SEMMELWEIS EGYETEM

DOKTORI ISKOLA

Ph.D. értekezések

3360.

KÁDÁR KRISTÓF GYÖRGY

A folyadék- és elektrolitháztartás szabályozásának élet- és kórélettana-Keringés és vérnyomás szabályozás

című program

Programvezető: Dr. Zsembery Ákos, egyetemi docens

Témavezetők: Dr. Zsembery Ákos, egyetemi docens

CALCIUM TRANSPORT IN HAT-7 CELLS: A CELLULAR MODEL OF AMELOGENESIS

PhD thesis

Kristóf Kádár, MD

Theoretical and Translational Medicine Division

Semmelweis University

Supervisor: Ákos Zsembery, MD, PhD

Official reviewers: Éva Ruisanchez, MD, PhD
Norbert Szentandrássy, MD, PhD

Head of the Complex Examination Committee: György Reusz MD, PhD, DSc

Members of the Complex Examination Committee: Zoltán Prohászka MD, DSc
Mihály Kovács PhD, DSc

Budapest

2025

Table of Contents

List of Abbreviations

2-APB	2-aminoethyl diphenylborinate
ACh	Acetylcholine
AE2	anion exchanger 2 (*Slc4a2)*
AI	amelogenesis imperfecta
ALP	alkaline phosphatase
AMBN	ameloblastin
AMELX, AMELY	amelogenin X and Y genes
AP	apical
APLP	tissue-nonspecific alkaline phosphatase
ATP	adenosine triphosphate
BL	basolateral
CA	carbonic anhydrase
cAMP	cyclic AMP
cDNA	complementary DNA
CFTR	cystic fibrosis transmembrane conductance regulator
Cldn	claudin
CRAC	Ca^{2+} release-activated Ca^{2+} (channel)
CREB	cyclic AMP responsive element binding protein
E18.5	(mice) embryonic day 18.5
EC_{50}	half maximal effective concentration
ECM	extracellular matrix
EHS	Engelbreth-Holm-Swarm
EMP	enamel matrix protein
ENAM	enamelin
EOE	enamel organ epithelium
ER	endoplasmic reticulum
ERM	epithelial cell rests of Malassez
FBS	fetal bovine serum
FTY720	2-amino-2-(2-[4-octylphenyl]ethyl)−1,3-propanediol), fingolimod

GPCR	G-protein coupled receptors
HAp	hydroxyapatite
hDPSCs	human dental pulp stem cells
HK-2	human kidney-2 epithelial cells
HSG	human submandibular gland
IC_{50}	half maximal inhibitory concentration
IEE	inner enamel epithelium
IP3	inositol 1,4,5-trisphosphate
IP_3R	inositol trisphosphate receptor
ITP	Inosine triphosphate
I-V	current-voltage
KLK4	kallikrein-related peptidase 4
KO	knockout
MHR1–4	N-terminal TRPM homologue region domains
MIC	magnesium inhibited cation (current)
MMP20	matrix metalloproteinase/metallopeptidase 20 (enamelysin)
NBCe1	Na^+-HCO_3^- cotransporter (*Slc4a4*)
NCKX	potassium-dependent sodium-calcium exchanger
NCX	Na^+/Ca^{2+} exchanger
NHE1	Na^+-H^+ exchanger 1
NKCC1	Na^+–K^+–$2Cl^-$ cotransporter 1
NSAID	non-steroidal anti-inflammatory drug
ODAM	odontogenic ameloblast-associated protein (Apin)
ORAI	calcium release-activated calcium channel protein
P14	postnatal day 14
P2X, P2Y	purinergic receptor X and Y
PI3K	phosphoinositide 3-kinase
PIP_2	phosphatidylinositol 4,5-bisphosphate
PL	papillary layer
PLC	phospholipase C
PMCA	plasma membrane Ca^{2+}-ATPases
qPCR	quantitative PCR

RA	ruffle-ended ameloblast
RGD	Arg-Gly-Asp
ROI	region of interest
SA	smooth-ended ameloblast
SCPPPQ1	secretory calcium-binding phosphoprotein-proline-glutamine-rich 1
SD	standard deviation
SEM	standard error of the mean
SERCA	sarcoendoplasmic reticulum calcium ATPase
shRNA	short/small hairpin RNA
SI	stratum intermedium
SLC24A4	solute carrier family 24, member 4 gene, encoding NCKX4
SLC26	solute carrier family 26
Slc26a4	pendrin
SLC41A1	solute Carrier Family 41 Member
SLC8A1	solute carrier family 8 member A1
SOCC	store-operated Ca^{2+} channel
SOCE	store-operated calcium entry
STIM	stromal interaction molecule
TER	transepithelial electrical resistance
TJP1	tight junction protein1
TP	Tomes' process
TRP	transient receptor potential
TRPM	transient receptor potential cation channel cubfamily M
TRPM7-KR	TRPM7 kinase-inactive knock-in mutant
UTP	uridine triphosphate
VSOR/VRAC Cl^-	volume-sensitive outwardly rectifying anion channel
WDR72	WD repeat domain 72
WT	wild-type
ZO-1	tight junction protein1

1. Introduction

Enamel, the hardest and most highly mineralized tissue in the human body, covers the crown of teeth and provides the mechanical resilience required for mastication. It is produced during tooth development by specialized epithelial cells, the ameloblasts, which disappear after tooth eruption. Mature enamel is acellular, avascular, inert, rigid, almost completely mineralized non-regenerative, with calcium (Ca^{2+}) as its predominant component. Consequently, one of the key functions of ameloblasts is the transport of calcium ions to the mineralization front. Although several Ca^{2+} channels and transporters have been identified in ameloblasts, the precise mechanisms governing Ca^{2+} transport during amelogenesis remain largely unresolved. Because ameloblasts are lost following eruption modeling of transport dynamics requires in vitro epithelial models of polarized ameloblast-like cells. This thesis summarizes my investigations into: (1) identifying the functional presence, Ca^{2+} conductance, and pH sensitivity of TRPM7, a divalent cation channel, in HAT-7 cells as an in vitro model of ameloblasts, and assessing its putative role in Ca^{2+} transport during amelogenesis; and (2) examining the functional presence of purinergic and cholinergic receptors in 3D cultures of these cells.

1.1 Overview of tooth development

Tooth development begins around the 6th week of embryogenesis and arises from two main tissue types: ectoderm, which gives rise to enamel, and neural crest-derived mesenchyme, which differentiates into pulp, dentin, cementum, periodontal ligament, and alveolar bone. The process is subdivided into distinct, histologically recognizable stages (Fig. 1). The first, the lamina (placode) stage (Fig. 1A), involves localized thickening of the oral epithelium, giving rise to dental placodes (1,2). This is followed by the bud stage (Fig. 1B), marked by ectomesenchymal condensation around epithelial invaginations. Next, in the cap stage (Fig. 1C), the invaginated oral epithelium develops into the enamel organ, while the underlying condensed mesenchyme forms the dental papilla. Late in this stage, histodifferentiation gives rise to pre-ameloblasts and odontoblasts (1,2). The subsequent bell stage is characterized by morphogenesis (Fig. 1D), where the final shape of the tooth crown is established, and the onset of enamel and dentin formation occurs. During this stage, the dental lamina degenerates, creating a connection between the developing tooth and surrounding tissues. Development of the secondary dentition begins

at approximately the 20th intrauterine week and continues until about 10 months after birth (1,2).

1.2 Overview of amelogenesis

Enamel is the hardest calcified tissue in the human body because of its high mineral composition and highly organized structure. Unlike bone, it lacks vital cells, contains no collagen, and cannot regenerate once formed, as the ameloblasts responsible for its secretion undergo apoptosis during tooth eruption (3). Mature enamel consists predominantly of minerals (≈ 95% by weight), with small contributions from water (2-4%) and organic material (1-2%). The most abundant ions are Ca^{2+} and PO_4^{3-}, accounting for approximately 37% and 17% of the mineral content by weight, respectively. Other ions are also present, including Mg^{2+} (0.22%), Na^{+} (0.70%), and K^{+} (0.03%). The inorganic phase is composed of carbonated hydroxyapatite (HAp, $Ca_5(PO_4)_3(OH)$) crystals, arranged into long, ribbon-like structures (3,4). These crystals are organized into enamel rods (prisms) with interrod enamel filling the spaces between them. Enamel rods extend through most of the enamel thickness, except in the aprismatic inner layer. In approximately three-quarters of each rod is encased by rod sheath, a mostly protein containing material, connecting the rod to the interrod enamel (3,4).

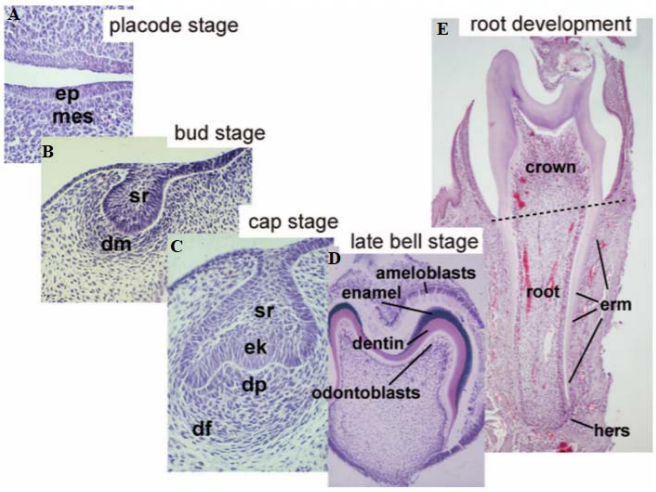

Figure 1. *Stages of tooth development. (A) placode (lamina) stage, (B bud stage, (C) cap stage, (D) bell stage, (E) root development. ep: epithelium; mes: ectomesenchyme; sr: stellate reticulum; dm: dental mesenchyme; dp: dental papilla; df: dental follicle; ek: enamel knot; erm: epithelial cell rests of Malassez; and hers: Hertwig's epithelial root sheath. Adapted from (1).*

This hierarchical structural organization, combined with its chemical composition, provides enamel with exceptional hardness and the ability to withstand high masticatory forces (5,6). However, enamel's brittleness and lack of regenerative capacity make it highly vulnerable to wear, erosion, and caries once damaged (3).

Amelogenesis is initiated at the bell stage of odontogenesis. Inner enamel epithelium (IEE) cells are induced by the underlying mesenchymal dental papilla to differentiate into ameloblasts (pre-secretory phase) as the basal lamina between IEE and papilla breaks down, and the cells get in a direct contact with pre-dentine. During this process, IEE cells are gradually transformed from a cuboidal into a columnar shape to form ameloblast (pre-secretory ameloblasts) (Fig 2A). Ameloblasts are specialized epithelial cells that provide the optimal environment for mineralization in amelogenesis by secreting ions and enamel matrix proteins (3,4,6).

Amelogenesis is divided into two major stages - the secretory and maturation stages - separated by a short transitional stage. The morphology, protein and ion secretion of ameloblasts is altered according to their stage-specific functions (3,4,6).

1.2.1 Secretory stage

In the secretory stage, ameloblasts elongate, their nuclei shift toward the basal pole, and a distal extension - the Tomes' process (TP) develops. The TP is critically involved in exocytosis of vesicles containing matrix proteins and in organizing growing crystals (4,7,8). Protein-synthesizing organelles, including the Golgi apparatus, rough endoplasmic reticulum, and mitochondria, are markedly increased (Figs. 2B-D) (8). The ameloblasts are tightly connected by junctional complexes, forming a selectively permeable barrier for ions between the interstitial space and the enamel matrix and considered both morphologically and functionally polarized (4,8). During this phase, nearly the entire enamel thickness is deposited, though the matrix remains soft—composed of roughly equal amounts of enamel matrix proteins (EMPs), mineral, and water—with only ~30% mineralization. The main function of secretory ameloblasts is the synthesis and secretion of EMPs: amelogenin, ameloblastin, and enamelin. Amelogenin, the most abundant (80–90%) (9), controls crystal growth and orientation (10-12). Ameloblastin (~5%) is thought to mediate adhesion of ameloblasts to the mineralization front (13,14), while enamelin (3–5%) contributes to crystal elongation and ribbon formation (10,15).

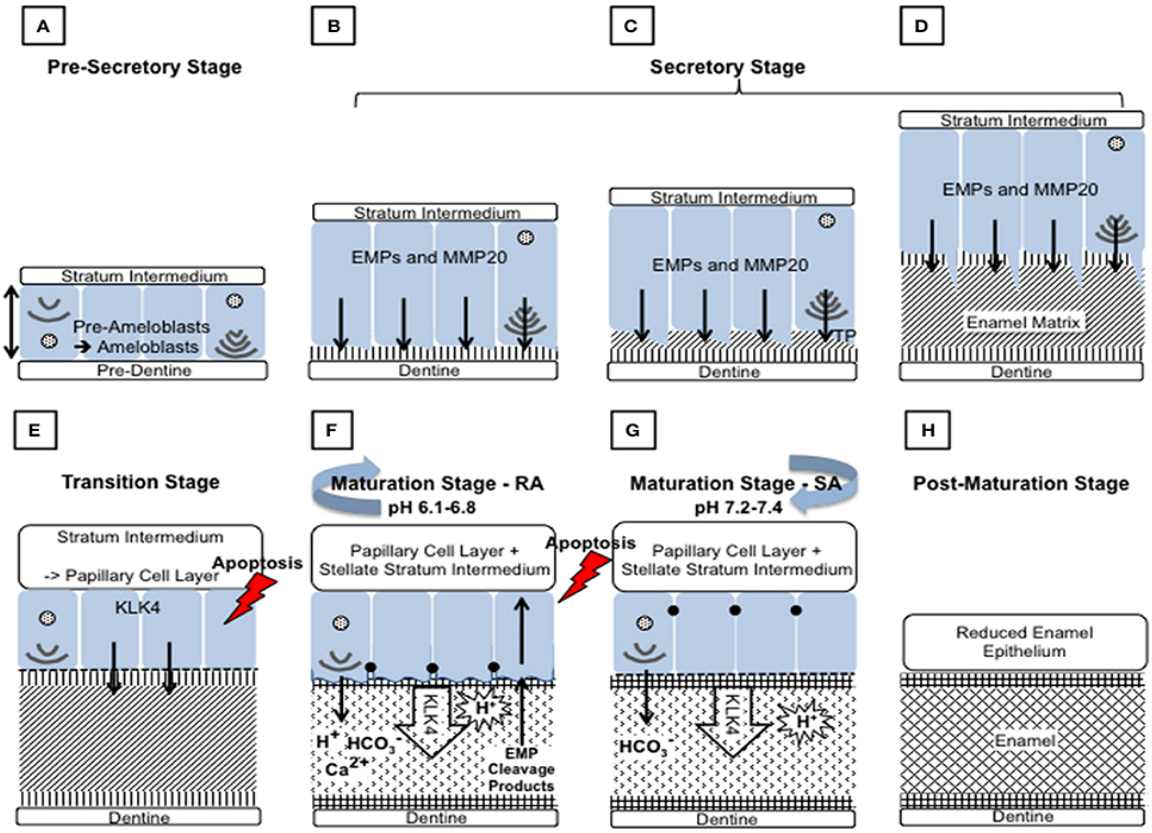

Figure 2*. Schematic diagram of the events during amelogenesis.* ***(A) Pre-secretory stage:*** *Ameloblasts (blue) differentiate from IEE cells in response to reciprocal signaling with the dental papilla. (B–D)* ***Secretory stage:*** *Ameloblasts secrete enamel matrix proteins (EMPs) via exocytosis from the Tomes' process (TP) while retreating from dentine, increasing enamel thickness.* ***(B) Initial secretion forms*** *aprismatic enamel closely associated with dentine mineral.* ***(C)*** *Further* ***development of the TP*** *allows EMP secretion from two domains, giving rise to prismatic and interprismatic enamel.* ***(D)*** *With progression, the TP lengthens and thins; secretion gradually ceases, thus the final enamel formed is aprismatic.* ***(E) Transition stage:*** *EMP secretion declines, and ameloblasts undergo reorganization, shortening to about half their height, reducing organelles, and losing the TP. Stellate reticulum, and outer enamel epithelium form the papillary layer (PL). (F–G)* ***Maturation stage:*** *enamel matrix undergoes complete mineralization through crystallite growth and EMP degradation/removal. Ameloblasts modulate cyclically between* ***ruffle-ended*** *(RA,* ***F)*** *and* ***smooth-ended*** *(SA,* ***G)*** *morphologies. RA ameloblasts form apical membrane infoldings with tight junctions, mediating ion transport and proton neutralization, while SA ameloblasts are more permeable, permitting water and protein passage.* ***(H) Post-maturation stage:*** *Ameloblasts and other enamel organ cells form the reduced enamel epithelium.*

Expression of amelogenin (16) and enamelin (10,17) declines in maturation, whereas ameloblastin persists (10,17). Mutations in the genes encoding amelogenin (*AMELX*, *AMELY*), ameloblastin (*AMBN*), or enamelin (*ENAM*) have been associated with amelogenesis imperfecta (AI), resulting a thinner or complete absent of enamel (hypoplastic AI) (6,10).

Enamel proteins continuous secreted and deposited on the enamel surface, while ameloblasts radially moving away from the site of secretion as enamel thickens and enamel crystals elongate (4). Upon secretion, amelogenin self-assembles into nanospheres serving as precursors of enamel rods, functioning as space fillers and scaffolds for the growth of apatite crystals (Fig. 2) (4,18). Simultaneously, Ca^{2+} and phosphate are transported through the ameloblast layer to supply ions for HAp crystal formation (3,6,19,20). In parallel, EMPs - particularly amelogenin - are proteolytically processed by enamelysin (MMP20), expressed predominantly during the secretory and early maturation stages (Figs. 2B-D), with maximal expression in secretion (21,22). MMP20-null mice exhibit defective mineralization, underscoring the essential role of proteolysis in proper enamel formation (3,6,11).

1.2.2 Transition stage

Once the full thickness of immature enamel has been deposited, secretory ameloblasts undergo marked morphological changes in a short transition stage (4). The cells become shorter, Tomes' processes are lost, and the abundance of intracellular organelles is reduced (4). Concurrently, the expression of *AMELX, AMELY, AMBN, ENAM* declines, while the expression of genes associated with ion transport, proteolysis, and pH regulation increases (4,23-25). Also, atypical basal lamina forms against enamel, and hemidesmosomes mediate adhesion. Surrounding stratum intermedium (SI), stellate reticulum, and outer enamel epithelium form the papillary layer (PL), which is vascularized and may assist with ion transport and protein removal. Approximately 25% of ameloblasts undergo apoptosis (Fig. 2E) (6).

1.2.3 Maturation stage

During the maturation stage, ameloblasts shorten while retaining apical–basal polarity. They alternate cyclically between two phenotypes: ruffle-ended (RA) and smooth-ended (SA) cells (Fig. 2) (26). These changes occur in coordinated groups, forming oblique bands of similar morphology across the crown. In rat incisors, SA waves occur at ~8.5-h

intervals, after which cells revert to the RA phenotype within ~2 h (27). Histological analyses show that ~70% of maturation ameloblasts are in the RA state and ~20% in the SA state at any given time. RA ameloblasts exhibit extensive apical membrane infoldings forming a striated border, with mitochondria clustered nearby - features consistent with intensive ion transport and endocytosis (8,26). Their apical junctions are tight, but basal junctions leaky. In contrast, SA cells lack the ruffled border, show leaky apical junctions but tight basal junctions, facilitating water and protein passage (Figs. 2F & 2G) (8,26). Functionally, RA ameloblasts mediate Ca^{2+} and phosphate transport into the enamel space, buffer protons generated during HAp growth, and internalize degraded proteins. Notably, phenotype cycling correlates with pH oscillations: enamel under RA cells is mildly acidic (pH ~6.2), whereas enamel under SA cells is near neutral (pH ~7.2) (28,29). The molecular machinery driving these cycles remains largely unresolved.

Protein secretion diminishes at this stage, limited mainly to amelotin, ODAM, and SCPPPQ1 (10,30). These proteins likely mediate adhesion of ameloblasts to the enamel, with ODAM also implicated in regulating MMP20 (31).

By the end of secretion, the bulk of enamel matrix is deposited but only ~30% mineralized. Initial HAp crystals elongate along the c-axis, forming thin ribbons embedded in EMPs. During maturation, ribbons thicken laterally (a- and b-axes), requiring proteolytic removal of EMPs. KLK4, a serine protease secreted by ameloblasts, degrades enamel proteins previously cleaved by MMP20 and functions across the wide pH range of maturation (Figs. 2F & 2G) (11). Mutations in KLK4, like those in MMP20, cause hypomaturation AI (6). Protein degradation products are endocytosed (7), with WDR72 implicated in this process (32).

Since the bulk mineralization occurs in this stage there is an intensive Ca^{2+} and phosphate transport through ameloblasts accompanied by HCO_3^- secretion to buffer extracellular acidity. Ion transport and crystal growth are most active in the RA phenotype. Through repeated RA/SA cycles, the enamel matrix is gradually converted into mature, fully mineralized tissue virtually devoid of organic material (3,6,19).

In the post-maturation (protective) stage, ameloblasts and associated enamel organ cells form the reduced enamel epithelium, which later contributes to the junctional epithelium of erupted teeth and provides a transient protective layer during the pre-eruptive phase.

1.3 Ca^{2+} transport in amelogenesis

Transepithelial calcium transport by ameloblasts is essential for enamel mineralization. Beyond its structural role in mineralized tissues, calcium (Ca^{2+}) also acts as a universal signaling messenger, regulating virtually all biological processes (33). Cytosolic Ca^{2+} is tightly maintained at ~100 nM, far below the ~1.0-1.3 mM extracellular concentration (33), since sustained elevations are cytotoxic. Cells utilize a highly conserved set of clearance mechanisms (33,34) and it is not unlikely, that transepithelial Ca^{2+} transport utilizes – at least partly - this same Ca^{2+} handling toolkit.

The bulk of calcium transport occurs during the maturation stage, whit total transport and rates are being highest. Cytosolic Ca^{2+} rises to ~230 nM in maturation ameloblasts versus ~135 nM in secretory cells (35), and ~86% of total calcium is acquired during this stage in rat incisors (36). Elevated mineral accretion has been confirmed by tracer, radiographic, and chemical analyses, with transport rates estimated up to fourfold higher than in the secretory stage (37). The average calcium transport rate falls within the range reported for intestinal transport under a 1.5 mmol/L Ca^{2+} load (37).

Although the precise mechanisms of Ca^{2+} transport remain poorly understood (20,36,37), it is hypothesized that calcium is transported via the enamel organ, moving from the basolateral to the apical side, crossing the ameloblast barrier (3,20,38). As ameloblasts are highly polarized cells forming a tight epithelial barrier, that restricts the intercellular movement of ions and minerals (36), passive paracellular Ca^{2+} transport is unlikely. Earlier models proposed that cyclic relocation of tight junctions during RA-SA modulation could “gate” paracellular movement (3,36), but this is limited since ~70% of ameloblasts are in the RA phase where distal junctions block enamel access (36). Moreover, ^{45}Ca tracer studies indicate that Ca^{2+} incorporation predominates during the RA stage (20,39). These findings support a transcellular route as the main pathway, involving three steps: Ca^{2+} entry, intracellular transit, and extrusion (37). Initially, Ca^{2+} uptake was thought to be passive, driven by the extracellular–intracellular gradient, with extrusion mediated by plasma membrane Ca^{2+}-ATPases (PMCAs) (40).

1.3.1 Transporters in Ca^{2+} secretion

During its transcellular transport Ca^{2+} should be secreted against its electochemical gradients. To achieve this, ameloblasts employ two major systems to extrude Ca^{2+}: ATP-dependent Ca^{2+} pumps and Na^{+}-dependent Ca^{2+} exchangers (19,20,38).

1.3.1.1 Plasma membrane Ca^{2+}-ATPases

PMCAs, are high-affinity, low-capacity Ca^{2+} pumps that translocate Ca^{2+} across the plasma membrane in exchange of protons (H^+) at the expense of ATP hydrolysis (1 Ca^{2+}/ATP) (41,42). Three isoforms (ATP2B1, ATP2B3, and ATP2B4) are expressed in ameloblasts with localization and intensity varying by stage and phenotype (43-46).

Earlier it studies reported the presence of PMCA in all stages of amelogenesis, with higher intensity in early maturation than in the secretory stage (44-46). In the secretory stage, expression was detected across the entire plasma membrane, whereas in RA cells localized at the distal ruffled border and SA cells along lateral and proximal membranes (44-46). In contrast, Robertson et al. have recently reported that PMCA1 and PMCA4 localizes to the basolateral membrane in both secretory and maturation ameloblasts (Fig. 3) (43). Functional PMCA pumps were reported on isolated rat secretory and maturation ameloblasts, using fura-2 Ca^{2+} imaging (47).

1.3.1.2 Na^+/Ca^{2+} exchangers (NCX/NCKX)

Na^+/Ca^{2+} exchangers uses the electrochemical Na^+ gradient to drive Ca^{2+} extrusion with low Ca^{2+} affinity but very high capacity (48). NCXs exchange 1 Ca^{2+} for 3 Na^+, while NCKXs exchange 1 Ca^{2+} and 1 K^+ for 4 Na^+ (49,50). Their activity is bidirectional: under physiological conditions they mediate forward-mode extrusion, but under altered electrochemical conditions they may operate in reverse mode, importing Ca^{2+} (49).

NCXs, encoded by *SLC8A* genes, were first identified in ameloblasts by Okumura et al. (51). NCX1 and NCX3, were found in both secretory and maturation ameloblasts (43,51), with mostly apical or apico-lateral distribution in immunohistochemistry studies. In a recent studies NCX1 was found in both the apical, middle and basal region of maturation ameloblasts (52), while others reported that the NCX3 protein expression in practically limited to the secretory phase (Fig. 3) (53). The functional presence of NCX transporters has also been demonstrated in primary cultured ameloblasts using fura-2 Ca^{2+} imaging (51). However, no mutations in *SLC8A* have been associated with amelogenesis imperfecta yet.

By contrast, strong evidence supports a critical role for NCKX transporters, especially NCKX4 (*SLC24A4)*. *SLC24A4* mRNA expression was identified in ameloblasts, highest among other members of the NCKX family (23,54), with markedly increase in gene expression during maturation (23). Its polarized localization at the distal pole of RA

ameloblasts - in contrast to a more diffuse distribution is SA phenotype, as well as its absence in the secretory stage - suggests a specialized role in Ca^{2+} extrusion during bulk enamel mineralization (Fig. 3) (23). Furthermore, mutations in *SLC24A4* cause enamel defects in both humans and mouse models, underscoring its key role in enamel biomineralization (25,55). Recent functional studies on isolated secretory and maturation ameloblasts found NCKX to be the dominant Na^{+}/Ca^{2+} exchanger (53).

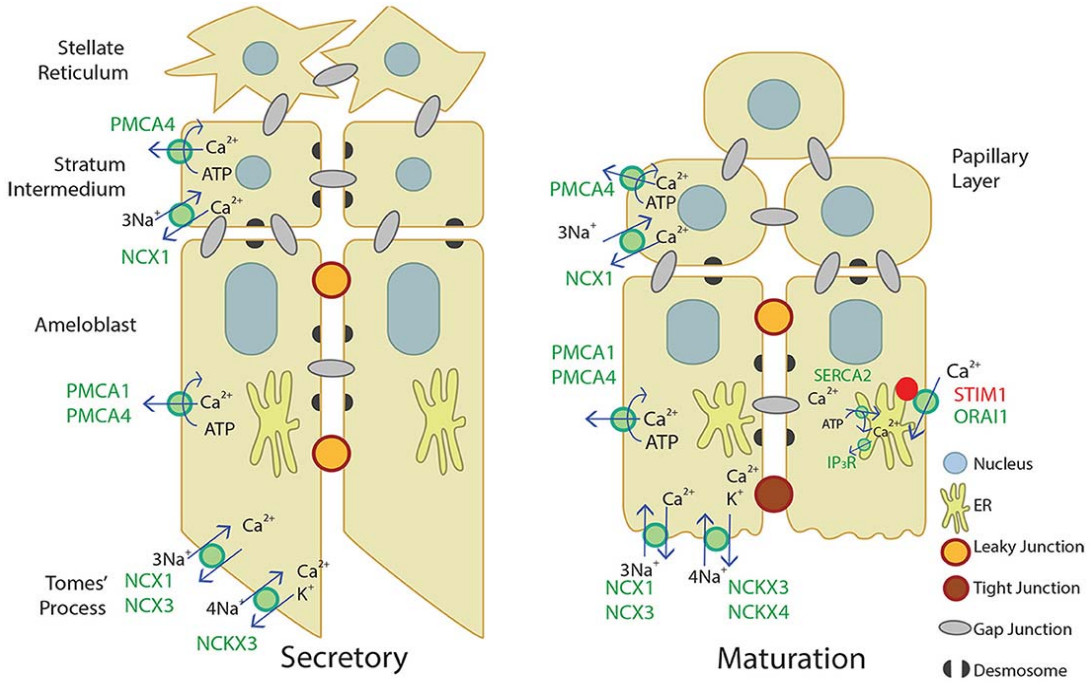

Figure 3. Transcellular calcium transport system during the secretory and maturation stages. *In the secretory stage, active Ca^{2+} transport across the lateral membrane is mainly mediated by PMCA1 and PMCA4. NCX1, NCX3, and NCKX3 contribute to Ca^{2+} extrusion via the Tomes' process. Ca^{2+} entry is predominantly mediated by CRAC channels activated upon ER store depletion through IP_3R. Cytosolic Ca^{2+} is cleared by SERCA2, replenishing ER stores, and by NCKX/NCX transporters at the apical membrane secreting Ca^{2+} into the enamel space to support mineralization. In the maturation stage, NCX1 and PMCA4 also export Ca^{2+} from the stratum intermedium/papillary layer. (43)*

1.3.2 Transporters in Ca^{2+} uptake

While the extrusion a Ca^{2+} to the enamel matrix seems be decoded to some extent, the cellular uptake and transit are less defined. Historically, Ca^{2+} influx into ameloblasts was thought to occur passively, driven by the steep extracellular–intracellular gradient, with cytosolic Ca^{2+} buffers such as parvalbumin and calbindin (9/28 kDa) regulating $[Ca^{2+}]_i$ as

Ca^{2+} moving from the basolateral to the apical pole (20,37,40). Since the deletion of otherwise abundantly expressed calbindins did not produce enamel defects (56,57), currently transorganellar routes are proposed (3,20,38,57). The endoplasmic reticulum (ER), with its continuous tubular network and Ca^{2+} buffering proteins (calreticulin, endoplasmin, ERp72, calnexin), as well as SERCA (sarcoendoplasmic reticulum calcium ATPase) pumps, is a logical candidate, with store-operated calcium entry as a plausible uptake mechanism (20,38,58).

Store-operated calcium entry (SOCE) mediated by Ca^{2+} release-activated Ca^{2+} (CRAC) channels, serves as a crucial and ubiquitously expressed pathway for calcium influx, particularly in non-excitable cells where it constitutes the primary mechanism for Ca^{2+} uptake (59). CRAC channels are composed of stromal interaction molecules STIM1 and STIM2, which act as Ca^{2+} sensors in the ER membrane, and ORAI proteins (ORAI1–3), which form the pore in the plasma membrane (59,60). Upon activation of cell surface receptors (mainly G-protein coupled receptors (GPCRs)), phospholipase C (PLC) is produced, leading to the generation of inositol 1,4,5-trisphosphate (IP_3), which binds to its receptors (IP_3R) on the ER membrane. This interaction induces the release of Ca^{2+} from ER stores via IP_3R channels (61,62). The resulting drop in ER luminal Ca^{2+} concentration triggers significant conformational changes in STIM proteins, enabling them to activate ORAI channels and initiate sustained calcium influx (Fig. 3) (59,60).

The transcripts and proteins of *Stim1* and *Stim2* have been reported to be upregulated during enamel maturation (24). In primary murine enamel cells, key CRAC channel components—including ORAI-3, STIM1, and STIM2 - were all expressed, with peak expression occurring during the maturation phase of enamel development.

While ORAI1 seemed to be the dominant isoform, considerable amount of ORAI2 and ORAI3 expression was also observed (35). STIM1 showed intensive cytosolic localization in RA, but significantly reduced immunoreactivity in SA phenotype (35). CRAC channel inhibitors such as synta-66, BTP-2, and GSK7975A in rat ameloblasts significantly reduced or nearly abolished Ca^{2+} influx through SOCE (35,63). Mice deficient in STIM1/2 or ORAI1, which exhibited impaired SOCE in ameloblasts, displayed enamel abnormalities ranging from pronounced hypomineralization to disrupted enamel crystal formation (58,64). Similarly, individuals with mutations in ORAI1 or STIM1 were found to have enamel defects classified as type 2 hypomineralized

AI (65,66).

Consistently, this several IP_3R subtypes were found to be upregulated during maturation (35) suggesting that in ameloblasts Ca^{2+} release from ER mediated by this pathway. A number of physiological agonists are known to induce Ca^{2+} release by GPCR activation, including ATP and acetylcholine (67). Nurbaeva et al. reported functional purinergic and cholinergic receptors on isolated secretory and maturation ameloblasts, with significantly stronger $[Ca^{2+}]_i$ responses in the maturation phenotype (35).

Alternative models of Ca^{2+} uptake and transit also exists like Golgi-derived vesicle packaging for apical exocytosis (20,68) and mitochondrial-mediated transport (20,69), with recent evidence showing elevated mitochondrial Ca^{2+} uptake in isolated maturation-stage ameloblasts (70). More importantly, the high relative abundance of TRPM7 in reported in the enamel organ during tooth development (71), together with defective enamel mineralization observed in TRPM7 mutant mice (71,72), suggests a putative role for TRPM7 in Ca^{2+} uptake.

1.4 pH regulation in amelogenesis

Acid–base balance is critical for enamel hydroxyapatite formation, as crystal growth requires tight regulation of ionic composition and extracellular pH (3,4,29). The formation of hydroxyapatite ($10Ca^{2+} + 6HPO_4^{2-} + 2H_2O \rightleftharpoons Ca_{10}(PO_4)_6(OH)_2 + 8H^+$) releases large amounts of protons, which must be neutralized or buffered. During the secretory stage, amelogenin contributes to pH buffering; however, since it is absent during maturation, current evidence suggests that ameloblasts neutralize the acidified enamel matrix (RA phase) by secreting HCO_3^- ions in the SA phase (8,36,73,74). Bicarbonate can be generated intracellularly by carbonic anhydrases (CA) or transported from the blood through dedicated ion transporters (e.g. NBCe1). CAs catalyze carbonic acid formation providing HCO_3^- and also H^+ (75). CA2 and CA6 are significantly upregulated in maturation ameloblasts (24). CA2, localized to the apical border of ruffle-ended cells, may act together with V-type ATPases (3,28,76).

Transporters of the SLC4 family mediate bicarbonate flux. Anion exchangers (AE1-3) were indentified in ameloblasts from which AE2 (*Slc4a2*) mostly expressed in maturation ameloblasts in basolateral localization. AE2 exchanges intracellular HCO_3^- for extracellular Cl^-, thereby supplying chloride into the cell (3,76-80). NBCe1 (*Slc4a4*), an electrogenic Na^+/HCO_3^- cotransporter also found basolaterally in both secretory and

maturation phase, with stronger expression during maturation (3,73,80,81) mediate a bicarbonate influx. Knockout of AE2 or NBCe1 leads to severe enamel defects in mice, demonstrating their essential role in mineralization (79,81).

CA generated protons are removed from ameloblasts via transporters and pumps. NHE1 (*Slc9a1*), a Na^+/H^+ exchanger, found basolaterally removes the proton using the Na^+ gradient (76,77), while V-type H^+-ATPases, localized at the apical border of maturation ameloblasts, extrude protons directly into the enamel space using ATP (76).

The bicarbonate is transported out from the cell in exchange of a Cl^- by specific members of the SLC26 family, *Slc26a3*, *Slc26a6*, and *Slc26a4* (pendrin) on the apical membrane (82,83). CFTR, a cAMP-regulated Cl^- channel likely mediates Cl^- efflux into the enamel matrix, providing Cl^- for re-entry in exchange for HCO_3^- via pendrin (19,74). CFTR is strongly upregulated during maturation and localized in the apical membrane (24,84-86). Mutations in *Cftr* cause enamel hypomineralization and abnormal crystal growth in animal models (87-89), while in humans, cystic fibrosis patients sometimes display enamel defects (90).

During maturation, the enamel matrix undergoes cyclic pH changes, becoming more acidic (pH ~6.2) in the RA phase when bulk Ca^{2+} transport occurs. It can be speculated that the acidic environment may modulate Ca^{2+} secretion directly or Ca^{2+} uptake indirectly by affecting intracellular pH.

1.5 TRPM7 channel

1.5.1 General properties

Among the TRP subfamilies, TRPM is the largest and features four melastatin homology regions (MHR1–4) at the N-terminal region. TRPM channels are expressed in various tissues and participate in diverse cellular functions, including regulation of cell proliferation, metabolism, apoptosis, and cancer development (91,92). TRPM2, TRPM3, TRPM6, TRPM7, and TRPM8 are Ca^{2+}-permeable and activated under stress conditions and TRPM2 and TRPM7 are classified as "chanzymes" due to their dual functionality as ion channels and enzymes (93).

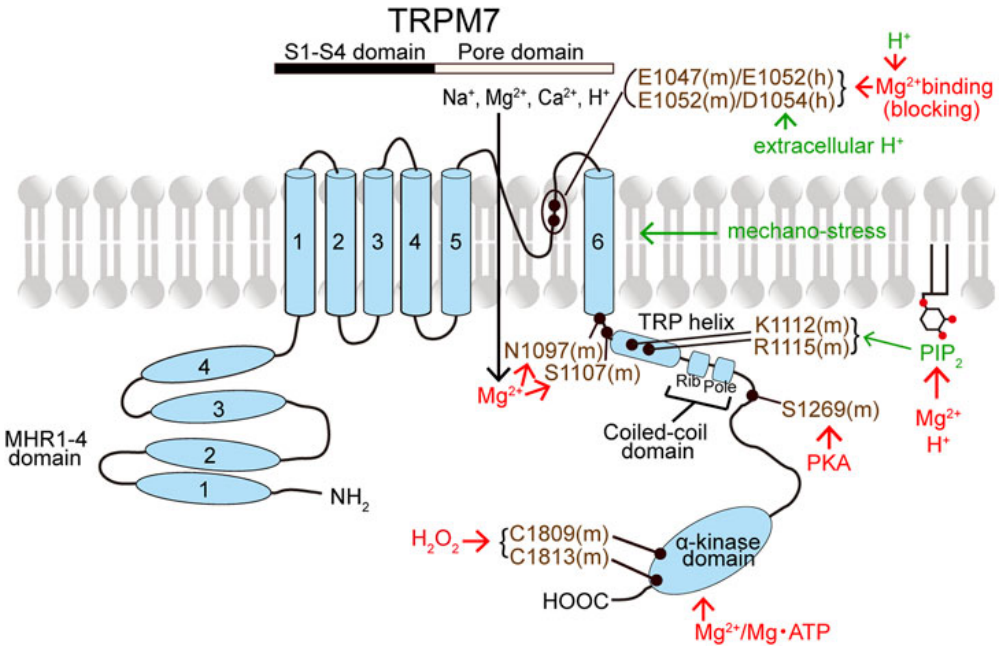

Figure 4. Topology model of a monomeric TRPM7 subunit with its modulators. *TRPM7 activators are shown in green, inhibitors in red, and residues in brown indicate the putative binding sites of these modulators (93)*

TRPM7 has MHR1–4 at its large N-terminus, followed by the conserved six transmembrane segments (S1–S6) with a pore-forming loop between S5 and S6, and a C-terminus comprising the TRP helix, the coiled-coil domain, and a unique α-kinase domain with an Mg^{2+}·ATP-binding site (Fig. 4) (93). Site-directed mutagenesis studies have shown that TRPM7's α-kinase activity and channel function operate independently (94,95). The protein kinase domain capable to phosphorylate of the α-helical tail of myosin II, a key regulator of cytoskeletal dynamics (93,96,97). Other identified substrates include TRPM6, annexin A1, eukaryotic elongation factor 2 kinase, tropomodulin, PLC-γ2, stromal interaction molecule 2 (98), SMAD2, Ras homologue family member A, and cAMP response element binding protein (93,96,97). TRPM7 can also autophosphorylate at a Ser/Thr-rich site in the C-terminal catalytic domain (93,96).The kinase can translocate to the nucleus in a Zn^{2+}-dependent manner, where it binds chromatin remodelling complexes and phosphorylates histones, thereby regulating gene expression (96,97,99).

TRPM7 single-channel currents have a conductance of ~40 pS at -70 mV in the absence of extracellular Mg^{2+} (100,101). Whole-cell I-V curves are nearly linear with weak inward rectification without extracellular divalent cations but become non-linear with

strong outward rectification in their presence, in particular Mg^{2+} acts as an open-channel blocker (95,102-104). In human TRPM7, residues D1054 and E1052 in the pore-forming region form the Mg^{2+}/Ca^{2+} binding and selectivity sites (105), whereas in mouse TRPM7, E1047 and E1052 play this role (Fig. 4) (106). TRPM7 conducts monovalent cations (Na^{+}, Cs^{+}) and divalent metal cations (Mg^{2+}, Ca^{2+}, Ba^{2+}, Sr^{2+}, Cd^{2+}, Zn^{2+}) (93,97,106,107), and in intracellular vesicles mediates ROS-induced Zn^{2+} release (107). The channel also exhibits proton permeability (108,109). Cation entry is driven by attraction to negatively charged glutamate and aspartate residues in the pore vestibule (105,108).

1.5.2 Regulation

1.5.2.1 Magnesium/Mg•nucleotides

Intracellular free Mg^{2+} is a key regulator of TRPM7 channel activity, maintaining its low activity under resting cellular conditions. Initially, intracellular Mg^{2+} was found to effectively inhibit channel activity in the micromolar range, with a complete block at 3 mM Mg^{2+} in whole cell patch-clamp experiments (103). The dose response curve found to be biphasic later on Jurkat T lymphocytes, suggesting two independent inhibition sites, one of high affinity (~10 μM) and one of low affinity (~165 μM) (110). Interestingly, Mg^{2+} inhibits TRPM7 in a manner similar to protons, as if protons can substitute for Mg^{2+} at the low-affinity inhibitory site. The primary effect of Mg^{2+} in multichannel patches is a reversible decrease in the number of conducting channels (111). Persistent low extracellular Mg^{2+} environment (400 nM or 8 μM for 1-3 day) also resulted channel activation due to depletion of intracellular Mg^{2+} (112). Extracellular application of Mg^{2+} resulted in a concentration-dependent inhibition of TRPM7 currents already in the micromolar range, suggesting that the channel conducts monovalent cations only in the absence of extracellular divalent cations (102,113,114). However, unlike intracellular cations, extracellular divalent cations inhibit TRPM7 through direct pore block rather than surface charge screening (102,114,115). Furthermore, the extracellular cation binding sites are not accessible from the cytoplasmic side; as a result, inhibition by intracellular Mg^{2+} or polyamines does not alter the current-voltage (I-V) relationship (115).

Similarly to Mg^{2+}, intracellular free Mg•ATP suppresses the channel activity, while its depletion augments it (94,103,115). Although it was previously advocated that,

essentially Mg^{2+} is responsible for its effect (103,115), Demeuse et al. demonstrated that, not just Mg•ATP but nearly all other magnesium–nucleotide complexes inhibit TRPM7, with nucleotides (except ITP) potentiating Mg^{2+}-mediated inhibition (94), They also proposed a hypothetical model of two different binding sites for Mg^{2+} and Mg•nucleotides with the latter being located at the site of the kinase and the former closer to the channel, acting synergistically (94).

The kinase activity of TRPM7 is not essential for its channel function, as mutations at two autophosphorylation sites or at a key catalytic residue that abolish kinase activity do not affect channel activity (116). However, the interaction between the channel and kinase domains plays a modulatory role by altering the channel's sensitivity to intracellular Mg^{2+} and Mg•ATP (94,117). More recently, it was demonstrated that this domain interaction enhances TRPM7 currents by reducing Mg^{2+}-dependent inhibition (118).

1.5.2.2 pH

Both extracellular and intracellular pH changes modulate TRPM7-related currents. TRPM7 currents are activated by cytosolic alkalinization (extracellular NH_4^+ application) and inhibited by intracellular acidification (extracellular acetate application) in rat basophilic leukemia (RBL) cells even in the presence of intracellular Mg^{2+} in whole-cell measurements. The activating effect of alkalinization was also observed in less invasive perforated patch recordings (100). Cytosolic protons inhibit TRPM7 with an IC_{50} corresponding to pH 6.3 (110). It has been suggested that both intracellular protons and Mg^{2+} inhibit TRPM7 in a similar, voltage-independent manner; however, protons appear to substitute only for the low-affinity Mg^{2+} inhibitory site (110). The inhibitory effect of protons primarily attributed to their interaction with PIP_2 and Mg^{2+} (100,119).

In HEK293 cells overexpressing TRPM7, lowering the extracellular pH produced a pH-dependent, marked potentiation of inward currents at negative membrane potentials (108,109), along with a moderate but significant increase in outward currents (108). Notably, this effect persisted even in the presence of 3 mM intracellular free Mg^{2+}. Similar findings have also been reported in case of endogenously expressed TRPM7 in RBL cells (108,113), HeLa cells (109), pig and rat ventricular myocytes (113). Authors suggested that the inward current under acidic conditions is, at least partially, carried by protons themselves. These currents were found to be potentiated in the absence and suppressed in the presence of Mg^{2+} and Ca^{2+} in the extracellular solution in freshly isolated human atrial

cardiomyocytes (120). It has been proposed that protons enhance the inward current by increasing the channel's permeability to monovalent cations, likely due to proton-induced displacement of divalent cations such as Ca^{2+} and Mg^{2+} from their inhibitory binding sites within the external pore (108). These binding sites are located in the pore region and include negatively charged residues (Fig. 4). Studies with charge-modifying mutations indicating electrostatic interactions as a likely mechanism (121).

1.5.2.3 PIP_2

As with many TRP channels, phosphatidylinositol 4,5-bisphosphate (PIP_2) stimuli have been implicated in the regulation of channel opening. It is now well established that TRPM7 activity depends on the presence of PIP_2 (100,113,122,123). However, the precise effects of PIP_2 depletion on TRPM7 gating remain controversial, as outcomes appear to vary depending on the method used and the extent of PIP_2 depletion or resynthesis (99). TRPM7-overexpressing HEK293 cells showed that PLC-mediated PIP_2 hydrolysis inhibited TRPM7 under low intracellular Mg^{2+}, with similar effects in ventricular fibroblasts (122,124) and prolonged PIP_2 depletion suppressed activity of both TRPM6 and TRPM7 (125). In contrast, transient PLC activation enhanced TRPM7 currents and Ca^{2+} influx (122), consistent with studies linking PLC stimuli to TRPM7-driven processes (99). Collectively, these results indicate biphasic PIP_2 dependence: transient depletion enhances TRPM7 activity, while excessive depletion inhibits it (122). The effects of PIP_2 on TRPM7 are closely tied to the modulatory effect of intracellular pH and Mg^{2+}. PIP_2 depletion sensitizes TRPM7 to Mg^{2+} and proton-mediated inhibition, while a point mutation that reduces Mg^{2+} sensitivity also renders currents resistant to PIP_2 depletion, protons, and polyamines (119). Conversely, divalent (Ca^{2+}, Mg^{2+}) and polyvalent cations (spermine, spermidine) inhibit PIP_2 hydrolysis (119,126), likely by charge shielding of phosphate head groups (100). This shielding may limit local PIP_2 availability for PLC, thereby modulating TRPM7 activity. While basal effects may be marginal, elevated cation or polyamine levels could strongly suppress PLC activity, especially during TRPM7 overexpression, (126). Alternatively, PIP_2 may act as a local Mg^{2+} chelator, promoting channel opening while enabling PLC-mediated modulation.

1.5.3 Inhibitors

Early inhibition studies of the TRPM7 channel employed non-specific blockers such as spermine, ruthenium red, trivalent cations, SKF-96365, and 2-aminoethyl

diphenylborinate (2-APB) (93,127,128). Several drug-like molecules were reported as TRPM7 inhibitors since, albeit effective only at high μM concentrations like nafamostat, carvacrol, 5-lipoxygenase inhibitors, midazolam, ginsenoside Rg3, ginsenoside-Rd, aripiprazole, quinine, CyPPA, dequalinium, SKA31, UCL1684 etc.(127,128). In contrast, the most extensively used inhibitors Waixenicin A, FTY720 and NS8593 suppress TRPM7 currents at low μM concentrations (127). More recently, a two highly selective, Mg^{2+}-independent compound, VER155008 (129) and the AKT inhibitor, CCT128930 (130) were reported.

1.5.3.1 NS8593

NS8593, N-[(1R)-1,2,3,4-tetrahydronaphthalen-1-yl]-1H-benzimidazol-2-amine, was initially synthesized as a potent and selective inhibitory gating modifier of small-conductance Ca^{2+}-activated K^+ (KCa2.1–2.3; SK) channels (131). NS8593 inhibits TRPM7 currents in an intracellular Mg^{2+}-dependent manner, with IC_{50} values of 1.6 μM in the absence and 5.9 μM in the presence of 0.3 mM $[Mg^{2+}]_i$. (132). Although broadly considered a non-selective cation channel blocker, at a concentration of 10 μM NS8593 selectively inhibits TRPM7 while sparing other TRP channels (132). NS8593 has been utilized in functional studies, such as demonstrating TRPM7-mediated Ca^{2+} influx in adipocytes (133), elucidating the role of TRPM7 in the pathogenesis of abdominal aortic aneurysm (134), and investigating TRPM7 function in primary ameloblast cells (135).

1.5.3.2 FTY720

FTY720 (2-amino-2-(2-[4-octylphenyl]ethyl)−1,3-propanediol), also known as fingolimod, is a sphingosine analogue originally recognized for its antitumor potential (136). Qin et al. (2013) demonstrated that FTY720 potently inhibit TRPM7 with IC_{50} = 0.72 ± 0.04 μM (137) in a kinase-independent manner. More recent studies have employed FTY720 as a pharmacological tool to establish TRPM7's roles in diverse physiological contexts, including macrophage proliferation and polarization (138), pathogenesis of abdominal aortic aneurysm (139) and odontoblast mechanosensitivity (140).

1.5.4 Activators

Earlier research primarily focused on TRPM7 inhibitors, more recent efforts have aimed to identify TRPM7 activators. Hofmann et al. reported 20 compounds capable of

activating TRPM7 channels including naltriben, clozapine, proadifen, doxepin, A3 hydrochloride, mibefradil, U-73343, CGP-74514A, metergoline, L-733,060, A-77636, ST-148, clemastine, desipramine, sertraline, methiothepin, NNC 55–0396, prochlorperazine, nortriptyline, and loperamide (141). Among these, naltriben and mibefradil have been the most extensively studied, and are now widely used as experimental tools to probe TRPM7 function.

1.5.4.1 Naltriben

Naltriben mesylate is a phenanthrene opioid with δ opioid antagonist properties (142). It has been identified as an effective activator of TRPM7 channels (141). Naltriben activates TRPM7 in a voltage-independent manner with an EC_{50} of 20.7 μM, and this activation is independent of intracellular Mg^{2+}. Furthermore, naltriben competes with NS8593, suggesting overlapping or interacting binding sites. Importantly, naltriben does not affect other TRP channels. The site of action is likely located within or near the TRP domain of TRPM7, as the S1107E mutant - Mg^{2+}-insensitive form of the channel - exhibited complete insensitivity to naltriben (Fig. 4). Recent studies gave a deeper insight into the mechanism of action of both naltriben and NS8593 (143). Naltriben has been widely used as a pharmacological tool to investigate TRPM7 function in diverse physiological and pathological contexts, including embryonic development (144), chondrogenesis (145), Mg^{2+} homeostasis (146), tumor progression through activation of the anti-inflammatory macrophage M2 phenotype (147), and ameloblast calcium transport during enamel formation (135).

1.5.4.2 Mibefradil

Mibefradil, a Cav3 T-type voltage-gated calcium channel antagonist originally developed for the treatment of hypertension and angina pectoris (148), is a benzimidazole compound structurally related to NS8593. It has been shown to activate TRPM7-mediated Ca^{2+} entry with an EC_{50} of 53 μM and to enhance TRPM7 currents at 100 μM in the presence of physiological intracellular Mg^{2+} concentrations (0.9 mM). This activation, however, was abolished at higher intracellular Mg^{2+} levels (1.8 mM), suggesting Mg^{2+}-sensitive modulation of TRPM7 activity (149). Mutation studies indicate TRP domain as its site of action. Importantly, mibefradil did not activate other TRP channels (149).

It has been proposed that TRPM7 agonists can be grouped into at least two classes: Type 1, represented by naltriben, which activates TRPM7 independently of intracellular Mg^{2+},

and Type 2, represented by mibefradil, which requires Mg^{2+} for activity (149). More recently, Souza Bomfim et al. suggested that mibefradil-induced increases in $[Ca^{2+}]_i$ occur through IP_3R channel activation and PLC-dependent signaling, leading to SOCE-mediated Ca^{2+} influx via ORAI channels (150). It is also noteworthy that, beyond TRPM7 activation, mibefradil inhibits voltage-dependent T-type Ca^{2+} channels (151) and volume-sensitive outwardly rectifying (VSOR/VRAC) Cl^- channels (152). Mibefradil has also been used to investigate TRPM7 function in embryo development (153).

1.5.5 Physiological role

Early studies in cultured cells identified TRPM7 as an essential Mg^{2+} channel (95,154), but it is also involved involved in Ca^{2+} signalling (97,104,155,156), vesicular Zn^{2+} release channel (107) mediating Zn^{2+}, Mg^{2+}, and Ca^{2+} influx in various processes (157-159). TRPM7-regulated Mg^{2+} plays a pivotal role in supporting the stability of DNA and RNA tertiary structures, energy metabolism, enzymatic activity, signaling pathways, cell cycle progression, and differentiation (160). The essential nature of TRPM7 for development and viability is underscored by the fact that global TRPM7 knockout in mice results in embryonic lethality (161), while cardiac-specific deletion impairs embryonic heart development. TRPM7's role in regulating cell differentiation has been demonstrated across multiple cell types (162). In mesenchymal stromal cells, TRPM7 senses shear stress, and its silencing accelerates osteogenic differentiation (163). Conversely, incorporation of Mg^{2+} into bone implant materials or coatings has been shown to enhance osseointegration (164), with evidence suggesting a potential role of TRPM7 in mediating this effect (165). TRPM7 mRNA expression was upregulated during osteogenic differentiation of human dental pulp stem cells (hDPSCs), whereas TRPM7-specific shRNA knockdown suppressed their osteogenic differentiation (166). More recently its role in muscle stem cell activation and muscle regeneration has also been suggested (167). Mechanistic studies suggest that, beyond its regulation of Ca^{2+} and Mg^{2+} homeostasis, TRPM7 can interact with receptor tyrosine kinase downstream effectors such as PI_3K, AKT, and ERK1/2, further influencing differentiation programs (162). TRPM7 has also been extensively studies in context of tumour formation and metastatic activity (168-171).

1.5.5.1 TRPM7 in the amelogenesis

Although the precise physiological functions of TRPM7 are not yet fully understood, its role in Mg^{2+} homeostasis suggested a potential involvement in skeletal development,

consistent with the association between Mg^{2+} deficiency and various skeletal pathologies (161). TRPM7 mRNA expression was found to be dramatically higher in teeth compared with other tissues such as brain, heart, lung, and kidney in E18.5 mice (71) TRPM7 was significantly upregulated in the maturation ameloblasts (72); mRNA and protein expression progressively increased from pre-secretory to maturation-stage ameloblasts, peaking during maturation (71,72). TRPM7 was also detected in odontoblasts and osteoblasts in addition to ameloblasts (71,72). Consistently with these findings, significantly hypomineralized craniofacial structures, including incisors, molars, and cranial bones were in found in heterozygous TRPM7 kinase-deficient mice (*Trpm7* $^{\Delta kinase/+}$). Enamel was severly hypoplastic, while histology and micro-CT analysis suggested that in dentin and bone matrix deposition occurred at levels comparable to wild-type mice; however, mineralization failed to progress normally (Fig. 5) (72).

Trpm7$^{\Delta kinase/+}$ mice exhibited ion channel dysfunction and hypomagnesaemia, while homozygous mutants were embryonically lethal (161). In heterozygotes, besides mineralization defect, alkaline phosphatase (ALP) activity was markedly reduced, but magnesium treatment partially restored ALP activity (72).

Kinase-inactive knock-in (K1646R) mutant (TRPM7 KR) mice, generated independently by two groups to assess TRPM7 kinase function without disrupting ion channel activity (159,172), displayed normal growth, body weight, food intake, and locomotor activity (172). TRPM7 KR mice showed deficient enamel pigmentation and decreased enamel thickness in both upper and lower incisors (Fig. 6).

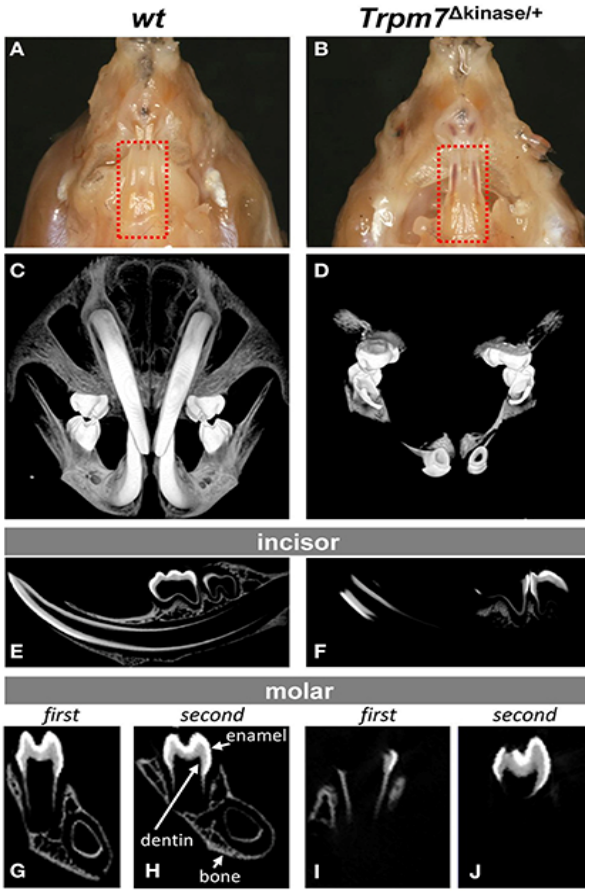

Figure 5. Hypomineralized enamel, dentin, and cranial bones in Trpm7$^{\Delta kinase/+}$ mice. (A, B) *Translucent mandibular incisors in P14 WT (A) versus transparent enamel in Trpm7$^{\Delta kinase/+}$ mice (B).* ***(C, D)*** *3D micro-CT reconstructions showing well-mineralized incisors, molars, and craniofacial bones in WT (C), but mineralization restricted to molar crowns and incisal ends in mutants at same intensity threshold (D).* ***(E, F)*** *Sagittal 2D micro-CT sections of hemimandibles showing strong contrast for enamel, dentin, and bone in WT (E) versus limited mineralization in mutants (F).* ***(G, H)*** *Well-mineralized enamel, dentin, and alveolar bone in WT first (G) and second (H) molars.* ***(I, J)*** *Partial mineralization in mutant first molar (I) and coronal enamel/dentin of second molar (J). (72)*

Scanning electron microscopy showed reduced rod density in the superficial while loosely arranged crystals and poorly packed rods in the deeper enamel layer. Surface hardness was also lower, with significantly reduced calcium content in the deep and elevated carbon content in both superficial and deep enamel layers (Fig. 7). However, the mineralization defect was considerably milder than what was reported in *Trpm7$^{\Delta kinase/+}$* mice. At the pre-secretory stage, ameloblasts displayed reduced Smad1/5/9, p38, and CREB phosphorylation. Immunoprecipitation confirmed direct binding of CREB to

TRPM7, indicating that the kinase domain may mediate ameloblast differentiation via CREB phosphorylation (71).

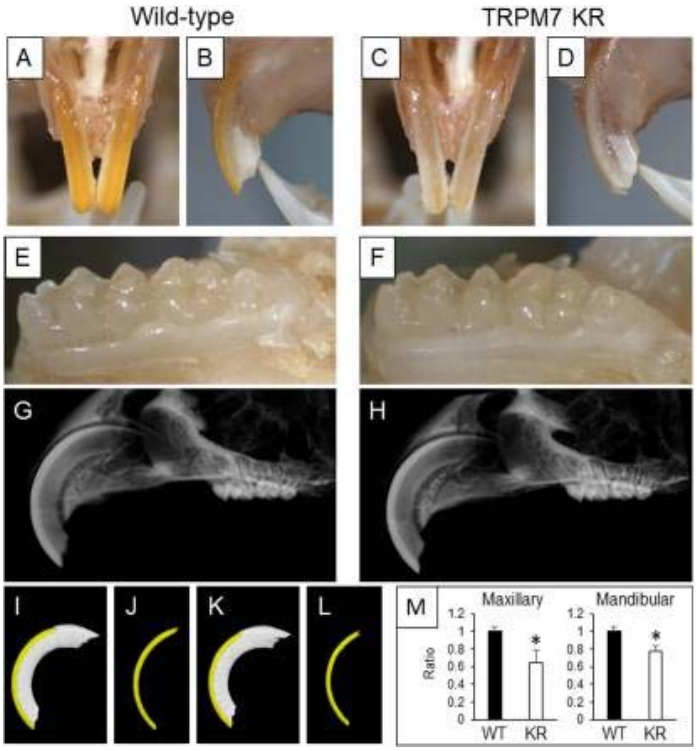

Figure 6. Enamel phenotype of TRPM7 KR mice (A–F) *Maxillary incisors in anterior (A, C) and lateral (B, D) views, and mandibular molars in occlusal view (E,F) from 20-week-old WT (A, B, E) and TRPM7 KR (C, D,F) mice.* ***(G, H)*** *Sagittal radiographs of maxillary incisors in 16-week-old WT (G) and TRPM7 KR (H).* ***(I–L)*** *3D micro-CT reconstructions of upper incisor enamel (yellow) with/without dentin (white) in WT (I, J) and TRPM7 KR (K, L). (M) Quantification of enamel volume in maxillary and mandibular incisors (12–16 weeks). Data are mean ± SD (n=3). *P < 0.05. KR: TRPM7 KR mutant; WT: wild-type. (71)*

A more recently developed a *K14-Cre;Trpm7$^{fl/fl}$* conditional knockout mice also exhibited a defective mineralization presented as reduced tooth pigmentation, fractured incisor tips, and a decreased area of high mineral density in molars (173). The enamel showed reduced calcification and microhardness, with significantly lower calcium and phosphorus content (173).

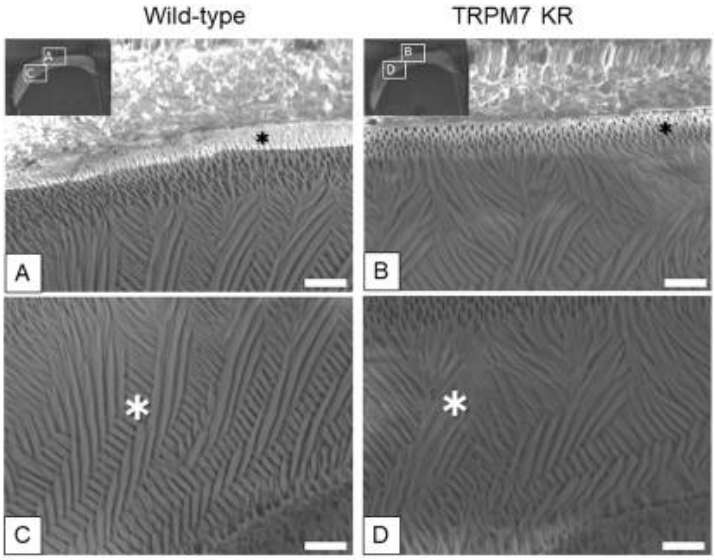

Figure 7. Enamel microstructure and mechanical properties in TRPM7 KR mice (A–D) *SEM of superficial (A, B) and deep (C, D) enamel layers from maxillary incisors of WT (A, C) and TRPM7 KR (B, D) mice. Inserts in (A, B) indicate magnified regions. *Regions analyzed by element mapping. Scale bar: 10 µm. modified from (71)*

Interestingly, the magnesium content of the enamel matrix was preserved, which somewhat contradicts the previously proposed role of TRPM7 in Mg^{2+} removal from the matrix (19). Histological analysis demonstrated ameloblast dysplasia with cyst-like stuctures at the maturation stage (173).

Collectively these data suggest an important role of TRPM7 in enamel mineralization, although its precise function yet to be fully elucidated.

1.6 Cellular models of amelogenesis

In mammals, ameloblasts disappear after amelogenesis, except in continuously growing rodent incisors, which are widely used for immunohistochemical and expression studies. However, these approaches offer only indirect insights, as most data on calcium transport come from tracers, staining, and expression analyses without functional validation. Consequently, current models of electrolyte transport remain largely hypothetical. To address this, suitable in vitro models needed for direct functional measurements ameloblast physiology. Immortalized cell lines, with their availability, relative stability and reproducibility compared to primary cultures, provide a common choice for such studies.

Important to note, however, that these cell lines typically cultured on flat plastic, glass, or functionalized surfaces covered by cell culture medium while in vivo cells reside within three-dimensional (3D) structures, surrounded by neighboring cells and extracellular matrix (ECM) (174). Notably, epithelial cells exhibit apical–basolateral polarization of transporters and receptors in their natural environment, a feature absent in standard culture.

1.6.1 Immortalized ameloblast cell lines

The two most widely used ameloblast-related cell lines are LS8 and ALC. LS8 cells were generated by introducing the polyoma virus large T-antigen into enamel organ epithelial (EOE) cells of newborn Swiss-Webster mice (175), whereas ALC cells were spontaneously immortalized from tooth germ organ cultures of newborn C57BL/6J mice (176). LS8 cells show higher mRNA levels of *AMELX, AMBN, ENAM*, and *MMP20* than ALC, but lack detectable protein expression of Amelx, Ambn, and Odam (177). In contrast, ALC cells express Odam and Klk4 and form calcified nodules in culture, resembling maturation-stage ameloblasts, while LS8 cells reflect a secretory phenotype. LS8 cells have been used to study Ca^{2+} transport, including TRPM7 function (135) and mitochondrial Ca^{2+} handling (70), whereas ALC cells have been applied to investigate Wnt/β-catenin signaling (178) and ameloblast–matrix interactions in 3D culture (179,180). A human ALC-like line (h-ALC) has also been established (181,182). Additional models include PABSo-E cells, derived from SV40-immortalized porcine molar EOE cells (183), used to study Ca^{2+}-sensing receptors (184) and endocytosis (185), and more recently EOE-3M and EOE-2M lines generated by HPV16 E6/E7 immortalization of mouse EOE cells, both expressing enamel matrix genes and proteases, with EOE-2M showing higher ALP levels (186).

1.6.1.1 HAT-7 cell line

The HAT-7 cell line was established from the cervical loop of rat incisors, the progenitor region of the enamel organ. HAT-7 cells exhibit key ameloblast characteristics, including expression of amelogenin and ameloblastin (187), as well as maturation-stage markers such as kallikrein-4 (Klk4) and amelotin. Previously these cells were used in gene expression studies on differentiation and circadian rhythm of ameloblasts (188-190).

Unlike previously described ameloblast-derived lines, HAT-7 cells can form a polarized epithelial layer with functional transport activity under specific culture conditions (77).

When seeded on permeable Transwell filters and exposed to differentiation stimuli-dexamethasone (10^{-8} M) and elevated extracellular Ca^{2+} (2.1 mM) - the cells upregulated tight junction proteins characteristic of maturation-stage ameloblasts, including ZO-1 (*Tjp1*), claudin-1 (*Cldn1*), claudin-4 (*Cldn4*), and claudin-8 (*Cldn8*), consistent with closed monolayer formation and increased transepithelial resistance. Key ion transporters involved in pH regulation (NHE1, NBCe1, AE2, pendrin, and CFTR) were detected by immunostaining and qPCR. Microfluorometry demonstrated the polarized functional activity of pH-modulating transporters and confirmed a regulated, vectorial basolateral-to-apical bicarbonate flux in polarized HAT-7 cells (77). Although there are several publications on membrane localization of these transporters (8,19), this was the first to demonstrate directional HCO_3^- transport in a cellular model, highlighting that HAT-7 cells under polarizing conditions can serve as a functional model system for studying transepithelial transport processes. This model has since been used to show that fluoride exposure does not affect bicarbonate transport but delays tight junction formation (78), and to demonstrate the functional presence of the Na^+-K^+-$2Cl^-$ cotransporter (NKCC1) at the basolateral membrane (78).

1.6.2 3D culture models

Increasing evidence suggests that conventional (unpolarized) 2D cultures fail to preserve key aspects of in vivo cell morphology and function (191-193). To overcome these limitations, 3D culture approaches have been adopted to promote differentiation toward ameloblast-like cells. Typically, immortalized ameloblast cell lines (e.g., ALC, HAT-7) are first expanded in 2D, then seeded - often together with fetal or postnatal dental mesenchymal cells - into ECM, most commonly Matrigel (21,194-196).

Basement membrane matrix extracts, commercially known as Matrigel, Cultrex, or EHS matrix, are widely used biological scaffolds (194,196,197). They are derived from the Engelbreth-Holm-Swarm (EHS) tumor and provides a rich source of basement membrane proteins. The main constituents include laminin, type IV collagen, heparan sulfate proteoglycan, and nidogen/entactin, while additional components comprise proteases (e.g., MMP-2, MMP-9) and growth factors such as TGFβ, FGF, EGF, PDGF, and IGF (194,196), although its biologically active components show considerable batch-to-batch variability (198-201). Collectively, these matrix components support cell adhesion, survival, and self-organization into 3D acinar-like or spheroidal structures, more closely

resembling the in vivo enamel organ microenvironment (196,197). These matrices provide a supportive microenvironment that closely mimics the in vivo extracellular milieu, thereby facilitating 3D organization and differentiation of ameloblast-like cells (196,197). In such conditions, 3D-cultured ameloblast-lineage cells typically show enhanced expression of enamel matrix proteins such as AMELX (21,202).

Two main techniques are used for matrix application. In the first, the matrix is spread onto a flat surface, allowed to gel, and then seeded with cells on top ("on-top" culture). In the second, cells are mixed with the matrix before gelling ("embedding" culture) (203). Upon contact with the matrix, many cell lines or primary cells cease proliferating and instead undergo differentiation, which varies by cell type. For example, human submandibular gland (HSG) cells form acinar-like structures and secrete amylase (204), while primary endothelial cells organize into capillary-like networks with lumens (205). We used Matrigel to create 3D culture from HAT-7 cells.

2. Aim and objectives

The aim of this thesis was to investigate changes of intracellular Ca^{2+} concentration in HAT-7 ameloblast cells under distinct conditions relevant to amelogenesis.

The objectives were as following:

1. To investigate the expression, functional presence and pH sensitivity of TRPM7 channels on cells grown in unpolarized culture
2. To study functional localization of TRPM7 channels in polarized cell monolayers
3. To investigate the effects of cholinergic and purinergic agonists on Ca^{2+} signal in 3D (spheroid) cell cultures

3. Methods

3.1 Cell culturing

3.1.1 Unpolarized monolayer culture

HAT-7 cells (206) were cultured in Dulbecco's modified Eagle's medium and Nutrient Mixture F-12 Ham medium (DMEM:F12; Sigma Aldrich) supplemented with 10% characterised fetal bovine serum (FBS; HyClone, Gibco), 100 U/ml penicillin and 100 mg/ml streptomycin (Sigma Aldrich) in standard conditions (37ºC, 5% CO_2). Subcultivation were performed in regular intervals using 0.25% trypsin-EDTA (Gibco).

3.1.2 Polarized monolayer (2D) culture

HAT-7 cells were grown on permeable polyester Transwell culture inserts with 0.4-µm pore size (Snapwell™ 12mm, Corning) for 2 days in standard culturing media (see above) followed by 3 days culturing in differentiation media (standard media supplemented with 2.1 M $CaCl_2$ and 10^{-5} mM dexamethasone, all Sigma). Transepithelial electrical resistance (TER) values were measured with an epithelial voltohmmeter (World Precision Instruments) daily, to monitor the paracellular permeability to electrolytes (barrier function), an important characteristic of secretory and absorptive epithelia.

3.1.3 3D (spheroid) culture

HAT-7 cells were grown within the gel layer of Matrigel® Basement Membrane Matrix (Corning). For seeding at low density to obtain single cell derived colonies within the Matrigel/, approximately 80,000 HAT-7 cells were resuspended in 160 µl Hepato-STIM® (BD Biosciences), a commercially available epithelial selection medium, supplemented with 10% HyClone fetal bovine serum (Thermo Scientific), 1% l-glutamine (Sigma-Aldrich), 100 U/ml penicillin and 10 g/ml streptomycin (Bori et al., 2016). The cell suspension was mixed with 400 µl of Matrigel and 70 µl aliquots were placed in eight individual wells of a 24-well Nunclon Sphera low-attachment plate (Thermo Fisher Scientific). The plate was incubated at 37°C to allow the Matrigel to solidify, and then 1 ml of the appropriate medium was added to each well. The culture medium was changed every other day. HAT-7 spheroids were released from the Matrigel matrix with trypsin/EDTA and resuspended in physiological salt solutions for further experiments.

3.2 RT-qPCR

In case of HAT-7 cells, grown as monolayers, total RNA was isolated using a GeneJET RNA Purification Kit (Thermo Scientific). Total RNA was isolated from 7-days HAT-7 spheroids using a NucleoSpin RNA XS kit (Macherey-Nagel). After RNA integrity check (1% agarose gel), RNA was reverse transcribed using a Maxima First Strand cDNA Synthesis Kit (Thermo Scientific). qPCR amplification was performed using either an ABI StepOne System or QuantStudio 5 using TaqMan Universal Master Mix II (Applied Biosystems) and TaqPath qPCR Master Mix, CG (Applied Biosystems) respectively.
The following TaqMan assays were used (all Life Technologies):

- TRPM7 (Rn01328216m1)
- Slc9a1/NHE1 (Rn00561924_m1)
- Slc4a2/AE2 (Rn00566910_m1)
- Slc4a4/NBCe1 (Rn00584747_m1)
- Slc26a4/pendrin (Rn00693043_m1)
- CFTR (Rn01455971_m1)
- Klk4 (Rn01498536_m1)
- Cldn1 (Rn00581740_m1)
- Cldn4 (Rn01196224_s1)
- Cldn8 (Rn01767199_s1)
- Tjp1/ZO-1 (Rn02116071_s1)

For internal control acidic ribosomal protein P0 (RPLP0; Rn00821065_g1) was used; each sample was measured in technical triplicates. To calculate elative fold changes the comparative Ct method ($2^{-\Delta\Delta CT}$) was used.

3.3 Immunohistochemistry

HAT-7 cells were fixed using a solution of 95% ethanol and 5% acetic acid. Hemimandibles were removed from 6-week-old C57BL/6 mice and fixed in 4% paraformaldehyde, demineralized with 8% EDTA, embedded in paraffin, and sectioned at a thickness of 5 μm. Following blocking with GeneTex Trident Universal protein blocking reagent, the tissue sections were incubated overnight at 4°C with the primary antibody - Abcam rabbit anti-TRPM7 (ab262698) at a 1:300 dilution. Subsequently, the slides were incubated for 1 hour at room temperature with the secondary antibody, FITC-

conjugated goat anti-rabbit IgG (Invitrogen, 1:400 dilution). Nuclear counterstaining was performed using 1 μg/ml Hoechst 33342 (Sigma) for 5 minutes at room temperature. As a negative control, non-specific rabbit IgG was applied. Imaging was carried out using a Leica TCS SP5 (Leica) confocal microscope.

3.4 Electrophysiology

Voltage-clamp recordings were performed using the standard whole-cell configuration with an Axopatch 200B amplifier (Axon Instruments). Micropipettes were fabricated from borosilicate glass capillaries (Harvard Apparatus) using a P-97 Flaming-Brown micropipette puller (Sutter Instrument). When filled with internal solution, pipettes had a tip resistance of 3–6 MΩ. The internal (pipette) solution contained (in mM): 120 $CsCH_4SO_4$, 20 NaCl, 10 HEPES, 2 EGTA, and 0.9 $MgCl_2$, adjusted to pH 7.2 with NaOH. In specific experiments, the intracellular Mg^{2+} concentration was modified to either 3.6 mM or approximately 0 mM (nominally Mg^{2+}-free). The standard external (bath) solution consisted of (in mM): 140 NaCl, 2.8 KCl, 1 $CaCl_2$, 1 $MgCl_2$, 10 HEPES, and 11 D-glucose, adjusted to pH 7.3. Solutions were delivered via continuous perfusion at 3 ml/min. When pharmacological agents were applied, recordings were taken after full exchange of the bath solution.

Whole-cell currents were recorded at a holding potential of –50 mV and during 30 ms voltage steps ranging from -100 mV to +100 mV in 20 mV increments, applied at 0.5 s intervals. Currents were corrected for pipette and whole-cell capacitance, as well as series resistance. Current-voltage relationships were constructed using stabilized current values measured 10 ms after the onset of each voltage step. To normalize for cell size, whole-cell currents were divided by membrane capacitance (typically 20–30 pF) and expressed as pA/pF. Leak subtraction was not applied, as baseline currents at the holding potential under unstimulated conditions remained below 0.5 pA/pF. Reversal potentials typically ranged from –50 to –55 mV.

Data acquisition and command protocols were managed using pClamp 11 software (Axon Instruments). Capacitative transients were compensated using analog settings, and series resistance was accepted if it remained below five times the pipette resistance. Data were analyzed using Clampfit 11 (Axon Instruments) and Microsoft Excel. All recordings were conducted at room temperature.

3.5 Ca^{2+} imaging

For unpolarized monolayer experiments, cells were cultured on coverslips for 2–3 days. In 3D culture experiments, spheroids were grown in Hepato-STIM medium for one week, then released from Matrigel using 0.25% Trypsin/EDTA and seeded at low density onto 25 mm coverslips pre-coated with 0.01% poly-L-lysine (Sigma-Aldrich). Cells or spheroids were incubated in a loading solution containing 4 µM fura-2 AM (Invitrogen), 0.08% F-127 (Sigma), and 1 mM probenecid (Invitrogen) in bath solution for 45–60 minutes at room temperature, followed by rinsing prior to calcium imaging. Coverslips were then mounted in a custom-built open perfusion chamber on an upright fluorescence microscope (Nikon TE600, Nikon) and continuously superfused with bath solution composed of (in mM): 137 NaCl, 5 KCl, 2 $CaCl_2$, 1 $MgCl_2$, 10 HEPES, and 10 glucose, adjusted to pH 7.4 with NaOH. For HAT-7 monolayer experiments, Mg^{2+} was excluded from the bath solution to eliminate its inhibitory effect on TRPM7 channel activity. In certain experiments, a nominally Ca^{2+}-free bath solution was used to assess the source of intracellular calcium ($[Ca^{2+}]_i$) responses.

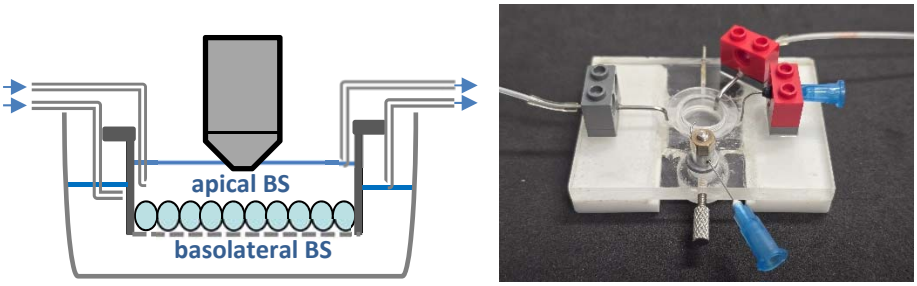

Figure 8. Custom made imaging chamber for Snapwell™ inserts

BS: bath soulution

In experiments involving HAT-7 cells cultured on Snapwell™ supports loading conditions were optimized to enhance fluorescence signal. Cells were incubated with 4 µM fura-2 AM, 0.08% F-127, and 1 mM probenecid in bath solution for 75–80 minutes at 37°C, followed by an additional 20–30 minutes in bath solution containing 1 mM probenecid at 37°C to allow de-esterification of the dye. All solutions were applied simultaneously to both the apical and basolateral sides. Probenecid was included to prevent rapid fura-2 efflux. The Snapwell™ inserts were then placed into a custom-built imaging chamber designed for separate perfusion of the apical and basolateral

compartments (Fig. 8) and mounted on the same fluorescence microscope described above.

Cells were illuminated alternately at 340 and 380 nm using a metal-halide lamp and an internal filter wheel (Prior Lumen 220 Pro). Imaging was conducted using either a cooled CCD camera (Retiga2000; QImaging) or an sCMOS camera (Prime BSI, Teledyne Photometrics), controlled via NIS AR software (Nikon), through a water-dipping objective (20x, NA 0.5, Nikon). The advantage of upright imaging is the reduction of background noise caused by membrane autofluorescence. Intracellular calcium changes were expressed as the ratio of fluorescence emitted at the two excitation wavelengths (F340/F380), normalized to baseline. Quantification was performed by selecting a region of interest (ROI) encompassing at least 50 cells.

3.6 Intracellular pH measurements

Real-time monitoring of intracellular pH changes was performed using microfluorometry with the pH-sensitive fluorescent dye BCECF, as previously described (77). In brief, cells cultured on coverslips were incubated with 4 μM BCECF-AM (Thermo Fisher Scientific) for 30 minutes. Following loading, coverslips were placed in a chamber mounted on a Nikon Eclipse TE200 (Nikon) inverted fluorescence microscope and continuously superfused at a rate of 3 ml/min with the same bath solution used in patch-clamp recordings. Fluorescence signals were recorded at 530 nm emission while alternating excitation wavelengths between 490 nm (pH-sensitive) and 440 nm (pH-insensitive), using a photomultiplier tube and amplifier system (Cairn Research). Data acquisition was controlled by DASYLab software (Measurement Computing), and the fluorescence ratio (F490/F440) was calculated every 5 seconds. Autofluorescence correction was applied at the end of each experiment by releasing intracellular BCECF with Triton X-100. The F490/F440 ratio values were then converted to pH using calibration data obtained via the high K^+/nigericin technique (77).

3.7 Statistical analysis

Data are expressed as mean ± SEM. Statistical significance was assessed using one-sample Student's t-tests, planned pairwise comparisons (paired or unpaired Student's two-sample t-tests), and one-way ANOVA followed by Dunnett's post hoc test. A p-value < 0.05 was considered statistically significant.

4. Results

4.1 TRPM7-mediated calcium transport in HAT-7 cells

4.1.1 TRPM7 expression in HAT-7 cells cultured as unpolarized monolayer

Quantitative gene expression analysis revealed that TRPM7 mRNA was highly upregulated in HAT-7 cells compared to other ion transporters and channels associated with amelogenesis, such as NHE1, CFTR, and pendrin (Fig. 9A). Immunostaining using a polyclonal antibody targeting the intracellular C-terminal region of human TRPM7 confirmed the presence of TRPM7 protein in HAT-7 cells (Fig. 9B). In vivo, TRPM7 exhibited a similar predominantly cytoplasmic localization in mouse maturation-stage ameloblasts (Fig. 9C).

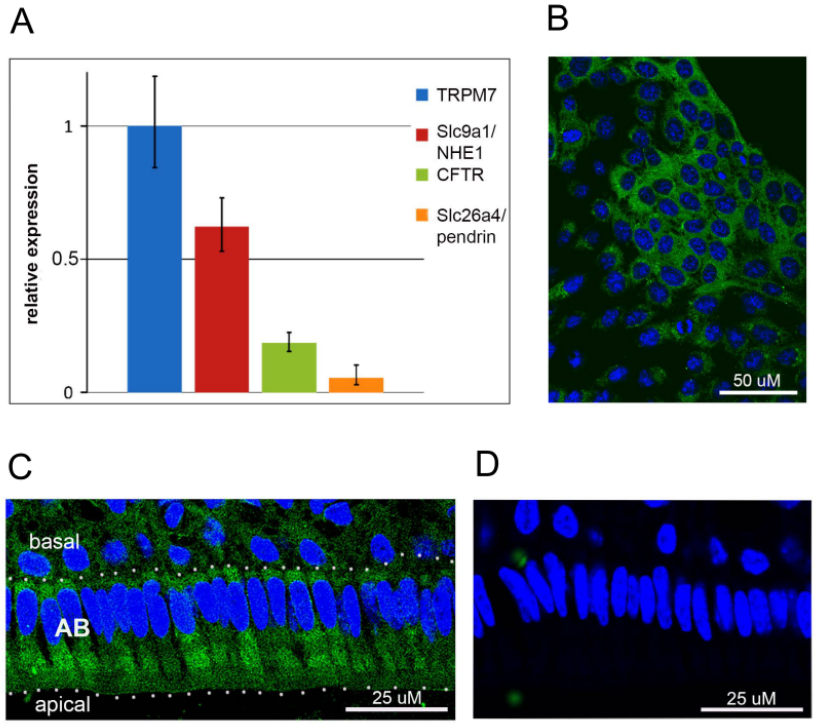

Figure 9. Expression of TRPM7 in HAT-7 cells and in mouse incisor. *A) mRNA expression levels of TRPM7, Slc9a1/NHE1, CFTR and Slc26a4/pendrin normalized to mean TRPM7 expression in HAT-7 cells. B, C) Immunostaining of TRPM7 protein (green) in HAT-7 cells grown on glass coverslips (B) and in maturation-stage ameloblasts (AB) from mouse incisor (C). D) Negative control staining using non-specific rabbit IgG in maturation-stage ameloblasts. Nuclei, blue. (207)*

4.1.2 Intracellular Ca^{2+} response to TRPM7 activators/inhibitors

To assess whether TRPM7 channels contribute directly to Ca^{2+} uptake in HAT-7 cells beyond their proposed role in modulating store-operated calcium entry pathways (135) ratiometric calcium imaging was used to directly measure intracellular Ca^{2+} responses. Cells were bathed a nominally Mg^{2+}-free extracellular solution to reduce competition between Mg^{2+} and Ca^{2+} for channel entry. Application of the TRPM7 activator naltriben (100 μM) resulted in a sustained and reversible increase in intracellular Ca^{2+} concentration ($[Ca^{2+}]_i$) of 32.6 ± 3.3% ($n = 9$, $p < 0.05$) (Figs. 10A & 10B). This increase was entirely eliminated in nominally Ca^{2+}-free extracellular environment, indicating that the rise in $[Ca^{2+}]_i$ was attributable to extracellular Ca^{2+} influx. Furthermore, co-application of the TRPM7 inhibitor NS8593 (20 μM) reduced the naltriben-induced $[Ca^{2+}]_i$ response by 56% ($n = 5$, $p < 0.01$) (Figs. 10A & 10B).

In a separate set of experiments, stimulation with a different TRPM7 activator, mibefradil (50 μM) increased $[Ca^{2+}]_i$ by 52 ± 5% ($n = 12$, $p < 0.05$) (Figs. 10C & 10D). Unlike naltriben, this response was only partially reduced by ~60% to 20 ± 2% ($n = 6$, $p < 0.004$) in a nominally Ca^{2+}-free extracellular solution, suggesting a partial involvement of intracellular store release (Figs. 10C & 10D). Depletion of intracellular Ca^{2+} stores with SERCA inhibitor thapsigargin (100 nM) completely abolished the mibefradil-induced $[Ca^{2+}]_i$ increase and even led to a transient decrease of 1.8 ± 0.2% below baseline ($n = 4$, $p < 0.05$) (Figs. 10C & 10D).

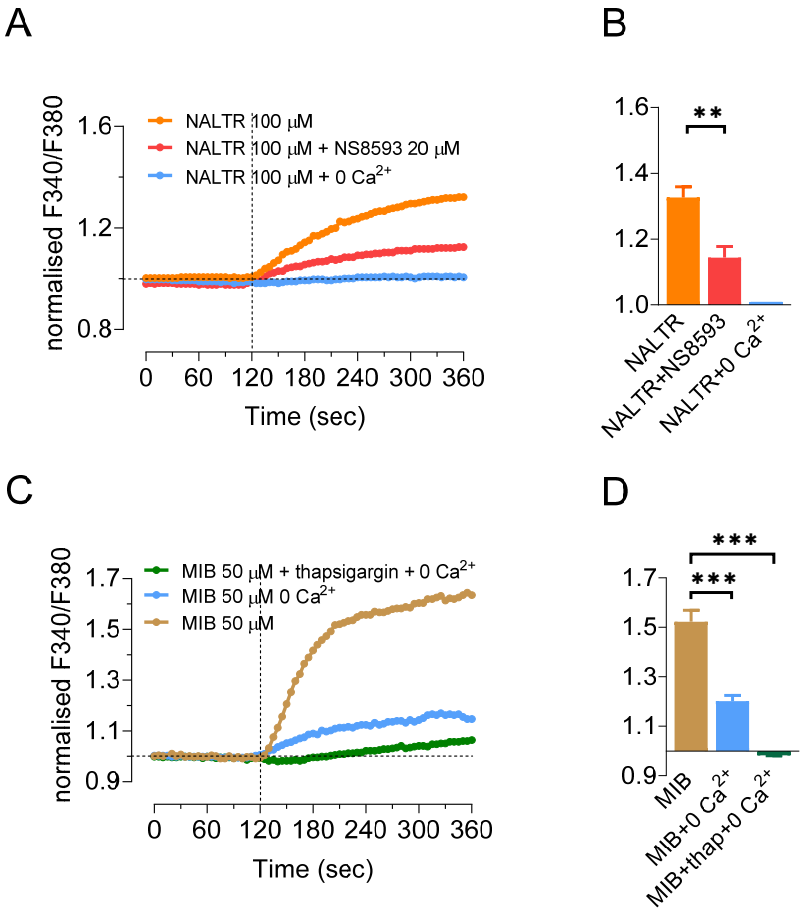

Figure 10. Changes in intracellular Ca^{2+} in response to TRPM7-specific activators and inhibitors. *A, B) $[Ca^{2+}]_i$ responses evoked by naltriben (100 μM, applied at 120 s) in the presence (n = 9) and absence of extracellular Ca^{2+}, and in the presence of 20 μM NS8593 (applied at 0 s, n = 5). C, D) $[Ca^{2+}]_i$ responses evoked by mibefradil (50 μM, applied at 120 s) in the presence (n = 12) and absence (n = 6) of extracellular Ca^{2+}, and following pretreatment with 100 nM thapsigargin (n = 4). Ca^{2+} was present in the bath solution unless the legend states otherwise. Data are presented as representative traces of changes in fura-2 fluorescence ratio normalized to baseline, and as mean peak values ± SEM (** p<0.01, *** p<0.001). (207)*

4.1.3 TRPM7-like ion currents in HAT-7 cells

A well-established electrophysiological feature of TRPM7 channels is an outwardly rectifying cation current - typically recorded as a Cs^+ current - which is enhanced by depletion of intracellular Mg^{2+} (103,110). Whole-cell patch-clamp recordings from HAT-7 cells, conducted under conditions designed to suppress other ionic currents, revealed a modest outwardly rectifying current (4.7 ± 0.14 pA/pF at +80 mV, n = 14) when the intracellular pipette solution contained a physiological Mg^{2+} concentration (0.9 mM).

Increasing intracellular Mg^{2+} to 3.6 mM led to a statistically significant reduction in current amplitude (3.6 ± 0.2 pA/pF at +80 mV, n = 14, $p < 0.05$). In contrast, complete removal of Mg^{2+} from the intracellular solution caused a pronounced, approximately six-fold increase in current (29.8 ± 2.4 pA/pF at +80 mV, n = 14, $p < 0.0001$).

Additional evidences were gathered using two established TRPM7 inhibitors: NS8593 (132) and FTY720 (137) which were tested on the Mg^{2+}-depletion-induced currents. In the absence of intracellular Mg^{2+}, application of 20 μM NS8593 reduced the current measured at +80 mV by approximately 60%, from 26.1 ± 3.0 to 10.4 ± 1.8 pA/pF (n = 5, $p < 0.05$) while treatment with 2 μM FTY720 produced an even greater inhibition, reducing the current by 90% (from 31.4 ± 5.2 to 3.4 ± 0.8 pA/pF, n = 5, $p < 0.001$).

The stimulatory effects of mibefradil (149) and naltriben (141), were also tested: under physiological intracellular Mg^{2+} conditions (0.9 mM). Application of extracellular mibefradil (50 μM) led to an approx. tenfold increase in outward current, rising from 4.0 ± 0.4 to 41.5 ± 9.7 pA/pF at +80 mV (n = 5, $p < 0.05$). Increasing the intracellular Mg^{2+} concentration to 3.6 mM significantly attenuated this mibefradil-induced current by approx. 75%, reducing it to 10.4 ± 3.6 pA/pF (n = 4, $p < 0.05$).

Application of 50 μM naltriben also significantly enhanced the outward current at +80 mV, increasing it from 2.7 ± 0.3 to 26.7 ± 3.5 pA/pF (n = 4, $p < 0.0001$). This naltriben-induced current was largely suppressed by the TRPM7 inhibitor NS8593 (20 μM), which reduced the current by approx. 80% to 5.2 ± 0.8 pA/pF (n = 4, $p < 0.05$).

4.1.4 Effect of SOCE inhibiton on Ca^{2+} response triggered by different TRPM7 activators

Souza Bomfim et al. (135) have recently suggested the involvement of store-operated calcium entry in TRPM7 activation-induced Ca^{2+} influx. Thus, responses to the TRPM7 activators were also investigated in the presence of the SOCE inhibitor BTP2 (208).

To assess SOCE activity, HAT-7 cells were pretreated with thapsigargin in a calcium-free extracellular solution to deplete ER calcium stores and the effect of extracellular Ca^{2+} repletion was then measured in the presence and absence of BTP2. Pretreatment (20 μM for 45 minutes) with and continuous application of BTP2 in the perfusate effectively inhibited SOCE-mediated calcium influx in unstimulated cells - resulting in a 92% reduction (n = 3, $p < 0.001$) (Figs. 11A & 11B).

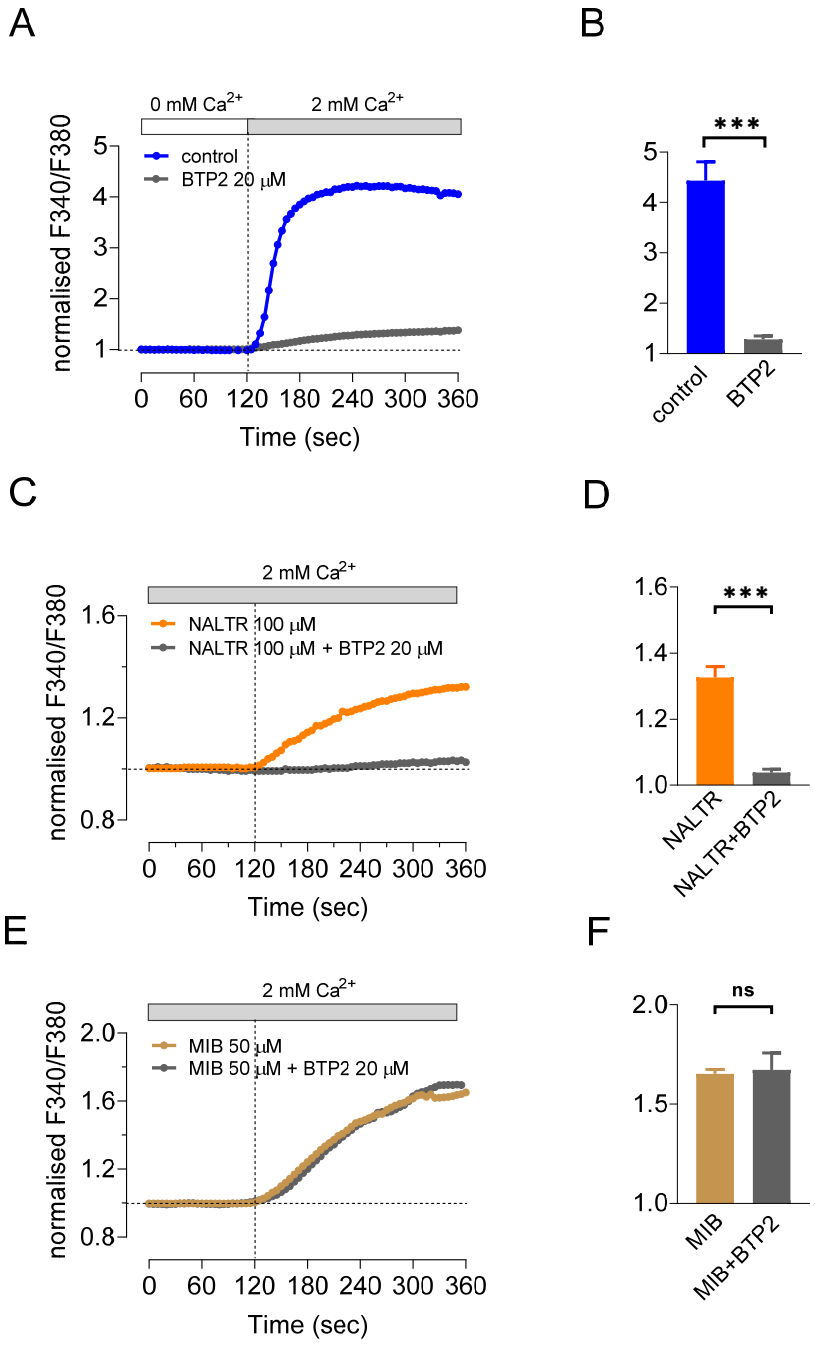

Figure 11. Changes in intracellular Ca^{2+} in response to TRPM7 activators and the SOCE inhibitor BTP2. *$[Ca^{2+}]_i$ responses resulted by repletion of extracellular Ca^{2+} in ER store-depleted cells (thapsigargin pretreatment, 100 nM, 20 min in Ca^{2+}-free bath solution), in the presence (n = 3) and absence of BTP2 (20 µM, applied at 0 s, n = 3) (A, B). $[Ca^{2+}]_i$ responses elicited by naltriben (100 µM, n = 4) (C, D) and mibefradil (50 µM, n = 5) (E, F) applied at 120 s in the presence and absence of BTP2 (20 µM, applied at 0 s). Data are presented as representative traces of changes in fura-2 fluorescence ratio normalized to baseline, and as mean peak values ± SEM (*** p<0.001). (207)*

We then evaluated the impact of BTP2 on Ca^{2+} influx triggered by naltriben (100 μM) and mibefradil (50 μM) in the absence of prior ER store depletion. Under normal extracellular Ca^{2+} conditions, naltriben-induced Ca^{2+} influx was almost completely abolished by BTP2, showing an 88% reduction ($n = 4$, $p < 0.001$) (Figs. 11C & 11D). In contrast, the Ca^{2+} influx elicited by mibefradil was completely unaffected by BTP2 ($n = 5$) (Figs. 11E & 11F). These findings indicate that naltriben-induced Ca^{2+} entry is largely dependent on the SOCE pathway, whereas mibefradil-induced Ca^{2+} influx more likely occurs directly through the TRPM7 channel itself.

4.1.5 Effect of pH on TRPM7 currents and Ca^{2+} influx

During enamel maturation, hydroxyapatite crystal formation generates large amounts of protons, and a cyclic acidification of the enamel matrix is observed (19,29,209). Therefore, we have also investigated the pH sensitivity of the observed TRPM7-related $[Ca^{2+}]_i$ responses and currents.

Whole-cell recordings from HAT-7 cells showed that lowering extracellular pH to 4.3 led to a seven-fold increase in outward current, from 6.6 ± 0.7 to 48.2 ± 4.6 pA/pF at +80 mV ($n = 4$, $p < 0.05$). This acidification-induced current was reduced by about half in the presence of the TRPM7 inhibitor FTY720 (2 μM), decreasing to 21.8 ± 1.3 pA/pF ($n = 4$, $p < 0.05$ vs. pH 4.3). A milder acidification from pH 7.3 to 6.3 - comparable to physiological conditions in maturation-stage ameloblasts - also caused a small but significant increase in current, from 4.3 ± 0.2 to 6.6 ± 0.6 pA/pF at +80 mV ($n = 5$, $p < 0.05$).

Furthermore, we have also tested the effects of both extracellular acidification and alkalization on $[Ca^{2+}]_i$ (Fig. 12A). Acidification to pH 6.9 resulted a mild, but highly significant decrease in $[Ca^{2+}]_i$ (10 ± 1.6%, $n = 8$, $p < 0.001$), while a mild alkalinization (pH 7.9) increased the $[Ca^{2+}]_i$ by 33 ± 8% ($n = 5$, $p < 0.05$). However, such changes in the extracellular millieau did not alter the mibefradil-triggered $[Ca^{2+}]_i$ responses (Fig. 12A).

Since cytosolic acidification disrupted the stability of the membrane-glass seal, we were unable to study the effect of intracellular acidification on TRPM7 currents using whole-cell recording. Hence, we were able to assess the pH sensitivity of TRPM7-mediated Ca^{2+}

influx using the ammonium prepulse technique, a well-established method of intracellular pH manipulation.

Application of 20 mM NH_4Cl for 2 minutes induced a transient intracellular alkalinization, followed by rapid acidification upon NH_4^+ withdrawal, as demonstrated by real-time BCECF fluorescence measurements (Fig. 12C). To prevent proton extrusion via Na^+/H^+ exchange, extracellular Na^+ was subsequently replaced with the impermeant cation $NMDG^+$, leading to a sustained intracellular acidification to approximately pH 6.4 (Fig. 12C). In separate calcium imaging experiments under the same conditions the NH_4^+-induced alkalinization caused a 35 ± 4.2% increase in $[Ca^{2+}]_i$ ($n = 9$, $p < 0.05$), which was abolished in a nominally Ca^{2+}-free extracellular solution (data not shown). The ensuing intracellular acidification triggered a modest but significant decrease in $[Ca^{2+}]_i$ of 12 ± 2% ($n = 6$, $p < 0.05$).

When applied under the intracellular acidification phase, both mibefradil (50 μM) and naltriben (100 μM) significantly enhanced the TRPM7-mediated Ca^{2+} influx beyond what was observed at normal pH_i. Specifically, mibefradil increased $[Ca^{2+}]_i$ by 78 ± 3.9% at low pH_i, compared to the 43 ± 6% measured at normal pH_i resulting an 81% relative increase ($n = 6$, $p < 0.05$) (Fig. 12D). Similarly, naltriben induced a 46 ± 16% relative increase in Ca^{2+} influx under acidic conditions ($n = 5$, $p < 0.05$), suggesting that intracellular protons potentiate TRPM7 activation. In this context it is important to note that changes in extracellular pH from 7.3 to 6.3 - mimicking physiological fluctuations at the apical surface of ameloblasts - can also cause a moderate and reversible intracellular acidification of 0.38 ± 0.032 pH units after 10 minutes ($n = 6$, $p < 0.05$), as measured by BCECF fluorescence (Fig. 12B).

In summary, these findings demonstrate functional TRPM7 channels in HAT-7 ameloblasts and suggest that, beyond modulating SOCE, TRPM7 may potentially act as a pH-sensitive pathway for Ca^{2+} uptake.

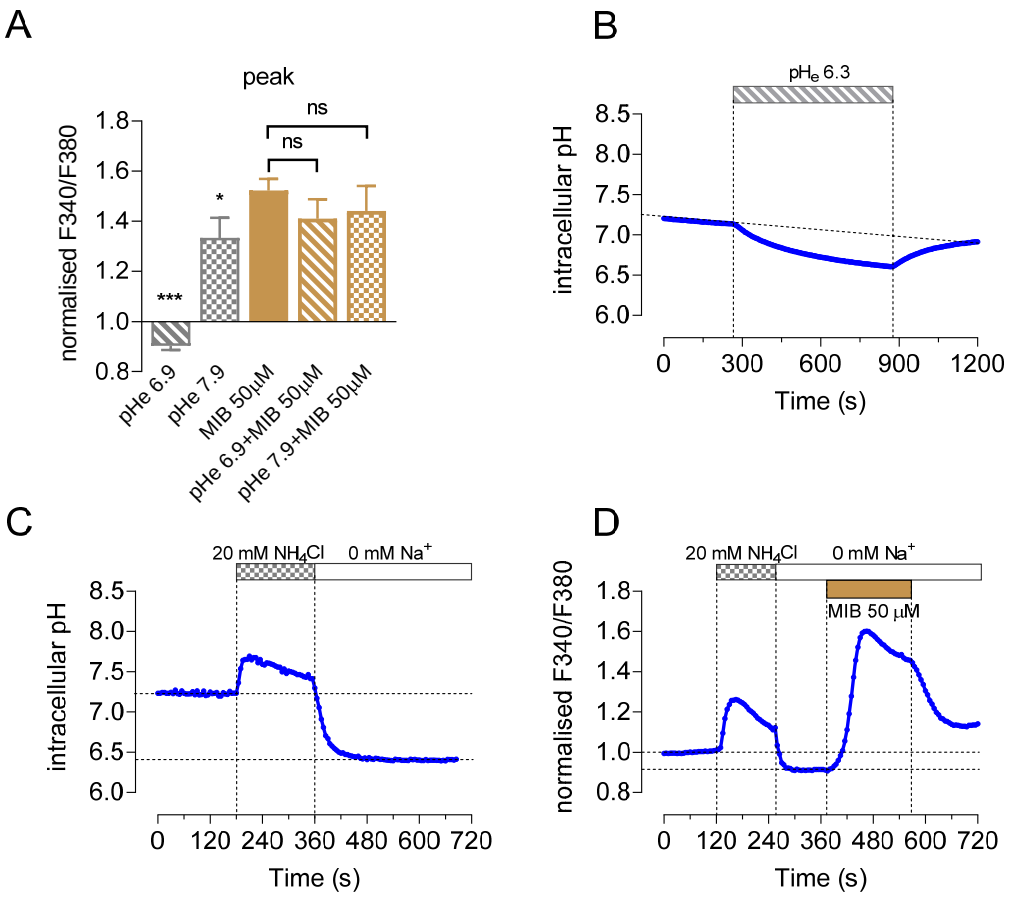

Figure 12. Effects of extra- and intracellular acidification on TRPM7-related ion currents and Ca^{2+} influx. *A) $[Ca^{2+}]_i$ responses to extracellular pH changes and mibefradil (50 µM) (fura-2 fluorescence ratio normalized to baseline, presented as mean peak values ± SEM; pH_e 6.9 n=8, pH_e 7.9 n=5, MIB 50 µM n=12, pH_e 6.9 + MIB 50 µM n=6, pH_e 6.7 + MIB 50 µM n=5, *** $p < 0.001$; * $p < 0.05$); B) Effect of extracellular acidification (pH 6.3) on intracellular pH measured by microfluorometry (BCECF, representative trace) C) Intracellular pH changes in response to an NH_4Cl pulse (20 mM) and a subsequent extracellular Na^+ removal measured by microfluorometry (BCECF, representative trace). D) Mibefradil-evoked Ca^{2+} response in acidic intracellular conditions measured by Ca^{2+} imaging (fura-2, representative trace; data are presented as changes in fura-2 fluorescence ratio normalized to baseline). (modified from (207))*

4.1.6 Polarization of TRPM7 activity in HAT-7 cells

To determine the functional polarization of TRPM7 channels, we used HAT-7 cells cultured on Transwell membranes under differentiating conditions as previously reported

by Bori et al (77). For calcium imaging experiments a custom-made chamber was constructed (Fig. 8), that enabled the separate perfusion of apical and basolateral surfaces of Snapwell™ inserts under an upright fluorescent microscope.

Similarly, to previous experiments, fura-2 ratiometric calcium imaging was used to directly measure intracellular Ca^{2+} responses. Mibefradil (50 µM) was applied separately either on the apical or on the basolateral side. Stimulation on the apical side increased $[Ca^{2+}]_i$ by 20.1 ± 1.8% (n = 4, $p < 0.002$) (Figs. 13A & 13B), while no significant increase was observed by basolateral application suggesting that TRPM7 channels are functionally present primarily on the apical side (apical v. basolateral, n=4, $p < 0.001$).

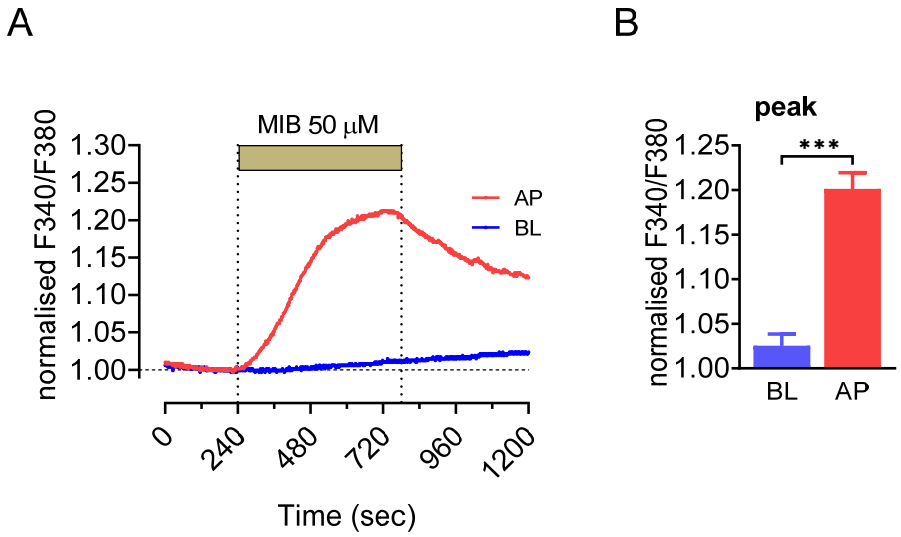

Figure 13. Changes in intracellular Ca^{2+} in response to polarized application of TRPM7 activator *A, B) $[Ca^{2+}]_i$ responses evoked by mibefradil (50 µM, applied either apically (AP, n=4) or basolaterally (BL, n=4) Data are presented as representative traces of changes in fura-2 fluorescence ratio normalized to baseline, and as mean peak values ± SEM (*** p<0.001, unpaired t-test).*

4.2 Purinergic and cholinergic signalization in 3D cultured HAT-7 cells

4.2.1 3D culture of HAT-7 cells

Cells suspension (Hepato-STIM media) of HAT-7 cells were mixed with Matrigel matrix and seeded in low-attachment plate wells. Spheroid development was monitored over a period of two weeks. After three days of culture a multicellular spherical appearance was observable and many spheroids reached 100 µm in diameter within one week (210). Interestingly, further prolongation of culturing period resulted in signs of disintegation.

For further experiments, spheroids grown for one week in Hepato-STIM media were used.

4.2.2 Transporter expression profile of HAT-7 cells in 3D culture

RNA expression levels of several tight junction proteins (claudin 1, 4, 8, and ZO-1), electrolyte transporters (NHE1, AE2, NBCEe1, pendrin, CFTR) as well as maturation-stage ameloblast marker KLK4 were compared between 2D monolayer and 3D culture conditions. *KLK4* had the highest expression level in spheroids, also the increase was approximately 70-fold compared to the monolayer culture. Spheroid cultures showed significant downregulation of tight junction proteins claudin-1, claudin-4, and ZO-1, with a concomitant increase in claudin-8. Among HCO_3^- transporters, pendrin (*SLC26A4*) and *CFTR* were significantly reduced, while minor decreases in *NHE1*, *AE2*, and *NBCe1* expressions were not statistically significant.

4.2.3 Intracellular calcium responses to purinergic and cholinergic stimuli

Previous studies have shown that electrolyte secretion of HAT-7 cells in 2D culture is activated by agonists known to mediate their effects by elevating intracellular cAMP and Ca^{2+}, such as forskolin and ATP, respectively (77). To test the presence of purinergic signalization in the spheroids, we measured the intracellular Ca^{2+} concentration $[Ca^{2+}]_i$ in response to purinergic agonists ATP (50 μM) and UTP (50 μM). Both ATP and UTP induced similar biphasic Ca^{2+} responses consisting of an initial transient peak and a sustained component provided that external Ca^{2+} (2 mM) was present. The absence of external Ca^{2+}, however, resulted only in transient Ca^{2+} responses for both agonists, suggesting that a Ca^{2+} influx from the extracellular space caused the sustained component (Figs. 14A-C). Since UTP does not stimulate ionotropic P2X receptors, we speculate that Ca^{2+} entry was due store-operated Ca^{2+} channels (SOCCs) activated by the depletion of intracellular Ca^{2+} stores.

Acetylcholine (ACh) has been reported to evoke $[Ca^{2+}]_i$ increase in freshly isolated rat ameloblasts (63). In our experiments, however, ACh analog, carbachol (100 μM), did not elicit $[Ca^{2+}]_i$ reponse (Fig. 14D) suggesting that neither muscarinic nor nicotinic functional ACh receptors are expressed in HAT-7 spheroids.

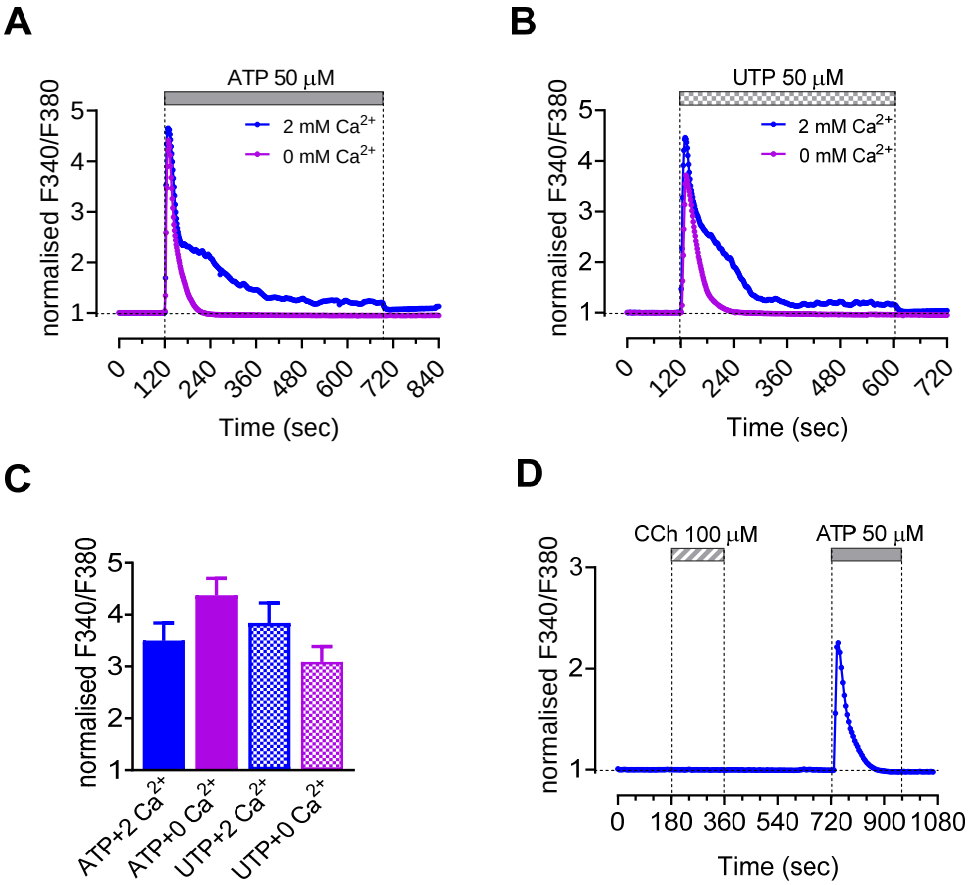

Figure 14. Intracellular Ca^{2+} responses of HAT-7 spheroids to different purinergic agonists and charbachol *(A-C) Changes in $[Ca^{2+}]_i$ in response to 50 μM ATP (n = 5) and 50 μM UTP (n = 3) in the presence and absence of extracellular calcium. Peak values (C) presented as means ± SEM (no significant difference). (D) Effect of carbachol (100 μM, n = 3) on $[Ca^{2+}]_i$. A subsequent ATP stimulus was introduced to test the responsiveness of the spheroids. Panels show representative traces. Data are presented as changes in fura-2 fluorescence ratio normalized to baseline. (210)*

5. Discussion

5.1 TRPM7-mediated calcium transport in HAT-7 cells

Our studies demonstrate abundant TRPM7 expression in HAT-7 cells at both mRNA and protein levels. These findings align with previous reports demonstrating high TRPM7 expression in ameloblasts and odontoblasts compared to other tissues (71), and a progressive increase in TRPM7 expression during ameloblast differentiation toward the maturation stage (72). Considering the recent classification of TRPM7 as a functional intracellular TRP channel (107), its predominant cytoplasmic localization is not suprising.

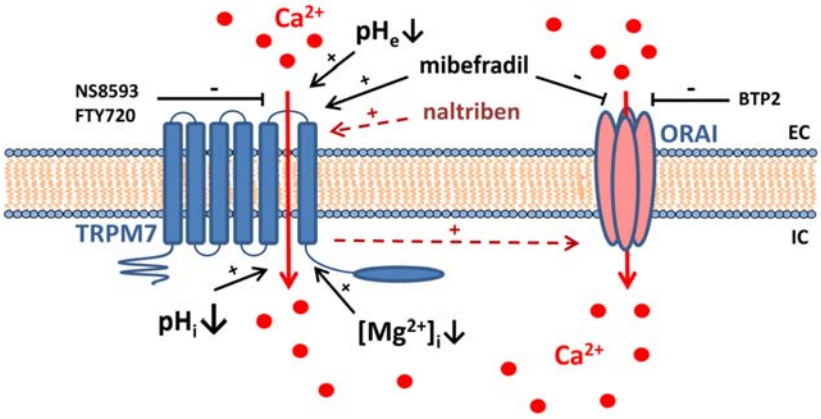

Figure 15. Proposed model for TRPM7-mediated Ca^{2+} entry in HAT-7 cells (207)

Transcellular Ca^{2+} transport towards the enamel space by ameloblasts requires Ca^{2+} uptake at the basolateral membrane to offset apical efflux. Similarly to what was reported in other cell types (133,140), TRPM7 activators significantly enhanced $[Ca^{2+}]_i$ in HAT-7 cells. Naltriben (141) induced a pronounced rise in $[Ca^{2+}]_i$, which was abolished in Ca^{2+}-free conditions, suggesting a potential role for TRPM7 in Ca^{2+} influx. However, the practically complete inhibition of this response by the SOCE blocker BTP2 indicates the involvement of ORAI channels, consistent with previous findings by Souza Bomfim et al. (Fig. 15) (135).

Our results are in line with studies in genetically modified mouse reporting distinct roles for the channel and kinase functions of TRPM7 in hard tissue mineralization (72). In the *Trpm7* $^{\Delta kinase/+}$mouse model, created by replacing exons 32–36 with a Neo cassette, reduced Mg^{2+} transport to bone (159) and enamel matrix (72) was observed, reflecting impaired TRPM7 channel function. Notably, mineralization defects in these mice were

more severe than in mice harboring a point mutation (TRPM7-KR) in the kinase domain with preserved channel activity (71). These findings suggest that TRPM7 contributes not only to SOCE-related Ca^{2+} transport but may also directly mediating Ca^{2+} influx through its channel function.

Another TRPM7 activator mibefradil (149), that is also a known blocker of voltage-gated Ca^{2+} channels, similarly triggered an increase in $[Ca^{2+}]_i$. Notably, this mibefradil-induced Ca^{2+} influx was unaffected by the SOCE inhibitor BTP2, suggesting that TRPM7 may mediate a Ca^{2+} entry pathway independent of store-operated mechanisms (Fig. 15). Furthermore, our results indicate that mibefradil not only promotes Ca^{2+} influx from the extracellular space but also mobilizes Ca^{2+} from intracellular stores. These findings are highly consistent with a recent report proposing that mibefradil elevates $[Ca^{2+}]_i$ via a phospholipase C-IP_3 receptor (PLC-IP_3R)-mediated signaling pathway (150). Additionally, we found that mibefradil caused a slight decrease in $[Ca^{2+}]_i$ in cells pre-treated with thapsigargin. This aligns with recent findings in endothelial and HK-2 epithelial cells, where mibefradil was shown to reduce ER Ca^{2+} leak following SERCA inhibition (211).

In our patch-clamp experiment performed in whole-cell configuration, depleting intracellular Mg^{2+} in HAT-7 cells triggered outward currents that were suppressed by established TRPM7 inhibitors NS8593 (132) and FTY720 (137), consistent with the known characteristics of TRPM7 (133,212). These findings further support the presence of functionally active TRPM7 channels in HAT-7 cells. The TRPM7 activators naltriben and mibefradil elicited similar outward currents, which were substantially attenuated by NS8593 and elevated intracellular Mg^{2+}. Notably, the extracellular solution in our experiments contained divalent cations, which likely prevented the inward currents commonly reported under divalent-free conditions (133,212).

Chubanov et al. suggested that two distinct types of TRPM7 activators exist: type 1 activators like naltriben, which stimulate the channel independently of intracellular Mg^{2+} levels, and type 2 activators like mibefradil, which are effective primarily under conditions of low intracellular Mg^{2+} (127). When intracellular Mg^{2+} is depleted, TRPM7 may operate as a divalent cation-permeable channel, a role that mibefradil appears to mimic. Faouzi et al. proposed that TRPM7-mediated Ca^{2+} influx is critical for maintaining ER Ca^{2+} stores in resting lymphocytes and for their replenishment following

Ca^{2+} signaling (98). They also emphasized the importance of TRPM7 kinase domain in regulating SOCE, a mechanism that may extend to ameloblasts. Also, in splenocytes of kinase-inactive mutant (TRPM7 KR) mice, SOCE was enhanced under resting conditions but suppressed upon activation (213).

Souza Bonfim et al. have recently advocated, that the $[Ca^{2+}]_i$ rise in response to mibefradil is the result of ER store release through the PLC-IP_3R signalization. In our experiments, the ER release related $[Ca^{2+}]_i$ component of mibefradil-triggered response was relatively small and inhibition of SOCE by BTP2 did not modulate the effect of mibefradil, suggesting the presence of a store-independent mechanism (Fig. 15). It is important to note that BTP2 largely inhibits ORAI1 and ORAI2 isoform (214) and ameloblast cells have shown to express also considerable amount of ORAI3, especially in maturation stage (35). However, further research is needed to clarify the seemingly different mechanisms by which naltriben and mibefradil exert their effects on $[Ca^{2+}]_i$ (Fig. 15).

Overall, these data suggest a complex, but rather unclear relationship between TRPM7 channel and the store-operated calcium entry. Similar connection was reported for other members of the TRPM family (215). Most authors hypothesize, that TRPM7 can modulate SOCE, primarily through indirect mechanisms such as phosphorylation of SOCE components via its enzymatic domain or by promoting mitochondrial Ca^{2+} accumulation (98,135,213,215).

Hydroxyapatite crystal formation during enamel matrix mineralization yields a substantial amount of protons, resulting in extracellular acidification (19,29,209). To promote enamel maturation, ameloblasts neutralizes this acidity through the coordinated activity of multiple acid-base transporters (19,29,77). Thus, local pH fluctuations are likely to modulate both Ca^{2+} uptake and secretion by ameloblasts.

TRPM7 channels are known to respond to both intra- and extracellular pH changes (108,110). In our study, extracellular acidification enhanced outward currents but had no effect on inward currents. By contrast, in HEK-293 cells overexpressing TRPM7, acidification increased both current directions (108). Notably, that study was conducted in the absence of extracellular Mg^{2+}, thus the lack of proton-induced inward currents in HAT-7 cells is potentially attributable to the presence of physiological Mg^{2+} levels in our experimental conditions.

In calcium imaging experiments of intact cells, the acidification of the extracellular millieau to pH 6.9 did not increase the mibefradil-evoked $[Ca^{2+}]_i$ response. This may be due to the mild pH decrease having little effect on Ca^{2+} influx. Alternatively, slight increase in Ca^{2+} entry was outweighed by significant stimulation of Ca^{2+} efflux. The latter would be consistent with the observed decrease of $[Ca^{2+}]_i$ in response to decreased pH_e. PMCA is potential mediator of this process since it extrudes Ca^{2+} ions against its electrochemical gradient in exchange of protons (42). Recently, Bonfim et al. reported a similar observation of PMCA-mediated $[Ca^{2+}]_i$ modulation in response to pH_e changes in primary culture of secretory and maturation ameloblasts (47).

We speculated that during enamel formation cyclical changes in extracellular pH at the apical membrane might potentially modulate Ca^{2+} uptake through basolateral TRPM7 channels in ameloblasts by influencing the intracellular pH. Indeed, in our experiments, extracellular pH of 6.3 – similar to what was observed in the apical surface of ameloblasts - caused a moderate and reversible intracellular acidification. Similar effect of extracellular pH was observed in rabbit lens epithelial cells (216). While direct electrophysiological assessment of intracellular pH effects was not feasible, our ammonium pulse experiments showed that intracellular acidification significantly enhanced Ca^{2+} influx triggered by both naltriben and mibefradil. Although this observation seems to contradict earlier findings that cytosolic acidification inhibits TRPM7 currents in Mg^{2+} -free conditions (100,106,110), it may be explained by the shared inhibitory site for protons and Mg^{2+} on TRPM7 (110). We hypothesize that, in intact cells, acidification reduces Mg^{2+} -mediated inhibition, thereby activating TRPM7 and promoting Ca^{2+} entry, whereas in Mg^{2+} -free patch-clamp conditions, proton binding alone suppresses channel activity. However, in a recent report NSAID-induced cytosolic acidification reversibly inhibited TRPM7 currents also in the presence of intracellular Mg^{2+} (217). It is also worth noting, that intracellular acidification protocol itself may also influence free $[Ca^{2+}]_i$ in intact cells. This can occur through reduced Ca^{2+} efflux due to the removal of extracellular Na^+, particularly in cells expressing Na^+/Ca^{2+} exchangers (49). Additionally, a drop in intracellular pH may alter the free intracellular levels of Ca^{2+} and Mg^{2+} by modulating their intracellular buffering by proteins (34) or ATP (218,219).

Our findings support the presence of functional TRPM7 channels in HAT-7 ameloblast cells, which may contribute to Ca^{2+} uptake depending on both intra- and extracellular pH

(Fig. 15). Based on data presented above, it was reasonable to assume that TRPM7 may play a role in the transport of divalent cations during amelogenesis, potentially as a distinct, pH-sensitive Ca^{2+} entry pathway on the basolateral membrane of the ameloblasts. To further elaborate this theory, we performed a series of calcium imaging experiments on HAT-7 cells cultured as polarized monolayer (77) using a custom-made chamber that enabled us to apply the activators/inhibitors to the apical or basolateral side separetly. In our experiments, mibefradil-elicited $[Ca^{2+}]_i$ response was only observable by the apical administration, suggesting a functional polarization of TRPM7 to the apical membrane. The precise subcellular localization of TRPM7 is still unclear. Most studies using immunfluorscent techniques observed strong cytoplasmic TRPM7 staining. More recently, TRPM7 has been shown to be abundantly present in intracellular vesicles as well (107). The role of TRPM7 in amelogenesis is not well understood. It is ubiquitously expressed throughout the body, and homozygous deletion of its kinase domain results in embryonic lethality (161). In the heterozygous kinase deleted mice model, reduced Mg^{2+} transport to both bone (159) and enamel matrix (72) was observed, reflecting the impaired TRPM7 channel function. In mice harboring a point mutation in the kinase domain with preserved channel activity, the mineralization defects were the less severe (71). It is also speculated that TRPM7 may be involved in Mg^{2+}/Ca^{2+} uptake that is required for the proper function of tissue-nonspecific alkaline phosphatase (APLP) (72). A recent study using epithelial cell–specific conditional TRPM7 knockout mice (173) reported defective enamel mineralization, characterized by reduced calcium and phosphorus levels but unchanged magnesium content in the enamel matrix - pointing to a more significant role for TRPM7 in calcium-related processes. However, the observed predominantly apical TRPM7 activity suggests that TRPM7 is unlikely to directly mediate transcellular Ca^{2+} transport during amelogenesis in our polarized HAT-7 ameloblast model.

We used an ameloblast-like cell line model for the amelogenesis related transport processes. Such model system harbors many known limitations including the discrepancies between cellular environments *in vitro* and *in vivo* (e.g. cell-cell, cell-matrix interactions), the alterations between the gene expression in primary and immortalized cells and the genetic drift during the consecutive passaging (191) that also constrains the validity of our conclusions. Although we believe that, these findings may contribute to the understanding of calcium transport during enamel formation. Nonetheless, further

studies are warranted to better perceive the role of ameloblasts in ion transport during amelogenesis.

5.2 Purinergic and cholinergic signalization in 3D cultured HAT-7 cells

To support the growth of HAT-7 cells in a 3D configuration, we employed Hepato-STIM medium supplemented with fetal bovine serum. This specialized medium is known to help maintain epithelial cell characteristics (220-222). Although initially developed for hepatocyte culture, Hepato-STIM has also been successfully applied to the growth of primary human salivary epithelial cells and lacrimal acinar cells (223).

We also used Matrigel as a scaffold to induce and promote spheroid formation by HAT-7 cells. Matrigel is a basement membrane derivative extracted from Engelbreth–Holm–Swarm mouse sarcoma cells, used extensively to establish spheroid and organoid cultures from various epithelial tissues including intestinal epithelial cells (224), pancreas (225,226), lacrimal glands (223,227) and salivary glands (204,220,228).

Matrigel's effect is thought to rely on of three key factors: i) it provides anchoring molecules, such as the Arg-Gly-Asp (RGD) sequence, which facilitate cell adhesion ii) it possesses an optimal stiffness that supports cell encapsulation and structural integrity and iii) it contains laminin-111, a key extracellular matrix component that independently delivers biological signals essential for spheroid and organoid formation and growth (224).

Previous studies have shown that porcine and human ameloblast-lineage cells form spherical, acinar-like structures resembling enamel pearls when cultured in Matrigel. Moreover, when ameloblast-lineage cells (202) or epithelial cells derived from human embryonic stem cells (229,230) are pre-cultured in Matrigel and then co-cultured with dental mesenchymal cells, they can give rise to tooth-like structures. Similarly, embedding mouse dental epithelial stem cells isolated from the posterior region of the incisor cervical loop in Matrigel also leads to spheroid formation (231). Using a 3D on-top culture approach and growth factor-reduced gel substrate (Geltrex), HAT-7 cells exhibited preferential elongation along the Z-axis, forming clusters of tall cells in the presence of ameloblastin or amelotin (179), consistent with observations in other ameloblast cell lines, such as ALC and LS8, under similar culture conditions (180). Our current achievement in reliably generating 3D HAT-7 spheroids using Hepato-STIM medium and a Matrigel matrix aligns well with these findings.

HAT-7 cells expressed tight junction proteins ZO-1, claudin-1, claudin-4, and claudin-8 at the mRNA level, regardless of whether they were cultured on porous Transwell inserts or within a 3D Matrigel matrix. When PCR results were normalized to the 2D culture condition, claudin-8 expression was elevated in spheroids, whereas ZO-1, claudin-1, and claudin-4 were downregulated. These findings are consistent with previous reports showing expression of claudin-1, -4, and -8 in maturation-stage ameloblasts (232,233). Notably, the expression of the maturation-stage ameloblast marker Klk4 was markedly increased, further suggesting a phenotypic transition toward the maturation stage during 3D spheroid formation (234,235).

Several electrolyte secreting epithelia are known to be regulated through purinergic or adrenergic signalization (236,237). Previous studies have shown that electrolyte secretion of HAT-7 cells in 2D culture is activated by agonists known to mediate their effects by elevating intracellular cAMP and Ca^{2+}, such as forskolin and ATP (77). Moreover, Nurbaeva et al. proposed that transcellular movement of Ca^{2+} in ameloblast involves G-protein coupled receptors and consequent Ca^{2+} release from the ER stores near the apical surface, potentially modulated by acetylcholine and/or ATP (63). In light of this data, we investigated GPCR-driven calcium signaling in HAT-7 spheroids. Adenosine activates P1 purinergic receptors, while extracellular nucleotides such as ATP, ADP, UTP, and UDP target P2 receptors, which are subdivided into ionotropic (P2X) and metabotropic (P2Y) subtypes. In the presence of extracellular Ca^{2+}, both ATP and UTP triggered biphasic Ca^{2+} responses in HAT-7 spheroids, indicating activation of metabotropic P2Y2 and/or P2Y4 receptors (238). Isolated secretory and maturation ameloblasts expressed mRNA for both receptors, with *P2ry2* being significantly upregulated during maturation (63). P2Y receptors have also been shown to regulate the Ca^{2+} extrusion pathway mediated by NCKX4 (239), a transporter essential for enamel maturation (20). Since UTP does not activate P2X receptors, the sustained phase of Ca^{2+} elevation is likely mediated by store-operated Ca^{2+} channels. Supporting this, Nurbaeva et al. demonstrated that ATP strongly induces store-operated Ca^{2+} entry in maturation-stage, but not secretory-stage ameloblasts (63).

6. Conclusions

1. HAT-7 ameloblast cells showed strong TRPM7 expression at both mRNA and protein levels.
2. TRPM7 activators mibefradil and naltriben elicited Ca^{2+} influx that was further potentiated by intracellular acidification, suggesting the functional presence and pH sensitivity of TRPM7 channels in unpolarized HAT-7 cells.
3. HAT-7 cells exhibited TRPM7-like transmembrane ion currents measured in whole-cell configuration of voltage clamp experiments. The currents were responsive to both stimulation and inhibition of TRPM7 channels, as well as were potentiated by extracellular acidification.
4. In polarized HAT-7 cells mibefradil elicited a polarized Ca^{2+} response, suggesting that functional TRPM7 channels are present predominantly in the apical membrane.
5. Spheroid (3D cultures) of HAT-7 cells showed intracellular Ca^{2+} responses characteristic to metabotropic P2Y2 and/or P2Y4 receptors, while there was no evidence of functional muscarinic or nicotinic ACh receptors.

In summary, HAT-7 ameloblast cells abundantly express functional TRPM7 channels. Under specific conditions, these channels possess Ca^{2+} conductance that is sensitive to changes in extra- and intracellular pH suggesting a potential connection between environmental pH changes and Ca^{2+} transport during amelogenesis. In HAT-7 cells cultured as a polarized monolayer, mibefradil-evoked Ca^{2+} signal is localized to the apical membrane suggesting polarized distribution of TRPM7 channel proteins. HAT-7 cells cultured as spheroids exhibited functional metabotropic purinergic signaling, whereas no evidence was found for the presence of functional cholinergic receptors. These findings suggest that HAT-7 ameloblast cells could serve as a suitable model for investigating calcium transport mechanisms during amelogenesis.

7. Summary

Enamel, the most highly mineralized tissue in the human body, covers the crown of teeth and provides mechanical resilience during mastication. It is formed by specialized epithelial cells, the ameloblasts, which disappear after eruption, leaving enamel acellular, avascular, inert, and non-regenerative. Since Ca^{2+} is the predominant mineral component, one of the key functions of ameloblasts is Ca^{2+} transport to the mineralization front. Although several channels and transporters have been identified, the precise mechanisms of Ca^{2+} transport during amelogenesis remain largely unresolved. TRPM7, a channel with a known role in Ca^{2+}, Zn^{2+}, and Mg^{2+} homeostasis, is abundantly expressed in ameloblasts, and TRPM7 deficiency leads to enamel hypomineralization.

Because ameloblasts are lost after eruption, functional modeling of transport dynamics requires in vitro model systems. HAT-7 ameloblast cells, previously shown to form polarized monolayer with vectorial bicarbonate transport, were therefore used to investigate the role of TRPM7 in Ca^{2+} transport. This thesis focused on: (1) identifying the functional presence, Ca^{2+} conductance, and pH sensitivity of TRPM7 in HAT-7 cells, and (2) examining purinergic and cholinergic receptor activity in 3D cultures of these cells.

HAT-7 cells expressed TRPM7 at both mRNA and protein levels and displayed TRPM7-like transmembrane currents in whole-cell patch-clamp recording. sensitive to extracellular acidification. TRPM7 activators (mibefradil and naltriben) induced Ca^{2+} influx, which was further enhanced by intracellular acidification, indicating functional and pH-sensitive TRPM7 channels in unpolarized cells. In polarized monolayers, mibefradil evoked Ca^{2+} responses predominantly at the apical membrane, suggesting polarized distribution of TRPM7 proteins. In 3D spheroid cultures, HAT-7 cells exhibited purinergic Ca^{2+} signaling characteristic of P2Y2/P2Y4 receptors, whereas no functional muscarinic or nicotinic acetylcholine receptors were detected.

Taken together, HAT-7 cells abundantly express functional TRPM7 channels with Ca^{2+} conductance modulated by intra- and extracellular pH. This suggests a potential link between environmental pH changes and Ca^{2+} transport during amelogenesis. Therefore, HAT-7 ameloblasts, cultured as unpolarised, polarized or 3D speroid culture could serve as a physiologically relevant in vitro model for investigating ion transport mechanisms in enamel formation.

8. Összefoglaló

A zománc az emberi szervezet leginkább mineralizált szövete, amely a biztosítja fogkorona mechanikai ellenállását a rágás során fellépő erőkkel szemben. A zománc kialakulásáért specializált hámsejtek az ameloblasztok felelősek, amelyek a fog előtörése után eltűnnek, így a zománc acelluláris, inaktív és nem regenerálódó szövet. Mivel a zománc fő alkotóeleme a kálcium, az ameloblasztok egyik legfontosabb feladata a Ca^{2+} transzportja a mineralizáció helyére. Bár számos Ca^{2+}-forgalomban résztvevő ioncsatornát és transzportert azonosítottak ameloblasztokon, a transzport pontos mechanizmusa nem ismert. A Mg^{2+}- Ca^{2+}-, és Zn^{2+}-homeosztázisban szerepet játszó TRPM7 bőségesen expresszálódik ameloblasztokban ugyanakkor a TRPM7 hiánya zománc-hipomineralizációhoz vezet. Az amelogenezis transzportdinamikájának vizsgálatára a HAT-7 ameloblaszt sejteket választottuk, amelyekről korábban kimutattuk, hogy képesek vektoriális bikarbonát-transzportra. A dolgozat két kutatási irány eredményeit ismerteti: (1) a TRPM7 funkcionális jelenlétének, Ca^{2+}-vezetőképességének és pH-érzékenységének azonosítása HAT-7 sejtekben, valamint (2) purinerg és kolinerg receptoraktivitás vizsgálata ezen sejtek 3D kultúráiban.

A HAT-7 sejtekben a TRPM7 mRNS- és fehérjeszinten is expresszálódott, és TRPM7-re jellemző, extracellulári acidifikációra érzékeny transzmembrán áramokat mértünk whole-cell patch-clamp technikával. A TRPM7 aktivátorok (mibefradil és naltriben) Ca^{2+} beáramlást indukáltak, amit az intracelluláris acidifikáció tovább fokozott, jelezve a TRPM7 csatornák funkcionális jelenlétét és pH-érzékenységét. Polarizált monolayer kultúrában vizsgálva elsősorban az apikális mibefradil váltott ki Ca^{2+} választ, ami a TRPM7 funkcionális polarizációjára utal. A Matrigel segítségével létrehozott 3D szferoid kultúrákban a HAT-7 sejtek P2Y2/P2Y4 receptorokra jellemző purinerg Ca^{2+} választ mutattak, míg működő muszkarinos vagy nikotinos acetilkolin receptorok jelenlétét nem sikerült kimutatni.

Összességében megállapítható, hogy a HAT-7 sejtek nagy mennyiségben expresszálnak funkcionáló TRPM7 csatornákat, amelyek érzékenyek az intra- és extracelluláris pH változásaira, ezáltal kapcsolatot jelenthetnek a zománc érése során zajló extracelluláris pH-változások és a Ca^{2+} transzport között. Az eredmények alapján a HAT-7 sejtek - nem polarizált, polarizált vagy 3D szferoid kultúrában - élettanilag releváns in vitro modellként szolgálhatnak a zománcképződés iontranszport-mechanizmusainak vizsgálatára.

9. References

1. Thesleff I, Tummers M. Tooth organogenesis and regeneration. In: The Stem Cell Research Community, editor. StemBook, http://www.stembook.org. 2009.

2. Chapter 5 - Development of the Tooth and Its Supporting Tissues. In: Nanci A, editor. Ten Cate's Oral Histology (Eighth Edition). St. Louis (MO): Mosby, 2013: 70-94.

3. Lacruz RS. Enamel: Molecular identity of its transepithelial ion transport system. Cell Calcium 2017; 65:1-7.

4. Lacruz RS, Habelitz S, Wright JT, Paine ML. Dental enamel formation and implications for oral health and disease. Physiol Rev 2017; 97(3):939-993.

5. Cui FZ, Ge J. New observations of the hierarchical structure of human enamel, from nanoscale to microscale. J Tissue Eng Regen Med 2007; 1(3):185-191.

6. Smith CEL, Poulter JA, Antanaviciute A, Kirkham J, Brookes SJ, Inglehearn CF, Mighell AJ. Amelogenesis Imperfecta; Genes, Proteins, and Pathways. Front Physiol 2017; 8:435.

7. Pham CD, Smith CE, Hu Y, Hu JC, Simmer JP, Chun YP. Endocytosis and Enamel Formation. Front Physiol 2017; 8:529.

8. Varga G, Keremi B, Bori E, Foldes A. Function and repair of dental enamel - Potential role of epithelial transport processes of ameloblasts. Pancreatology 2015; 15(4 Suppl):S55-S60.

9. Hu JC, Chun YH, Al HT, Simmer JP. Enamel formation and amelogenesis imperfecta. Cells Tissues Organs 2007; 186(1):78-85.

10. Chun YP, Foster BL, Liang T, Kawasaki K. Functions of secretory calcium-binding phosphoproteins in dental mineralization. J Bone Miner Res 2025; 40(8):909-930.

11. Pandya M, Diekwisch TGH. Amelogenesis: Transformation of a protein-mineral matrix into tooth enamel. J Struct Biol 2021; 213(4):107809.

12. Simmer JP, Hu JC, Hu Y, Zhang S, Liang T, Wang SK, Kim JW, Yamakoshi Y, Chun YH, Bartlett JD, Smith CE. A genetic model for the secretory stage of dental enamel formation. J Struct Biol 2021; 213(4):107805.

13. Fukumoto S, Kiba T, Hall B, Iehara N, Nakamura T, Longenecker G, Krebsbach PH, Nanci A, Kulkarni AB, Yamada Y. Ameloblastin is a cell adhesion molecule required for maintaining the differentiation state of ameloblasts. J Cell Biol 2004; 167(5):973-983.

14. Kegulian NC, Visakan G, Bapat RA, Moradian-Oldak J. Ameloblastin and its multifunctionality in amelogenesis: A review. Matrix Biol 2024; 131:62-76.

15. Hu JC, Hu Y, Lu Y, Smith CE, Lertlam R, Wright JT, Suggs C, McKee MD, Beniash E, Kabir ME, Simmer JP. Enamelin is critical for ameloblast integrity and enamel ultrastructure formation. PLoS One 2014; 9(3):e89303.

16. Lacruz RS, Smith CE, Chen YB, Hubbard MJ, Hacia JG, Paine ML. Gene-expression analysis of early- and late-maturation-stage rat enamel organ. Eur J Oral Sci 2011; 119 Suppl 1(Suppl 1):149-157.

17. Uchida T, Tanabe T, Fukae M, Shimizu M, Yamada M, Miake K, Kobayashi S. Immunochemical and immunohistochemical studies, using antisera against porcine 25 kDa amelogenin, 89 kDa enamelin and the 13-17 kDa nonamelogenins, on immature enamel of the pig and rat. Histochemistry 1991; 96(2):129-138.

18. Martinez-Avila O, Wu S, Kim SJ, Cheng Y, Khan F, Samudrala R, Sali A, Horst JA, Habelitz S. Self-assembly of filamentous amelogenin requires calcium and phosphate: from dimers via nanoribbons to fibrils. Biomacromolecules 2012; 13(11):3494-3502.

19. Bronckers AL. Ion Transport by Ameloblasts during Amelogenesis. J Dent Res 2017; 96(3):243-253.

20. Nurbaeva MK, Eckstein M, Feske S, Lacruz RS. Ca(2+) transport and signalling in enamel cells. J Physiol 2017; 595(10):3015-3039.

21. Hermans F, Hasevoets S, Vankelecom H, Bronckaers A, Lambrichts I. From Pluripotent Stem Cells to Organoids and Bioprinting: Recent Advances in Dental Epithelium and Ameloblast Models to Study Tooth Biology and Regeneration. Stem Cell Rev Rep 2024; 20(5):1184-1199.

22. Llano E, Pendas AM, Knauper V, Sorsa T, Salo T, Salido E, Murphy G, Simmer JP, Bartlett JD, Lopez-Otin C. Identification and structural and functional

characterization of human enamelysin (MMP-20). Biochemistry 1997; 36(49):15101-15108.

23. Hu P, Lacruz RS, Smith CE, Smith SM, Kurtz I, Paine ML. Expression of the sodium/calcium/potassium exchanger, NCKX4, in ameloblasts. Cells Tissues Organs 2012; 196(6):501-509.

24. Lacruz RS, Smith CE, Bringas P, Jr., Chen YB, Smith SM, Snead ML, Kurtz I, Hacia JG, Hubbard MJ, Paine ML. Identification of novel candidate genes involved in mineralization of dental enamel by genome-wide transcript profiling. J Cell Physiol 2012; 227(5):2264-2275.

25. Wang S, Choi M, Richardson AS, Reid BM, Seymen F, Yildirim M, Tuna E, Gencay K, Simmer JP, Hu JC. STIM1 and SLC24A4 Are Critical for Enamel Maturation. J Dent Res 2014; 93(7 Suppl):94S-100S.

26. Josephsen K, Fejerskov O. Ameloblast modulation in the maturation zone of the rat incisor enamel organ. A light and electron microscopic study. J Anat 1977; 124(Pt 1):45-70.

27. Smith CE, McKee MD, Nanci A. Cyclic induction and rapid movement of sequential waves of new smooth-ended ameloblast modulation bands in rat incisors as visualized by polychrome fluorescent labeling and GBHA-staining of maturing enamel. Adv Dent Res 1987; 1(2):162-175.

28. Sasaki S, Takagi T, Suzuki M. Cyclical changes in pH in bovine developing enamel as sequential bands. Arch Oral Biol 1991; 36(3):227-231.

29. Varga G, DenBesten P, Racz R, Zsembery A. Importance of bicarbonate transport in pH control during amelogenesis - need for functional studies. Oral Dis 2018; 24(6):879-890.

30. Moffatt P, Wazen RM, Dos Santos NJ, Nanci A. Characterisation of secretory calcium-binding phosphoprotein-proline-glutamine-rich 1: a novel basal lamina component expressed at cell-tooth interfaces. Cell Tissue Res 2014; 358(3):843-855.

31. Moffatt P, Smith CE, St-Arnaud R, Nanci A. Characterization of Apin, a secreted protein highly expressed in tooth-associated epithelia. J Cell Biochem 2008; 103(3):941-956.

32. Katsura K, Nakano Y, Zhang Y, Shemirani R, Li W, Den BP. WDR72 regulates vesicle trafficking in ameloblasts. Sci Rep 2022; 12(1):2820.

33. Bootman MD, Bultynck G. Fundamentals of Cellular Calcium Signaling: A Primer. Cold Spring Harb Perspect Biol 2020; 12(1).

34. Eisner D, Neher E, Taschenberger H, Smith G. Physiology of intracellular calcium buffering. Physiol Rev 2023; 103(4):2767-2845.

35. Nurbaeva MK, Eckstein M, Concepcion AR, Smith CE, Srikanth S, Paine ML, Gwack Y, Hubbard MJ, Feske S, Lacruz RS. Dental enamel cells express functional SOCE channels. Sci Rep 2015; 5:15803.

36. Smith CE. Cellular and chemical events during enamel maturation. Crit Rev Oral Biol Med 1998; 9(2):128-161.

37. Hubbard MJ. Calcium transport across the dental enamel epithelium. Crit Rev Oral Biol Med 2000; 11(4):437-466.

38. Costiniti V, Bomfim GH, Mitaishvili E, Son GY, Li Y, Lacruz RS. Calcium Transport in Specialized Dental Epithelia and Its Modulation by Fluoride. Front Endocrinol (Lausanne) 2021; 12:730913.

39. Takano Y, Crenshaw MA, Reith EJ. Correlation of 45Ca incorporation with maturation ameloblast morphology in the rat incisor. Calcif Tissue Int 1982; 34(2):211-213.

40. Bawden JW. Calcium transport during mineralization. Anat Rec 1989; 224(2):226-233.

41. Stafford N, Wilson C, Oceandy D, Neyses L, Cartwright EJ. The Plasma Membrane Calcium ATPases and Their Role as Major New Players in Human Disease. Physiol Rev 2017; 97(3):1089-1125.

42. Thomas RC. The plasma membrane calcium ATPase (PMCA) of neurones is electroneutral and exchanges 2 H+ for each Ca2+ or Ba2+ ion extruded. J Physiol 2009; 587(2):315-327.

43. Robertson SYT, Wen X, Yin K, Chen J, Smith CE, Paine ML. Multiple Calcium Export Exchangers and Pumps Are a Prominent Feature of Enamel Organ Cells. Front Physiol 2017; 8:336.

44. Salama AH, Zaki AE, Eisenmann DR. Cytochemical localization of Ca2+-Mg2+ adenosine triphosphatase in rat incisor ameloblasts during enamel secretion and maturation. J Histochem Cytochem 1987; 35(4):471-482.

45. Borke JL, Zaki AE, Eisenmann DR, Ashrafi SH, Ashrafi SS, Penniston JT. Expression of plasma membrane Ca++ pump epitopes parallels the progression of enamel and dentin mineralization in rat incisor. J Histochem Cytochem 1993; 41(2):175-181.

46. Zaki AE, Hand AR, Mednieks MI, Eisenmann DR, Borke JL. Quantitative immunocytochemistry of Ca(2+)-Mg2+ ATPase in ameloblasts associated with enamel secretion and maturation in the rat incisor. Adv Dent Res 1996; 10(2):245-251.

47. Bomfim GHS, Giacomello M, Lacruz RS. PMCA Ca(2+) clearance in dental enamel cells depends on the magnitude of cytosolic Ca(2). FASEB J 2023; 37(1):e22679.

48. Niggli E, Lederer WJ. Activation of Na-Ca exchange current by photolysis of "caged calcium". Biophys J 1993; 65(2):882-891.

49. Lytton J. Na+/Ca2+ exchangers: three mammalian gene families control Ca2+ transport. Biochem J 2007; 406(3):365-382.

50. Gagnon KB, Delpire E. Sodium Transporters in Human Health and Disease. Front Physiol 2020; 11:588664.

51. Okumura R, Shibukawa Y, Muramatsu T, Hashimoto S, Nakagawa K, Tazaki M, Shimono M. Sodium-calcium exchangers in rat ameloblasts. J Pharmacol Sci 2010; 112(2):223-230.

52. Mahdee AF, Ali AH, Gillespie JI. Structural and functional relations between the connective tissue and epithelium of enamel organ and their role during enamel maturation. J Mol Histol 2021; 52(5):975-989.

53. Souza Bomfim GH, Mitaishvili E, Schnetkamp PPM, Lacruz RS. Na+/Ca2+ exchange in enamel cells is dominated by the K+-dependent NCKX exchanger. J Gen Physiol 2024; 156(1):e202313372.

54. Lacruz RS, Smith CE, Kurtz I, Hubbard MJ, Paine ML. New paradigms on the transport functions of maturation-stage ameloblasts. J Dent Res 2013; 92(2):122-129.

55. Parry DA, Poulter JA, Logan CV, Brookes SJ, Jafri H, Ferguson CH, Anwari BM, Rashid Y, Zhao H, Johnson CA, Inglehearn CF, Mighell AJ. Identification of mutations in SLC24A4, encoding a potassium-dependent sodium/calcium exchanger, as a cause of amelogenesis imperfecta. Am J Hum Genet 2013; 92(2):307-312.

56. Hubbard MJ, McHugh NJ, Mangum JE. Exclusion of all three calbindins from a calcium-ferry role in rat enamel cells. Eur J Oral Sci 2011; 119 Suppl 1:112-119.

57. Turnbull CI, Looi K, Mangum JE, Meyer M, Sayer RJ, Hubbard MJ. Calbindin independence of calcium transport in developing teeth contradicts the calcium ferry dogma. J Biol Chem 2004; 279(53):55850-55854.

58. Eckstein M, Vaeth M, Fornai C, Vinu M, Bromage TG, Nurbaeva MK, Sorge JL, Coelho PG, Idaghdour Y, Feske S, Lacruz RS. Store-operated Ca(2+) entry controls ameloblast cell function and enamel development. JCI Insight 2017; 2(6):e91166.

59. Prakriya M, Lewis RS. Store-Operated Calcium Channels. Physiol Rev 2015; 95(4):1383-1436.

60. Rubaiy HN. ORAI Calcium Channels: Regulation, Function, Pharmacology, and Therapeutic Targets. Pharmaceuticals (Basel) 2023; 16(2):162.

61. Park HS, Betzenhauser MJ, Zhang Y, Yule DI. Regulation of Ca(2)(+) release through inositol 1,4,5-trisphosphate receptors by adenine nucleotides in parotid acinar cells. Am J Physiol Gastrointest Liver Physiol 2012; 302(1):G97-G104.

62. Wagner LE, Yule DI. Differential regulation of the InsP(3) receptor type-1 and -2 single channel properties by InsP(3), Ca(2)(+) and ATP. J Physiol 2012; 590(14):3245-3259.

63. Nurbaeva MK, Eckstein M, Devotta A, Saint-Jeannet JP, Yule DI, Hubbard MJ, Lacruz RS. Evidence That Calcium Entry Into Calcium-Transporting Dental Enamel Cells Is Regulated by Cholecystokinin, Acetylcholine and ATP. Front Physiol 2018; 9:801.

64. Eckstein M, Vaeth M, Aulestia FJ, Costiniti V, Kassam SN, Bromage TG, Pedersen P, Issekutz T, Idaghdour Y, Moursi AM, Feske S, Lacruz RS. Differential regulation of Ca(2+) influx by ORAI channels mediates enamel mineralization. Sci Signal 2019; 12(578):eaav4663.

65. Lian J, Cuk M, Kahlfuss S, Kozhaya L, Vaeth M, Rieux-Laucat F, Picard C, Benson MJ, Jakovcevic A, Bilic K, Martinac I, Stathopulos P, Kacskovics I, Vraetz T, Speckmann C, Ehl S, Issekutz T, Unutmaz D, Feske S. ORAI1 mutations abolishing store-operated Ca(2+) entry cause anhidrotic ectodermal dysplasia with immunodeficiency. J Allergy Clin Immunol 2018; 142(4):1297-1310.

66. McCarl CA, Picard C, Khalil S, Kawasaki T, Rother J, Papolos A, Kutok J, Hivroz C, Ledeist F, Plogmann K, Ehl S, Notheis G, Albert MH, Belohradsky BH, Kirschner J, Rao A, Fischer A, Feske S. ORAI1 deficiency and lack of store-operated Ca2+ entry cause immunodeficiency, myopathy, and ectodermal dysplasia. J Allergy Clin Immunol 2009; 124(6):1311-1318.

67. Foskett JK, White C, Cheung KH, Mak DO. Inositol trisphosphate receptor Ca2+ release channels. Physiol Rev 2007; 87(2):593-658.

68. Eisenmann DR, Ashrafi S, Zaki AE. Multi-method analysis of calcium localization in the secretory ameloblast. J Dent Res 1982; Spec No:1555-1562.

69. Takano Y, Matsuo S, Wakisaka S, Ichikawa H, Nishikawa S, Akai M. Histochemical localization of calcium in the enamel organ of rat incisors in early-stage amelogenesis. Acta Anat (Basel) 1989; 134(4):305-311.

70. Costiniti V, Bomfim GHS, Neginskaya M, Son GY, Mitaishvili E, Giacomello M, Pavlov E, Lacruz RS. Mitochondria modulate ameloblast Ca(2+) signaling. FASEB J 2022; 36(2):e22169.

71. Ogata K, Tsumuraya T, Oka K, Shin M, Okamoto F, Kajiya H, Katagiri C, Ozaki M, Matsushita M, Okabe K. The crucial role of the TRPM7 kinase domain in the early stage of amelogenesis. Sci Rep 2017; 7(1):18099.

72. Nakano Y, Le MH, Abduweli D, Ho SP, Ryazanova LV, Hu Z, Ryazanov AG, Den Besten PK, Zhang Y. A Critical Role of TRPM7 As an Ion Channel Protein in

Mediating the Mineralization of the Craniofacial Hard Tissues. Front Physiol 2016; 7:258.

73. Ji M, Xiao L, Xu L, Huang S, Zhang D. How pH is regulated during amelogenesis in dental fluorosis. Exp Ther Med 2018; 16(5):3759-3765.

74. Lacruz RS, Nanci A, Kurtz I, Wright JT, Paine ML. Regulation of pH During Amelogenesis. Calcif Tissue Int 2010; 86(2):91-103.

75. Supuran CT. Carbonic anhydrases--an overview. Curr Pharm Des 2008; 14(7):603-614.

76. Josephsen K, Takano Y, Frische S, Praetorius J, Nielsen S, Aoba T, Fejerskov O. Ion transporters in secretory and cyclically modulating ameloblasts: a new hypothesis for cellular control of preeruptive enamel maturation. Am J Physiol Cell Physiol 2010; 299(6):C1299-C1307.

77. Bori E, Guo J, Racz R, Burghardt B, Foldes A, Keremi B, Harada H, Steward MC, Den BP, Bronckers AL, Varga G. Evidence for Bicarbonate Secretion by Ameloblasts in a Novel Cellular Model. J Dent Res 2016; 95(5):588-596.

78. Racz R, Foldes A, Bori E, Zsembery A, Harada H, Steward MC, DenBesten P, Bronckers ALJJ, Gerber G, Varga G. No Change in Bicarbonate Transport but Tight-Junction Formation Is Delayed by Fluoride in a Novel Ameloblast Model. Front Physiol 2017; 8:940.

79. Lyaruu DM, Bronckers AL, Mulder L, Mardones P, Medina JF, Kellokumpu S, Oude Elferink RP, Everts V. The anion exchanger Ae2 is required for enamel maturation in mouse teeth. Matrix Biol 2008; 27(2):119-127.

80. Paine ML, Snead ML, Wang HJ, Abuladze N, Pushkin A, Liu W, Kao LY, Wall SM, Kim YH, Kurtz I. Role of NBCe1 and AE2 in secretory ameloblasts. J Dent Res 2008; 87(4):391-395.

81. Lacruz RS, Nanci A, White SN, Wen X, Wang H, Zalzal SF, Luong VQ, Schuetter VL, Conti PS, Kurtz I, Paine ML. The sodium bicarbonate cotransporter (NBCe1) is essential for normal development of mouse dentition. J Biol Chem 2010; 285(32):24432-24438.

82. Bronckers AL, Guo J, Zandieh-Doulabi B, Bervoets TJ, Lyaruu DM, Li X, Wangemann P, DenBesten P. Developmental expression of solute carrier family 26A member 4 (SLC26A4/pendrin) during amelogenesis in developing rodent teeth. Eur J Oral Sci 2011; 119 Suppl 1(Suppl 1):185-192.

83. Seidler U, Nikolovska K. Slc26 Family of Anion Transporters in the Gastrointestinal Tract: Expression, Function, Regulation, and Role in Disease. Compr Physiol 2019; 9(2):839-872.

84. Becker HM, Seidler UE. Bicarbonate secretion and acid/base sensing by the intestine. Pflugers Arch 2024; 476(4):593-610.

85. Bronckers A, Kalogeraki L, Jorna HJ, Wilke M, Bervoets TJ, Lyaruu DM, Zandieh-Doulabi B, DenBesten P, de JH. The cystic fibrosis transmembrane conductance regulator (CFTR) is expressed in maturation stage ameloblasts, odontoblasts and bone cells. Bone 2010; 46(4):1188-1196.

86. Crawford I, Maloney PC, Zeitlin PL, Guggino WB, Hyde SC, Turley H, Gatter KC, Harris A, Higgins CF. Immunocytochemical localization of the cystic fibrosis gene product CFTR. Proc Natl Acad Sci U S A 1991; 88(20):9262-9266.

87. Sui W, Boyd C, Wright JT. Altered pH regulation during enamel development in the cystic fibrosis mouse incisor. J Dent Res 2003; 82(5):388-392.

88. Arquitt CK, Boyd C, Wright JT. Cystic fibrosis transmembrane regulator gene (CFTR) is associated with abnormal enamel formation. J Dent Res 2002; 81(7):492-496.

89. Wright JT, Kiefer CL, Hall KI, Grubb BR. Abnormal enamel development in a cystic fibrosis transgenic mouse model. J Dent Res 1996; 75(4):966-973.

90. Azevedo TD, Feijo GC, Bezerra AC. Presence of developmental defects of enamel in cystic fibrosis patients. J Dent Child (Chic) 2006; 73(3):159-163.

91. Dhakal S, Lee Y. Transient Receptor Potential Channels and Metabolism. Mol Cells 2019; 42(8):569-578.

92. Wong KK, Banham AH, Yaacob NS, Nur Husna SM. The oncogenic roles of TRPM ion channels in cancer. J Cell Physiol 2019; 234(9):14556-14573.

93. Okada Y, Numata T, Sabirov RZ, Kashio M, Merzlyak PG, Sato-Numata K. Cell death induction and protection by activation of ubiquitously expressed anion/cation channels. Part 3: the roles and properties of TRPM2 and TRPM7. Front Cell Dev Biol 2023; 11:1246955.

94. Demeuse P, Penner R, Fleig A. TRPM7 channel is regulated by magnesium nucleotides via its kinase domain. J Gen Physiol 2006; 127(4):421-434.

95. Schmitz C, Perraud AL, Johnson CO, Inabe K, Smith MK, Penner R, Kurosaki T, Fleig A, Scharenberg AM. Regulation of vertebrate cellular Mg2+ homeostasis by TRPM7. Cell 2003; 114(2):191-200.

96. Liang HY, Chen Y, Wei X, Ma GG, Ding J, Lu C, Zhou RP, Hu W. Immunomodulatory functions of TRPM7 and its implications in autoimmune diseases. Immunology 2022; 165(1):3-21.

97. Chubanov V, Kottgen M, Touyz RM, Gudermann T. TRPM channels in health and disease. Nat Rev Nephrol 2024; 20(3):175-187.

98. Faouzi M, Kilch T, Horgen FD, Fleig A, Penner R. The TRPM7 channel kinase regulates store-operated calcium entry. J Physiol 2017; 595(10):3165-3180.

99. Visser D, Middelbeek J, van Leeuwen FN, Jalink K. Function and regulation of the channel-kinase TRPM7 in health and disease. Eur J Cell Biol 2014; 93(10-12):455-465.

100. Kozak JA, Matsushita M, Nairn AC, Cahalan MD. Charge screening by internal pH and polyvalent cations as a mechanism for activation, inhibition, and rundown of TRPM7/MIC channels. J Gen Physiol 2005; 126(5):499-514.

101. Li M, Jiang J, Yue L. Functional characterization of homo- and heteromeric channel kinases TRPM6 and TRPM7. J Gen Physiol 2006; 127(5):525-537.

102. Kerschbaum HH, Kozak JA, Cahalan MD. Polyvalent cations as permeant probes of MIC and TRPM7 pores. Biophys J 2003; 84(4):2293-2305.

103. Nadler MJ, Hermosura MC, Inabe K, Perraud AL, Zhu Q, Stokes AJ, Kurosaki T, Kinet JP, Penner R, Scharenberg AM, Fleig A. LTRPC7 is a Mg.ATP-regulated divalent cation channel required for cell viability. Nature 2001; 411(6837):590-595.

104. Runnels LW, Yue L, Clapham DE. TRP-PLIK, a bifunctional protein with kinase and ion channel activities. Science 2001; 291(5506):1043-1047.

105. Numata T, Okada Y. Molecular determinants of sensitivity and conductivity of human TRPM7 to Mg2+ and Ca2+. Channels (Austin) 2008; 2(4):283-286.

106. Li M, Du J, Jiang J, Ratzan W, Su LT, Runnels LW, Yue L. Molecular determinants of Mg2+ and Ca2+ permeability and pH sensitivity in TRPM6 and TRPM7. J Biol Chem 2007; 282(35):25817-25830.

107. Abiria SA, Krapivinsky G, Sah R, Santa-Cruz AG, Chaudhuri D, Zhang J, Adstamongkonkul P, DeCaen PG, Clapham DE. TRPM7 senses oxidative stress to release Zn(2+) from unique intracellular vesicles. Proc Natl Acad Sci U S A 2017; 114(30):E6079-E6088.

108. Jiang J, Li M, Yue L. Potentiation of TRPM7 inward currents by protons. J Gen Physiol 2005; 126(2):137-150.

109. Numata T, Okada Y. Proton conductivity through the human TRPM7 channel and its molecular determinants. J Biol Chem 2008; 283(22):15097-15103.

110. Chokshi R, Matsushita M, Kozak JA. Detailed examination of Mg2+ and pH sensitivity of human TRPM7 channels. Am J Physiol Cell Physiol 2012; 302(7):C1004-C1011.

111. Chokshi R, Matsushita M, Kozak JA. Sensitivity of TRPM7 channels to Mg2+ characterized in cell-free patches of Jurkat T lymphocytes. Am J Physiol Cell Physiol 2012; 302(11):C1642-C1651.

112. Mellott A, Rockwood J, Zhelay T, Luu CT, Kaitsuka T, Kozak JA. TRPM7 channel activity in Jurkat T lymphocytes during magnesium depletion and loading: implications for divalent metal entry and cytotoxicity. Pflugers Arch 2020; 472(11):1589-1606.

113. Gwanyanya A, Amuzescu B, Zakharov SI, Macianskiene R, Sipido KR, Bolotina VM, Vereecke J, Mubagwa K. Magnesium-inhibited, TRPM6/7-like channel in cardiac myocytes: permeation of divalent cations and pH-mediated regulation. J Physiol 2004; 559(Pt 3):761-776.

114. Kozak JA, Kerschbaum HH, Cahalan MD. Distinct properties of CRAC and MIC channels in RBL cells. J Gen Physiol 2002; 120(2):221-235.

115. Kozak JA, Cahalan MD. MIC channels are inhibited by internal divalent cations but not ATP. Biophys J 2003; 84(2 Pt 1):922-927.

116. Matsushita M, Kozak JA, Shimizu Y, McLachlin DT, Yamaguchi H, Wei FY, Tomizawa K, Matsui H, Chait BT, Cahalan MD, Nairn AC. Channel function is dissociated from the intrinsic kinase activity and autophosphorylation of TRPM7/ChaK1. J Biol Chem 2005; 280(21):20793-20803.

117. Yu H, Zhang Z, Lis A, Penner R, Fleig A. TRPM7 is regulated by halides through its kinase domain. Cell Mol Life Sci 2013; 70(15):2757-2771.

118. Inoue H, Murayama T, Kobayashi T, Konishi M, Yokoyama U. The zinc-binding motif of TRPM7 acts as an oxidative stress sensor to regulate its channel activity. J Gen Physiol 2021; 153(6):e202012708.

119. Zhelay T, Wieczerzak KB, Beesetty P, Alter GM, Matsushita M, Kozak JA. Depletion of plasma membrane-associated phosphoinositides mimics inhibition of TRPM7 channels by cytosolic Mg(2+), spermine, and pH. J Biol Chem 2018; 293(47):18151-18167.

120. Macianskiene R, Almanaityte M, Jekabsone A, Mubagwa K. Modulation of Human Cardiac TRPM7 Current by Extracellular Acidic pH Depends upon Extracellular Concentrations of Divalent Cations. PLoS One 2017; 12(1):e0170923.

121. Numata T, Sato-Numata K, Okada Y. TRPM7 is involved in acid-induced necrotic cell death in a manner sensitive to progesterone in human cervical cancer cells. Physiol Rep 2019; 7(13):e14157.

122. Langeslag M, Clark K, Moolenaar WH, van Leeuwen FN, Jalink K. Activation of TRPM7 channels by phospholipase C-coupled receptor agonists. J Biol Chem 2007; 282(1):232-239.

123. Macianskiene R, Gwanyanya A, Vereecke J, Mubagwa K. Inhibition of the magnesium-sensitive TRPM7-like channel in cardiac myocytes by nonhydrolysable GTP analogs: involvement of phosphoinositide metabolism. Cell Physiol Biochem 2008; 22(1-4):109-118.

124. Runnels LW, Yue L, Clapham DE. The TRPM7 channel is inactivated by PIP(2) hydrolysis. Nat Cell Biol 2002; 4(5):329-336.

125. Xie J, Sun B, Du J, Yang W, Chen HC, Overton JD, Runnels LW, Yue L. Phosphatidylinositol 4,5-bisphosphate (PIP(2)) controls magnesium gatekeeper TRPM6 activity. Sci Rep 2011; 1:146.

126. Seo JB, Jung SR, Huang W, Zhang Q, Koh DS. Charge Shielding of PIP2 by Cations Regulates Enzyme Activity of Phospholipase C. PLoS One 2015; 10(12):e0144432.

127. Chubanov V, Gudermann T. Mapping TRPM7 Function by NS8593. Int J Mol Sci 2020; 21(19):7017.

128. Cheng XY, Li SF, Chen Y, Zhao YJ, Hu W, Lu C, Zhou RP. Transient receptor potential melastatin 7 and their modulators. Eur J Pharmacol 2022; 931:175180.

129. Rossig A, Hill K, Norenberg W, Weidenbach S, Zierler S, Schaefer M, Gudermann T, Chubanov V. Pharmacological agents selectively acting on the channel moieties of TRPM6 and TRPM7. Cell Calcium 2022; 106:102640.

130. Guan Z, Chen X, Fang S, Ji Y, Gao Z, Zheng Y. CCT128930 is a novel and potent antagonist of TRPM7 channel. Biochem Biophys Res Commun 2021; 560:132-138.

131. Strobaek D, Hougaard C, Johansen TH, Sorensen US, Nielsen EO, Nielsen KS, Taylor RD, Pedarzani P, Christophersen P. Inhibitory gating modulation of small conductance Ca2+-activated K+ channels by the synthetic compound (R)-N-(benzimidazol-2-yl)-1,2,3,4-tetrahydro-1-naphtylamine (NS8593) reduces afterhyperpolarizing current in hippocampal CA1 neurons. Mol Pharmacol 2006; 70(5):1771-1782.

132. Chubanov V, Schnitzler M, Meissner M, Schafer S, Abstiens K, Hofmann T, Gudermann T. Natural and synthetic modulators of SK (K(ca)2) potassium channels inhibit magnesium-dependent activity of the kinase-coupled cation channel TRPM7. Br J Pharmacol 2012; 166(4):1357-1376.

133. Inoue H, Inazu M, Konishi M, Yokoyama U. Functional expression of TRPM7 as a Ca(2+) influx pathway in adipocytes. Physiol Rep 2019; 7(20):e14272.

134. Zong P, Li CX, Feng J, Yue Z, Nethramangalath T, Xie Y, Qin X, Cicchetti M, Cai Y, Jellison E, Matsushita M, Runnels LW, Yue L. TRPM7 channel activity promotes the pathogenesis of abdominal aortic aneurysms. Nat Cardiovasc Res 2025; 4(2):197-215.

135. Souza Bomfim GH, Costiniti V, Li Y, Idaghdour Y, Lacruz RS. TRPM7 activation potentiates SOCE in enamel cells but requires ORAI. Cell Calcium 2020; 87:102187.

136. Adachi K, Chiba K. FTY720 story. Its discovery and the following accelerated development of sphingosine 1-phosphate receptor agonists as immunomodulators based on reverse pharmacology. Perspect Medicin Chem 2007; 1:11-23.

137. Qin X, Yue Z, Sun B, Yang W, Xie J, Ni E, Feng Y, Mahmood R, Zhang Y, Yue L. Sphingosine and FTY720 are potent inhibitors of the transient receptor potential melastatin 7 (TRPM7) channels. Br J Pharmacol 2013; 168(6):1294-1312.

138. Schilling T, Miralles F, Eder C. TRPM7 regulates proliferation and polarisation of macrophages. J Cell Sci 2014; 127(Pt 21):4561-4566.

139. Wang X, Wang M, Zhu TT, Zheng ZJ, Li S, Sui ZY, Guo X, Wu S, Zhang NN, Yu ZY, Hu CP, Tang YB, Wang Q, Zhang Z. The TRPM7 chanzyme in smooth muscle cells drives abdominal aortic aneurysm in mice. Nat Cardiovasc Res 2025; 4(2):216-234.

140. Won J, Vang H, Kim JH, Lee PR, Kang Y, Oh SB. TRPM7 Mediates Mechanosensitivity in Adult Rat Odontoblasts. J Dent Res 2018; 97(9):1039-1046.

141. Hofmann T, Schafer S, Linseisen M, Sytik L, Gudermann T, Chubanov V. Activation of TRPM7 channels by small molecules under physiological conditions. Pflugers Arch 2014; 466(12):2177-2189.

142. Sofuoglu M, Portoghese PS, Takemori AE. Differential antagonism of delta opioid agonists by naltrindole and its benzofuran analog (NTB) in mice: evidence for delta opioid receptor subtypes. J Pharmacol Exp Ther 1991; 257(2):676-680.

143. Nadezhdin KD, Correia L, Narangoda C, Patel DS, Neuberger A, Gudermann T, Kurnikova MG, Chubanov V, Sobolevsky AI. Structural mechanisms of TRPM7 activation and inhibition. Nat Commun 2023; 14(1):2639.

144. Carvacho I, Ardestani G, Lee HC, McGarvey K, Fissore RA, Lykke-Hartmann K. TRPM7-like channels are functionally expressed in oocytes and modulate post-fertilization embryo development in mouse. Sci Rep 2016; 6:34236.

145. Qian N, Ichimura A, Takei D, Sakaguchi R, Kitani A, Nagaoka R, Tomizawa M, Miyazaki Y, Miyachi H, Numata T, Kakizawa S, Nishi M, Mori Y, Takeshima H. TRPM7 channels mediate spontaneous Ca(2+) fluctuations in growth plate chondrocytes that promote bone development. Sci Signal 2019; 12(576):eaaw4847.

146. Tashiro M, Inoue H, Konishi M. Modulation of Mg(2+) influx and cytoplasmic free Mg(2+) concentration in rat ventricular myocytes. J Physiol Sci 2019; 69(1):97-102.

147. Nascimento DC, V, Sun Y, Venkatesan M, De La Chapa J, Ramachandran K, Jasrotia RS, Drel V, Chai X, Mishra BB, Madesh M, Singh BB. Naltriben promotes tumor growth by activating the TRPM7-mediated development of the anti-inflammatory M2 phenotype. NPJ Precis Oncol 2025; 9(1):29.

148. Frishman WH. Mibefradil: A New Selective T-Channel Calcium Antagonist for Hypertension and Angina Pectoris. J Cardiovasc Pharmacol Ther 1997; 2(4):321-330.

149. Schafer S, Ferioli S, Hofmann T, Zierler S, Gudermann T, Chubanov V. Mibefradil represents a new class of benzimidazole TRPM7 channel agonists. Pflugers Arch 2016; 468(4):623-634.

150. Souza Bomfim GH, Mitaishvili E, Aguiar TF, Lacruz RS. Mibefradil alters intracellular calcium concentration by activation of phospholipase C and IP(3) receptor function. Mol Biomed 2021; 2(1):12.

151. Viana F, Van den Bosch L, Missiaen L, Vandenberghe W, Droogmans G, Nilius B, Robberecht W. Mibefradil (Ro 40-5967) blocks multiple types of voltage-gated calcium channels in cultured rat spinal motoneurones. Cell Calcium 1997; 22(4):299-311.

152. Nilius B, Prenen J, Kamouchi M, Viana F, Voets T, Droogmans G. Inhibition by mibefradil, a novel calcium channel antagonist, of Ca(2+)- and volume-activated Cl- channels in macrovascular endothelial cells. Br J Pharmacol 1997; 121(3):547-555.

153. Bernhardt ML, Stein P, Carvacho I, Krapp C, Ardestani G, Mehregan A, Umbach DM, Bartolomei MS, Fissore RA, Williams CJ. TRPM7 and CaV3.2 channels mediate

Ca(2+) influx required for egg activation at fertilization. Proc Natl Acad Sci U S A 2018; 115(44):E10370-E10378.

154. Chubanov V, Waldegger S, Schnitzler M, Vitzthum H, Sassen MC, Seyberth HW, Konrad M, Gudermann T. Disruption of TRPM6/TRPM7 complex formation by a mutation in the TRPM6 gene causes hypomagnesemia with secondary hypocalcemia. Proc Natl Acad Sci U S A 2004; 101(9):2894-2899.

155. Schappe MS, Szteyn K, Stremska ME, Mendu SK, Downs TK, Seegren PV, Mahoney MA, Dixit S, Krupa JK, Stipes EJ, Rogers JS, Adamson SE, Leitinger N, Desai BN. Chanzyme TRPM7 Mediates the Ca(2+) Influx Essential for Lipopolysaccharide-Induced Toll-Like Receptor 4 Endocytosis and Macrophage Activation. Immunity 2018; 48(1):59-74.

156. Schappe MS, Stremska ME, Busey GW, Downs TK, Seegren PV, Mendu SK, Flegal Z, Doyle CA, Stipes EJ, Desai BN. Efferocytosis requires periphagosomal Ca(2+)-signaling and TRPM7-mediated electrical activity. Nat Commun 2022; 13(1):3230.

157. Jin J, Desai BN, Navarro B, Donovan A, Andrews NC, Clapham DE. Deletion of Trpm7 disrupts embryonic development and thymopoiesis without altering Mg2+ homeostasis. Science 2008; 322(5902):756-760.

158. Mittermeier L, Demirkhanyan L, Stadlbauer B, Breit A, Recordati C, Hilgendorff A, Matsushita M, Braun A, Simmons DG, Zakharian E, Gudermann T, Chubanov V. TRPM7 is the central gatekeeper of intestinal mineral absorption essential for postnatal survival. Proc Natl Acad Sci U S A 2019; 116(10):4706-4715.

159. Ryazanova LV, Hu Z, Suzuki S, Chubanov V, Fleig A, Ryazanov AG. Elucidating the role of the TRPM7 alpha-kinase: TRPM7 kinase inactivation leads to magnesium deprivation resistance phenotype in mice. Sci Rep 2014; 4:7599.

160. Al Alawi AM, Majoni SW, Falhammar H. Magnesium and Human Health: Perspectives and Research Directions. Int J Endocrinol 2018; 2018:9041694.

161. Ryazanova LV, Rondon LJ, Zierler S, Hu Z, Galli J, Yamaguchi TP, Mazur A, Fleig A, Ryazanov AG. TRPM7 is essential for Mg(2+) homeostasis in mammals. Nat Commun 2010; 1:109.

162. Zou ZG, Rios FJ, Montezano AC, Touyz RM. TRPM7, Magnesium, and Signaling. Int J Mol Sci 2019; 20(8):1877.

163. Liu YS, Liu YA, Huang CJ, Yen MH, Tseng CT, Chien S, Lee OK. Mechanosensitive TRPM7 mediates shear stress and modulates osteogenic differentiation of mesenchymal stromal cells through Osterix pathway. Sci Rep 2015; 5:16522.

164. Wang S, Zhao X, Hsu Y, He Y, Wang F, Yang F, Yan F, Xia D, Liu Y. Surface modification of titanium implants with Mg-containing coatings to promote osseointegration. Acta Biomater 2023; 169:19-44.

165. Zhang Y, Xu J, Ruan YC, Yu MK, O'Laughlin M, Wise H, Chen D, Tian L, Shi D, Wang J, Chen S, Feng JQ, Chow DH, Xie X, Zheng L, Huang L, Huang S, Leung K, Lu N, Zhao L, Li H, Zhao D, Guo X, Chan K, Witte F, Chan HC, Zheng Y, Qin L. Implant-derived magnesium induces local neuronal production of CGRP to improve bone-fracture healing in rats. Nat Med 2016; 22(10):1160-1169.

166. Cui L, Xu SM, Ma DD, Wu BL. The effect of TRPM7 suppression on the proliferation, migration and osteogenic differentiation of human dental pulp stem cells. Int Endod J 2014; 47(6):583-593.

167. Hirano K, Nakabayashi C, Sasaki M, Suzuki M, Aoyagi Y, Tanaka K, Murakami A, Tsuchiya M, Umemoto E, Takabayashi S, Kitajima Y, Ono Y, Matsukawa T, Matsushita M, Ohkawa Y, Mori Y, Hara Y. Mg(2+) influx mediated by TRPM7 triggers the initiation of muscle stem cell activation. Sci Adv 2025; 11(14):eadu0601.

168. Wang ZB, Zhang X, Xiao F, Liu ZQ, Liao QJ, Wu N, Wang J. Roles of TRPM7 in ovarian cancer. Biochem Pharmacol 2023; 217:115857.

169. Izaguirre-Hernandez IY, Sumoza-Toledo A. Potential functions of TRPM2 and TRPM7 channels in the tumor microenvironment. J Leukoc Biol 2025; 117(7):qiaf098.

170. Ji D, Fleig A, Horgen FD, Feng ZP, Sun HS. Modulators of TRPM7 and its potential as a drug target for brain tumours. Cell Calcium 2022; 101:102521.

171. Koles L, Ribiczey P, Szebeni A, Kadar K, Zelles T, Zsembery A. The Role of TRPM7 in Oncogenesis. Int J Mol Sci 2024; 25(2):719.

172. Kaitsuka T, Katagiri C, Beesetty P, Nakamura K, Hourani S, Tomizawa K, Kozak JA, Matsushita M. Inactivation of TRPM7 kinase activity does not impair its channel function in mice. Sci Rep 2014; 4:5718.

173. Shin M, Matsushima A, Kajiya H, Okamoto F, Ogata K, Oka K, Ohshima H, Bartlett JD, Okabe K. Conditional knockout of transient receptor potential melastatin 7 in the enamel epithelium: Effects on enamel formation. Eur J Oral Sci 2023; 131(2):e12920.

174. Edmondson R, Broglie JJ, Adcock AF, Yang L. Three-dimensional cell culture systems and their applications in drug discovery and cell-based biosensors. Assay Drug Dev Technol 2014; 12(4):207-218.

175. Chen LS, Couwenhoven RI, Hsu D, Luo W, Snead ML. Maintenance of amelogenin gene expression by transformed epithelial cells of mouse enamel organ. Arch Oral Biol 1992; 37(10):771-778.

176. Nakata A, Kameda T, Nagai H, Ikegami K, Duan Y, Terada K, Sugiyama T. Establishment and characterization of a spontaneously immortalized mouse ameloblast-lineage cell line. Biochem Biophys Res Commun 2003; 308(4):834-839.

177. Sarkar J, Simanian EJ, Tuggy SY, Bartlett JD, Snead ML, Sugiyama T, Paine ML. Comparison of two mouse ameloblast-like cell lines for enamel-specific gene expression. Front Physiol 2014; 5:277.

178. Guan X, Xu M, Millar SE, Bartlett JD. Beta-catenin is essential for ameloblast movement during enamel development. Eur J Oral Sci 2016; 124(3):221-227.

179. Visakan G, Bapat RA, Su J, Moradian-Oldak J. Modeling ameloblast-matrix interactions using 3D cell culture. Front Physiol 2022; 13:1069519.

180. Visakan G, Su J, Moradian-Oldak J. Ameloblastin promotes polarization of ameloblast cell lines in a 3-D cell culture system. Matrix Biol 2022; 105:72-86.

181. DenBesten PK, Machule D, Zhang Y, Yan Q, Li W. Characterization of human primary enamel organ epithelial cells in vitro. Arch Oral Biol 2005; 50(8):689-694.

182. Yan Q, Zhang Y, Li W, DenBesten PK. Differentiation of human ameloblast-lineage cells in vitro. Eur J Oral Sci 2006; 114 Suppl 1:154-158.

183. DenBesten PK, Gao C, Li W, Mathews CH, Gruenert DC. Development and characterization of an SV40 immortalized porcine ameloblast-like cell line. Eur J Oral Sci 1999; 107(4):276-281.

184. Mathias RS, Mathews CH, Machule C, Gao D, Li W, DenBesten PK. Identification of the calcium-sensing receptor in the developing tooth organ. J Bone Miner Res 2001; 16(12):2238-2244.

185. Duan X, Mao Y, Wen X, Yang T, Xue Y. Excess fluoride interferes with chloride-channel-dependent endocytosis in ameloblasts. J Dent Res 2011; 90(2):175-180.

186. MacDougall M, Mamaeva O, Lu C, Chen S. Establishment and characterization of immortalized mouse ameloblast-like cell lines. Orthod Craniofac Res 2019; 22 Suppl 1(Suppl 1):134-141.

187. Kawano S, Saito M, Handa K, Morotomi T, Toyono T, Seta Y, Nakamura N, Uchida T, Toyoshima K, Ohishi M, Harada H. Characterization of dental epithelial progenitor cells derived from cervical-loop epithelium in a rat lower incisor. J Dent Res 2004; 83(2):129-133.

188. Harada H, Ichimori Y, Yokohama-Tamaki T, Ohshima H, Kawano S, Katsube K, Wakisaka S. Stratum intermedium lineage diverges from ameloblast lineage via Notch signaling. Biochem Biophys Res Commun 2006; 340(2):611-616.

189. Matsumoto A, Harada H, Saito M, Taniguchi A. Induction of enamel matrix protein expression in an ameloblast cell line co-cultured with a mesenchymal cell line in vitro. In Vitro Cell Dev Biol Anim 2011; 47(1):39-44.

190. Zheng L, Seon YJ, Mourao MA, Schnell S, Kim D, Harada H, Papagerakis S, Papagerakis P. Circadian rhythms regulate amelogenesis. Bone 2013; 55(1):158-165.

191. Segeritz CP, Vallier L. Chapter 9 - Cell Culture: Growing Cells as Model Systems In Vitro. In: Jalali M, Saldanha FYL, Jalali M, editors. Basic Science Methods for Clinical Researchers. Boston: Academic Press, 2017: 151-172.

192. Pampaloni F, Reynaud EG, Stelzer EH. The third dimension bridges the gap between cell culture and live tissue. Nat Rev Mol Cell Biol 2007; 8(10):839-845.

193. Mazzoleni G, Di LD, Steimberg N. Modelling tissues in 3D: the next future of pharmaco-toxicology and food research? Genes Nutr 2009; 4(1):13-22.

194. Kleinman HK, Martin GR. Matrigel: basement membrane matrix with biological activity. Semin Cancer Biol 2005; 15(5):378-386.

195. Li W, Machule D, Gao C, DenBesten PK. Growth of ameloblast-lineage cells in a three-dimensional Matrigel environment. Eur J Oral Sci 2006; 114 Suppl 1:159-163.

196. Taghizadeh M, Taghizadeh A, Kim HS. Mechanobiological engineering strategies for organoid culture. APL Bioeng 2025; 9(3):031501.

197. Fang Y, Eglen RM. Three-Dimensional Cell Cultures in Drug Discovery and Development. SLAS Discov 2017; 22(5):456-472.

198. Hofer M, Lutolf MP. Engineering organoids. Nat Rev Mater 2021; 6(5):402-420.

199. Kozlowski MT, Crook CJ, Ku HT. Towards organoid culture without Matrigel. Commun Biol 2021; 4(1):1387.

200. Kratochvil MJ, Seymour AJ, Li TL, Pasca SP, Kuo CJ, Heilshorn SC. Engineered materials for organoid systems. Nat Rev Mater 2019; 4(9):606-622.

201. Aisenbrey EA, Murphy WL. Synthetic alternatives to Matrigel. Nat Rev Mater 2020; 5(7):539-551.

202. He P, Zhang Y, Kim SO, Radlanski RJ, Butcher K, Schneider RA, DenBesten PK. Ameloblast differentiation in the human developing tooth: effects of extracellular matrices. Matrix Biol 2010; 29(5):411-419.

203. Lee GY, Kenny PA, Lee EH, Bissell MJ. Three-dimensional culture models of normal and malignant breast epithelial cells. Nat Methods 2007; 4(4):359-365.

204. Szlavik V, Vag J, Marko K, Demeter K, Madarasz E, Olah I, Zelles T, O'Connell BC, Varga G. Matrigel-induced acinar differentiation is followed by apoptosis in HSG cells. J Cell Biochem 2008; 103(1):284-295.

205. Kubota Y, Kleinman HK, Martin GR, Lawley TJ. Role of laminin and basement membrane in the morphological differentiation of human endothelial cells into capillary-like structures. J Cell Biol 1988; 107(4):1589-1598.

206. Kawano S, Morotomi T, Toyono T, Nakamura N, Uchida T, Ohishi M, Toyoshima K, Harada H. Establishment of dental epithelial cell line (HAT-7) and the cell differentiation dependent on Notch signaling pathway. Connect Tissue Res 2002; 43(2-3):409-412.

207. Kadar K, Juhasz V, Foldes A, Racz R, Zhang Y, Lochli H, Kato E, Koles L, Steward MC, DenBesten P, Varga G, Zsembery A. TRPM7-Mediated Calcium Transport in HAT-7 Ameloblasts. Int J Mol Sci 2021; 22(8):3992.

208. Jairaman A, Prakriya M. Molecular pharmacology of store-operated CRAC channels. Channels (Austin) 2013; 7(5):402-414.

209. Damkier HH, Josephsen K, Takano Y, Zahn D, Fejerskov O, Frische S. Fluctuations in surface pH of maturing rat incisor enamel are a result of cycles of H(+)-secretion by ameloblasts and variations in enamel buffer characteristics. Bone 2014; 60:227-234.

210. Foldes A, Sang-Ngoen T, Kadar K, Racz R, Zsembery A, DenBesten P, Steward MC, Varga G. Three-Dimensional Culture of Ameloblast-Originated HAT-7 Cells for Functional Modeling of Defective Tooth Enamel Formation. Front Pharmacol 2021; 12:682654.

211. Li P, Rubaiy HN, Chen GL, Hallett T, Zaibi N, Zeng B, Saurabh R, Xu SZ. Mibefradil, a T-type Ca(2+) channel blocker also blocks Orai channels by action at the extracellular surface. Br J Pharmacol 2019; 176(19):3845-3856.

212. Macianskiene R, Martisiene I, Zablockaite D, Gendviliene V. Characterization of Mg(2)(+)-regulated TRPM7-like current in human atrial myocytes. J Biomed Sci 2012; 19:75.

213. Beesetty P, Wieczerzak KB, Gibson JN, Kaitsuka T, Luu CT, Matsushita M, Kozak JA. Inactivation of TRPM7 kinase in mice results in enlarged spleens, reduced T-cell proliferation and diminished store-operated calcium entry. Sci Rep 2018; 8(1):3023.

214. Zhang X, Xin P, Yoast RE, Emrich SM, Johnson MT, Pathak T, Benson JC, Azimi I, Gill DL, Monteith GR, Trebak M. Distinct pharmacological profiles of ORAI1, ORAI2, and ORAI3 channels. Cell Calcium 2020; 91:102281.

215. Souza Bomfim GH, Niemeyer BA, Lacruz RS, Lis A. On the Connections between TRPM Channels and SOCE. Cells 2022; 11(7):1190.

216. Yawata K, Nagata M, Narita A, Kawai Y. Effects of long-term acidification of extracellular pH on ATP-induced calcium mobilization in rabbit lens epithelial cells. Jpn J Physiol 2001; 51(1):81-87.

217. Chokshi R, Bennett O, Zhelay T, Kozak JA. NSAIDs Naproxen, Ibuprofen, Salicylate, and Aspirin Inhibit TRPM7 Channels by Cytosolic Acidification. Front Physiol 2021; 12:727549.

218. Kim SJ, Cho IG, Kang HS, Kim JS. pH-dependent modulation of intracellular free magnesium ions with ion-selective electrodes in papillary muscle of guinea pig. J Vet Sci 2006; 7(1):31-36.

219. Gunzel D, Zimmermann F, Durry S, Schlue WR. Apparent intracellular Mg2+ buffering in neurons of the leech Hirudo medicinalis. Biophys J 2001; 80(3):1298-1310.

220. Szlavik V, Szabo B, Vicsek T, Barabas J, Bogdan S, Gresz V, Varga G, O'Connell B, Vag J. Differentiation of primary human submandibular gland cells cultured on basement membrane extract. Tissue Eng Part A 2008; 14(11):1915-1926.

221. Maria OM, Tran SD. Human mesenchymal stem cells cultured with salivary gland biopsies adopt an epithelial phenotype. Stem Cells Dev 2011; 20(6):959-967.

222. Hegyesi O, Foldes A, Bori E, Nemeth Z, Barabas J, Steward MC, Varga G. Evidence for Active Electrolyte Transport by Two-Dimensional Monolayers of Human Salivary Epithelial Cells. Tissue Eng Part C Methods 2015; 21(12):1226-1236.

223. Schonthal AH, Warren DW, Stevenson D, Schecter JE, Azzarolo AM, Mircheff AK, Trousdale MD. Proliferation of lacrimal gland acinar cells in primary culture. Stimulation by extracellular matrix, EGF, and DHT. Exp Eye Res 2000; 70(5):639-649.

224. Huang J, Jiang Y, Ren Y, Liu Y, Wu X, Li Z, Ren J. Biomaterials and biosensors in intestinal organoid culture, a progress review. J Biomed Mater Res A 2020; 108(7):1501-1508.

225. Bakhti M, Scheibner K, Tritschler S, Bastidas-Ponce A, Tarquis-Medina M, Theis FJ, Lickert H. Establishment of a high-resolution 3D modeling system for studying pancreatic epithelial cell biology in vitro. Mol Metab 2019; 30:16-29.

226. Molnar R, Madacsy T, Varga A, Nemeth M, Katona X, Gorog M, Molnar B, Fanczal J, Rakonczay Z, Jr., Hegyi P, Pallagi P, Maleth J. Mouse pancreatic ductal organoid culture as a relevant model to study exocrine pancreatic ion secretion. Lab Invest 2020; 100(1):84-97.

227. Massie I, Spaniol K, Barbian A, Geerling G, Metzger M, Schrader S. Development of lacrimal gland spheroids for lacrimal gland tissue regeneration. J Tissue Eng Regen Med 2018; 12(4):e2001-e2009.

228. Maria OM, Zeitouni A, Gologan O, Tran SD. Matrigel improves functional properties of primary human salivary gland cells. Tissue Eng Part A 2011; 17(9-10):1229-1238.

229. Zheng L, Warotayanont R, Stahl J, Kunimatsu R, Klein O, DenBesten PK, Zhang Y. Inductive ability of human developing and differentiated dental mesenchyme. Cells Tissues Organs 2013; 198(2):99-110.

230. Zheng LW, Linthicum L, DenBesten PK, Zhang Y. The similarity between human embryonic stem cell-derived epithelial cells and ameloblast-lineage cells. Int J Oral Sci 2013; 5(1):1-6.

231. Natsiou D, Granchi Z, Mitsiadis TA, Jimenez-Rojo L. Generation of Spheres from Dental Epithelial Stem Cells. Front Physiol 2017; 8:7.

232. Inai T, Sengoku A, Hirose E, Iida H, Shibata Y. Differential expression of the tight junction proteins, claudin-1, claudin-4, occludin, ZO-1, and PAR3, in the ameloblasts of rat upper incisors. Anat Rec (Hoboken) 2008; 291(5):577-585.

233. Hata M, Kawamoto T, Kawai M, Yamamoto T. Differential expression patterns of the tight junction-associated proteins occludin and claudins in secretory and mature ameloblasts in mouse incisor. Med Mol Morphol 2010; 43(2):102-106.

234. Bronckers AL, Lyaruu DM, Jalali R, DenBesten PK. Buffering of protons released by mineral formation during amelogenesis in mice. Eur J Oral Sci 2016; 124(5):415-425.

235. Nunez SM, Chun YP, Ganss B, Hu Y, Richardson AS, Schmitz JE, Fajardo R, Yang J, Hu JC, Simmer JP. Maturation stage enamel malformations in Amtn and Klk4 null mice. Matrix Biol 2016; 52-54:219-233.

236. Verschuren EHJ, Castenmiller C, Peters DJM, Arjona FJ, Bindels RJM, Hoenderop JGJ. Sensing of tubular flow and renal electrolyte transport. Nat Rev Nephrol 2020; 16(6):337-351.

237. Hill DB, Button B, Rubinstein M, Boucher RC. Physiology and pathophysiology of human airway mucus. Physiol Rev 2022; 102(4):1757-1836.

238. Guns PJ, Korda A, Crauwels HM, Van AT, Robaye B, Boeynaems JM, Bult H. Pharmacological characterization of nucleotide P2Y receptors on endothelial cells of the mouse aorta. Br J Pharmacol 2005; 146(2):288-295.

239. Yang X, Lytton J. Purinergic stimulation of K+-dependent Na+/Ca2+ exchanger isoform 4 requires dual activation by PKC and CaMKII. Biosci Rep 2013; 33(6):e00087.

10. Bibliography of the candidates's publications

Publications related to the thesis

Földes Anna, Sang-Ngoen Thanyaporn, **Kádár Kristóf**, Rácz Róbert, Zsembery Ákos, DenBesten Pamela, Steward Martin C, Varga Gábor

Three-Dimensional Culture of Ameloblast-Originated HAT-7 Cells for Functional Modeling of Defective Tooth Enamel Formation

FRONTIERS IN PHARMACOLOGY 12 Paper: 682654, 14 p. (2021)

Közlemény: 32052747 | Szakcikk (Folyóiratcikk) | Tudományos

Scopus - Pharmacology (medical) SJR indikátor: Q1

Scopus - Pharmacology SJR indikátor: Q1

IF: 5,988

Kádár Kristóf, Juhász Viktória, Földes Anna, Rácz Róbert, Zhang Y, Löchli Heike, Kató Erzsébet, Köles László, Steward Martin C, DenBesten Pamela, Varga Gábor, Zsembery Ákos

Trpm7-mediated calcium transport in hat-7 ameloblasts

INTERNATIONAL JOURNAL OF MOLECULAR SCIENCES 22: 8 Paper: 3992, 14 p. (2021)

Közlemény: 31981561 | Szakcikk (Folyóiratcikk) | Tudományos

Scopus - Spectroscopy SJR indikátor: D1

Scopus - Computer Science Applications SJR indikátor: Q1

Scopus - Inorganic Chemistry SJR indikátor: Q1

Scopus - Medicine (miscellaneous) SJR indikátor: Q1

Scopus - Organic Chemistry SJR indikátor: Q1

Scopus - Physical and Theoretical Chemistry SJR indikátor: Q1

Scopus - Catalysis SJR indikátor: Q2

Scopus - Molecular Biology SJR indikátor: Q2

IF: 6,208

Publications unrelated to the thesis

Tóth Béla Ernő, Takács István, Valkusz Zsuzsanna, Jakab Attila, Fülöp Zsanett, **Kádár Kristóf**, Putz Zsuzsanna, Kósa János Pál, Lakatos Péter

Effects of Vitamin D3 Treatment on Polycystic Ovary Symptoms: A Prospective Double-Blind Two-Phase Randomized Controlled Clinical Trial

NUTRIENTS 17: 7 Paper: 1246, 20 p. (2025)

Közlemény: 36084573 | Szakcikk (Folyóiratcikk) | Tudományos

Scopus - Food Science SJR indikátor: D1

Scopus - Nutrition and Dietetics SJR indikátor: D1

IF: 5,0

Köles László, Ribiczey Polett, Szebeni Andrea, **Kádár Kristóf,** Zelles Tibor, Zsembery Ákos

The Role of TRPM7 in Oncogenesis

INTERNATIONAL JOURNAL OF MOLECULAR SCIENCES 25: 2 Paper: 719, 31 p. (2024)

Közlemény: 34530291 | Összefoglaló cikk (Folyóiratcikk) | Tudományos

Scopus - Organic Chemistry SJR indikátor: D1

Scopus - Spectroscopy SJR indikátor: D1

Scopus - Computer Science Applications SJR indikátor: Q1

Scopus - Inorganic Chemistry SJR indikátor: Q1

Scopus - Medicine (miscellaneous) SJR indikátor: Q1

Scopus - Physical and Theoretical Chemistry SJR indikátor: Q1

Scopus - Catalysis SJR indikátor: Q2

Scopus - Molecular Biology SJR indikátor: Q2

IF: 4,9

Máthé Domokos, Szalay Gergely, Cseri Levente, Kis Zoltán, Pályi Bernadett, Földes Gábor, Kovács Noémi, Fülöp Anna, Szepesi Áron, Hajdrik Polett, Csomos Attila, Zsembery Ákos, **Kádár Kristóf**, Katona Gergely, Mucsi Zoltán, Rózsa Balázs József, Kovács Ervin

Monitoring correlates of SARS-CoV-2 infection in cell culture using a two-photon-active calcium-sensitive dye
CELLULAR AND MOLECULAR BIOLOGY LETTERS 29: 1 Paper: 105, 16 p. (2024)
Közlemény: 35139761 | Szakcikk (Folyóiratcikk) | Tudományos
Scopus - Biochemistry SJR indikátor: D1
Scopus - Cell Biology SJR indikátor: Q1
Scopus - Molecular Biology SJR indikátor: Q1
IF: 10,2

Tóth Béla E, Takács I, **Kádár K**, Mirani Sara, Vecsernyés M, Lakatos Péter
Safety and Efficacy of Loading Doses of Vitamin D: Recommendations for Effective Repletion
PHARMACEUTICALS 17: 12 Paper: 1620, 24 p. (2024)
Közlemény: 35659250 | Szakcikk (Folyóiratcikk) | Tudományos
Scopus - Drug Discovery SJR indikátor: Q1
Scopus - Pharmaceutical Science SJR indikátor: Q1
Scopus - Molecular Medicine SJR indikátor: Q2
IF: 4,8

Sramkó Bendegúz, Földes Anna, **Kádár Kristóf,** Varga Gábor, Zsembery Ákos, Pircs Karolina
The Wisdom in Teeth: Neuronal Differentiation of Dental Pulp Cells
CELLULAR REPROGRAMMING 25: 1 pp. 32-44. (2023)
Közlemény: 33616728 | Összefoglaló cikk (Folyóiratcikk) | Tudományos
Scopus - Biotechnology SJR indikátor: Q3
Scopus - Cell Biology SJR indikátor: Q4
Scopus - Developmental Biology SJR indikátor: Q4
IF: 1,2

Zsembery Ákos, **Kádár Kristóf,** Jaikumpun P, Deli Mária Anna, Jakab Ferenc, Dobay Orsolya

Bicarbonate: An Ancient Concept to Defeat Pathogens in Light of Recent Findings Beneficial for COVID-19 Patients? (2020)
Közlemény: 32202726 | Csak repozitóriumban hozzáférhető közlemény (Egyéb) | Tudományos

Fábián Zoltán, **Kádár Kristóf**, Patonay Lajos, Nagy Krisztián
Application of 3D printed biocompatible plastic surgical template for the reconstruction of a nasoalveolar cleft with preoperative volume analysis
MATERIALE PLASTICE 56: 2 pp. 413-415. (2019)
Közlemény: 30847059 | Rövid közlemény (Folyóiratcikk) | Tudományos
Scopus - Chemistry (miscellaneous) SJR indikátor: Q3
Scopus - Materials Chemistry SJR indikátor: Q3
Scopus - Mechanics of Materials SJR indikátor: Q3
Scopus - Polymers and Plastics SJR indikátor: Q3
IF: 1,517

Nagy Krisztina, Láng Orsolya, Láng Júlia, Perczel-Kovách Katalin, Gyulai-Gaál Szabolcs, **Kádár Kristóf**, Kőhidai László, Varga Gábor
A novel hydrogel scaffold for periodontal ligament stem cells
INTERVENTIONAL MEDICINE AND APPLIED SCIENCE 10: 3 pp. 162-170. (2018)
Közlemény: 3408039 | Szakcikk (Folyóiratcikk) | Tudományos
Scopus - Medicine (miscellaneous) SJR indikátor: Q3

Földes Anna, **Kádár Kristóf**, Kerémi Beáta, Zsembery Ákos, Gyires Klára, Zádori Zoltán Sándor, Varga Gábor
Mesenchymal stem cells of dental origin - their potential for anti-inflammatory and regenerative actions in brain and gut damage
CURRENT NEUROPHARMACOLOGY 14: 8 pp. 914-934. (2016)
Közlemény: 3007107 | Összefoglaló cikk (Folyóiratcikk) | Tudományos
Scopus - Medicine (miscellaneous) SJR indikátor: Q1
Scopus - Neurology (clinical) SJR indikátor: Q1
Scopus - Pharmacology (medical) SJR indikátor: Q1

Scopus - Pharmacology SJR indikátor: Q1
Scopus - Psychiatry and Mental Health SJR indikátor: Q1
Scopus - Neurology SJR indikátor: Q2
IF: 3,365

Rácz Gábor Zoltán, **Kádár Kristóf**, Földes Anna, Kálló Karola, Perczel-Kovách Katalin, Kerémi Beáta, Nagy Ákos, Varga Gábor
Immunomodulatory and potential therapeutic role of mesenchymal stem cells in periodontitis
JOURNAL OF PHYSIOLOGY AND PHARMACOLOGY 65: 3 pp. 327-339. (2014)
Közlemény: 2604580 | Összefoglaló cikk (Folyóiratcikk) | Tudományos
Scopus - Medicine (miscellaneous) SJR indikátor: Q2
Scopus - Pharmacology SJR indikátor: Q2
Scopus - Physiology SJR indikátor: Q3
IF: 2,386

Király Mariann, **Kádár Kristóf**, Horváthy Dénes Balázs, Nardai Péter, Rácz Gábor Zoltán, Lacza Zsombor, Varga Gábor, Gerber Gábor
Integration of neuronally predifferentiated human dental pulp stem cells into rat brain in vivo
NEUROCHEMISTRY INTERNATIONAL 59: 3 pp. 371-381. (2011)
Közlemény: 1433593 | Szakcikk (Folyóiratcikk) | Tudományos
Scopus - Cell Biology SJR indikátor: Q2
Scopus - Cellular and Molecular Neuroscience SJR indikátor: Q3
IF: 2,857

Király Mariann, Porcsalmy Balázs, Pataki Ágnes, **Kádár Kristóf**, Jelitai Márta, Molnár Bálint, Hermann Péter, Gera István, Grimm Wolf-Dieter, Ganss Bernhard, Zsembery Ákos, Varga Gábor
Simultaneous pkc and camp activation induces differentiation of human dental pulp stem cells into functionally active neurons
NEUROCHEMISTRY INTERNATIONAL 55: 5 pp. 323-332. (2009)

Közlemény: 109839 | Szakcikk (Folyóiratcikk) | Tudományos
Scopus - Cell Biology SJR indikátor: Q2
Scopus - Cellular and Molecular Neuroscience SJR indikátor: Q2
IF: 3,541

Kádár Kristóf, Porcsalmy Balázs, Király Mariann, Molnár Bálint, Jobbágy-Óvári Gabriella, Somogyi Eszter, Hermann Péter, Gera István, Varga Gábor
Humán fogbél eredetű őssejtek izolálása, tenyésztése és jellemzése [Isolating, culturing and characterizing stem cells of human dental pulp origin]
FOGORVOSI SZEMLE 102: 5 pp. 175-181. (2009)
Közlemény: 1386494 | Szakcikk (Folyóiratcikk) | Tudományos
Scopus - Medicine (miscellaneous) SJR indikátor: Q4

Kádár Kristóf, Király Mariann, Porcsalmy Balázs, Molnár Bálint, Rácz Gábor Zoltán, Blazsek József, Kálló Karola, Szabó EL, Gera István, Gerber Gábor, Varga Gábor
Differentiation potential of stem cells from human dental origin - promise for tissue engineering
JOURNAL OF PHYSIOLOGY AND PHARMACOLOGY 60: Suppl 7 pp. 167-175. (2009)
Közlemény: 1390629 | Szakcikk (Folyóiratcikk) | Tudományos
Scopus - Medicine (miscellaneous) SJR indikátor: Q2
Scopus - Pharmacology SJR indikátor: Q2
Scopus - Physiology SJR indikátor: Q3
IF: 1,489

Molnár Bálint, **Kádár Kristóf**, Király Mariann, Porcsalmy Balázs, Somogyi Eszter, Hermann Péter, Grimm Wolf-Dieter, Gera István, Varga Gábor
Emberi foggyökérhártya eredetű őssejtek izolálása, tenyésztése és jellemzése [Isolation, cultivation and characterisation of stem cells in human periodontal ligament]
FOGORVOSI SZEMLE 101: 4 pp. 155-161. (2008)
Közlemény: 1386499 | Szakcikk (Folyóiratcikk) | Tudományos
Scopus - Medicine (miscellaneous) SJR indikátor: Q3

Book chapters

Kádár Kristóf

Ionizáló sugárzások és sugárterápia következtében kialakuló orális tünetek

In: Nagy Ákos (szerk.) A magyarországi fogorvosképzés módszertani és tartalmi modernizációja korszerű hosszanti digitális tananyagfejlesztéssel három nyelven

Budapest, Magyarország: Dialóg Campus Kiadó, Nordex Kft. (2014) 1,217 p. pp. 129-136.

Közlemény: 2952941 | Felsőoktatási tankönyv része (Könyvrészlet) | Oktatási

Kádár Kristóf

Centrális és perifériás keringési elégtelenség; Shock – Orális vonatkozások

In: Nagy Ákos (szerk.) A magyarországi fogorvosképzés módszertani és tartalmi modernizációja korszerű hosszanti digitális tananyagfejlesztéssel három nyelven

Budapest, Magyarország: Dialóg Campus Kiadó, Nordex Kft. (2014) 1,217 p. pp. 224-235.

Közlemény: 2952943 | Felsőoktatási tankönyv része (Könyvrészlet) | Oktatási

Kádár Kristóf

Keményszövetek vizsgálata

In: Nagy Ákos (szerk.) A magyarországi fogorvosképzés módszertani és tartalmi modernizációja korszerű hosszanti digitális tananyagfejlesztéssel három nyelven

Budapest, Magyarország: Dialóg Campus Kiadó, Nordex Kft. (2014) 1,217 p. pp. 354-359.

Közlemény: 2952946 | Felsőoktatási tankönyv része (Könyvrészlet) | Oktatási

Kádár Kristóf

Radiation, oral symptoms associated with radiotherapy

In: Nagy Ákos (szerk.) Digital method and content development of the Hungarian higher education in dentistry in Hungarian, German and English

Budapest, Magyarország: Dialóg Campus Kiadó, Nordex Kft. (2014) 1,217 p. pp. 129-137.

Közlemény: 3242345 | Utánközlés (Könyvrészlet) | Oktatási

Kádár Kristóf

Cardiac insufficiency and shock - oral aspects

In: Nagy Ákos (szerk.) Digital method and content development of the Hungarian higher education in dentistry in Hungarian, German and English

Budapest, Magyarország: Dialóg Campus Kiadó, Nordex Kft. (2014) 1,217 p. pp. 226-236.

Közlemény: 3242355 | Utánközlés (Könyvrészlet) | Tudományos

Kádár Kristóf

Practices: Investigation methods of mineralised tissues

In: Nagy Ákos (szerk.) Digital method and content development of the Hungarian higher education in dentistry in Hungarian, German and English

Budapest, Magyarország: Dialóg Campus Kiadó, Nordex Kft. (2014) 1,217 p. pp. 353-358.

Közlemény: 3242361 | Utánközlés (Könyvrészlet) | Oktatási

Kádár Kristóf

Ionisierende Strahlungen und Radiotherapieflogenden orale Symptomen

In: Nagy Ákos (szerk.) Digitale Methodik und Inhaltmodernisierung der ungarischen zahnmedizinischen Hochschulausbildung auf Ungarisch, Englisch und Deutsch

Budapest, Magyarország: Dialóg Campus Kiadó, Nordex Kft. (2014) 1,259 p. pp. 136-143.

Közlemény: 3242637 | Utánközlés (Könyvrészlet) | Oktatási

Kádár Kristóf

Zentrale und periphere Kreislafstörungen; Schock und orale Symptome

In: Nagy Ákos (szerk.) Digitale Methodik und Inhaltmodernisierung der ungarischen zahnmedizinischen Hochschulausbildung auf Ungarisch, Englisch und Deutsch

Budapest, Magyarország: Dialóg Campus Kiadó, Nordex Kft. (2014) 1,259 p. pp. 233-244.

Közlemény: 3242641 | Utánközlés (Könyvrészlet) | Oktatási

Kádár Kristóf

Praktiken: Mineralisierte Gewebe

In: Nagy Ákos (szerk.) Digitale Methodik und Inhaltmodernisierung der ungarischen zahnmedizinischen Hochschulausbildung auf Ungarisch, Englisch und Deutsch

Budapest, Magyarország: Dialóg Campus Kiadó, Nordex Kft. (2014) 1,259 p. pp. 363-367.

Közlemény: 3242643 | Utánközlés (Könyvrészlet) | Oktatási

11. Acknowledgments

My warmest thanks go to my family.
To my late **mother**, who loved and supported me throughout her life, and from whom I learned how fascinating the world can be - especially science. She taught me the basics of scientific thinking and rigor, and I miss her deeply.
To my dear **father**, who always loved me and supported me in everything I pursued.
And to my dear **brother**, who never stopped believing in me.

I express my sincere gratitude to my tutor, **Dr. Ákos Zsembery**, the current head of the Department, and to **Professor Dr. Gábor Varga**, the former head, for providing me with the opportunity to pursue science, and for their guidance, patience, and support throughout my PhD program and my years in the Department.

My special thanks go to my colleague, **Dr. Anna Földes**, for her guidance, support, advice and participation in my projects, and to **Dr. Beáta Kerémi** for her support and invaluable advice during my PhD studies and the many years we worked together in the Department.

I am deeply indebted to **Dr. Martin C. Steward** for his invaluable guidance, advice, and help in our projects.

I thank **Dr. Róbert Rácz** for his support and participation in our scientific projects.

I am grateful to all my co-authors and collaborators for their contributions.

My heartfelt thanks go to **Humli Viktória** and **Csörögi Gáborné (Ildikó ☺)** for their continuous support.

I also thank **Dr. József Blazsek (Jóska ☺)** for all his valuable comments and suggestions.

My thanks extend to all colleagues in the Department of Oral Biology, including **Dr. Tibor Zelles, Dr. László Köles, and Dr. Judit Szepesy**.

Finally, I thank all my family members, friends, and colleagues not listed here for their advice, friendship, and encouragement.